

	<p>Research and Development Programme on Seismic Ground Motion</p> <p>CONFIDENTIAL <i>Restricted to SIGMA scientific partners and members of the consortium, please do not pass around</i></p>	<p>Ref : SIGMA-2014-D3-115 Version : 01</p> <p>Date : Page :</p>
--	--	--



CHARACTERIZING SITE METADATA OF ACCELEROMETRIC NETWORK STATIONS : RESULTS AND METHODOLOGICAL FEEDBACK FROM A RAP STATION SURVEY

AUTHORS			REVIEW			APPROVAL		
NOM	DATE	VISA	NOM	DATE	VISA	NOM	DATE	VISA
A. DECHAMP (CEA)			M. GRANET (EOST)		In written review attached	F. Hollender		
			F. PACOR (INGV Milano)		In written review attached	G. Senfaute		

DISSEMINATION: Authors; Steering Committee; Work Package leaders, Scientific Committee, Archiving.

	<p>Research and Development Programme on Seismic Ground Motion</p> <p>CONFIDENTIAL <i>Restricted to SIGMA scientific partners and members of the consortium, please do not pass around</i></p>	<p>Ref : SIGMA-2014-D3-115 Version : 01</p> <p>Date : Page :</p>
--	--	--

Executive Summary

FINAL DOCUMENT



CHARACTERIZING SITE METADATA OF ACCELEROMETRIC NETWORK STATIONS : RESULTS AND METHODOLOGICAL FEEDBACK FROM A RAP STATION SURVEY

Aline DECHAMP, Sylvette THOMASSIN,

Fabrice HOLLENDER, Cécile CORNOU

(6 May 2014 – Version 1)

AUTHORS			REVIEW			APPROVAL		
NOM	DATE	VISA	NOM	DATE	VISA	NOM	DATE	VISA
A. DECHAMP (CEA)			M. GRANET (EOST)			F. Hollender		
			F. PACOR (INGV Milano)			G. Senfaute		

	<p style="text-align: center;">Research and Development Programme on Seismic Ground Motion</p> <p style="text-align: center;">CONFIDENTIAL <i>Restricted to SIGMA and CASHIMA scientific partners and members of the consortium, please do not pass around</i></p>	<p>Ref : SIGMA-2014-D3-115 Version : 01</p> <hr/> <p>Date : 06/05/2014 Page : 112</p>
--	--	---

Executive Summary

Accelerometric station metadata are of a paramount importance for an optimal use of corresponding accelerograms into seismic hazard studies, for example GMPEs derivation. These metadata should give reliable information about the local site conditions in order to be able to evaluate (among other things) the site effects that affect the data. The French Accelerometric Permanent Network (RAP: Réseau Accélérométrique Permanent) still needs an important effort to optimize the quality of station metadata in order to reach the same level of quality that the one reached by neighbor countries, as Italy or Switzerland where an important effort was done over the last recent years.

Different approaches can be used to evaluate site conditions. The present work, conducted within the SIGMA/WP3 project, had two main objectives: 1. the production of metadata for a first set of RAP stations; 2. A methodological effort (complementary to the InterPacific subproject) that aims to test the non-invasive approaches on sites that are not always favorable to the implementation of surface wave approaches, in a “productivity” context (one day per site), then compare the possible results of surface wave methods to the GIM methods.

The survey was performed on 9 stations. We obtained reliable results (Vs profile, Vs30, class soil...) on at least 5 of them (PYLI, PYAS, PYLU, PYBB and PYAT) up to 130 to 350 m depth (depending on the site). On two other stations (PYLL and EPF) the investigation ranges were more limited but still allow giving Vs30 bounds. On the two last station (PYOR and PYLO), the surface wave upper mode identification was more complex and the results may strongly depend on this identification. The final results given in this report for those both stations are likely exact, but it is reasonable to keep in mind this mode identification issue. Further processing and/or acquisitions on these sites may improve the robustness of the results.

From a methodological point of view, the major learning is that surface-wave methods can be applied for site characterization of accelerometric network stations, that is to say, even when survey and processing complications are cumulated (strong topography, difficult access to sites, time constraints, a priori “rock stations” for which the amount of surface wave within the ambient vibration wave field is low). Of course, some acquisition and/or processing did not produce results (eg. SPAC processing), but on each site, we could produce information that enhance the site condition knowledge.

On 9 stations, we did not identify any true “reference station” since all station are characterized by amplification. For the most “rigid” sites (PYLI, Vs30=1150 m/s; PYAS, Vs30=1000 m/s), we systematically found a quite soft layer underling the “true rock” that induces an high frequency site effect, even if these site are classified in the EC8 “A class”. As comparison, these stations were considered as reference station with a Vs30 of 2000 m/s within previous work.

We also illustrated that this high frequency site effect could be different between stations (here PYLI and PYAS) even for quite similar Vs30 values. The Vs30 cannot characterize alone such amplification effects.

Even if we did not identify reference station in our work, it seems important to add a clear identification “flag” within in accelerometric database metadata for stations that are really reference stations. The characterization of the possible high-frequency site effect for “rock” station (that cannot be considered as “reference station”) has also an influence on the kappa parameter determination.

TABLE OF CONTENTS

1 INTRODUCTION AND OBJECTIVES.....	5
1.1 CONTEXT AND OVERALL OBJECTIVES	5
1.2 CHOICE OF INVESTIGATED STATIONS AND WORK ORGANIZATION	5
2 ACQUISITION AND PROCESSING METHODOLOGY.....	7
2.1 ACQUISITION.....	8
2.1.1 MASW	8
2.1.2 AMBIENT VIBRATION ARRAY (AVA).....	8
2.1.3 TOPOGRAPHIC MEASUREMENTS.....	8
2.2 PROCESSING.....	8
2.2.1 MASW	8
2.2.2 AMBIENT VIBRATION ARRAYS	8
2.3 INVERSION	9
3 PRESENTATION OF SURVEYS, PROCESSING AND INVERSION FOR ALL INVESTIGATED STATIONS.....	9
3.1 PYLL	9
3.1.1 STATIONS INFORMATION	9
3.1.2 MEASUREMENTS	12
3.1.3 PROCESSING	13
3.1.4 INVERSION	18
3.2 PYOR	20
3.2.1 STATIONS INFORMATION	20
3.2.2 MEASUREMENTS	22
3.2.3 PROCESSING	23
3.2.4 INVERSION	27
3.3 PYLI	30
3.3.1 STATIONS INFORMATION	30
3.3.2 MEASUREMENTS	32
3.3.3 PROCESSING	33
3.3.4 INVERSION	38
3.4 PYAS.....	41
3.4.1 STATIONS INFORMATION	41
3.4.2 MEASUREMENTS	42
3.4.3 PROCESSING	43
3.4.4 INVERSION	49

3.5	PYLU	52
3.5.1	STATIONS INFORMATION	52
3.5.2	MEASUREMENTS	54
3.5.3	PROCESSING	55
3.5.4	INVERSION	60
3.6	PYBB	63
3.6.1	STATIONS INFORMATION	63
3.6.2	MEASUREMENTS	65
3.6.3	PROCESSING	66
3.6.4	INVERSION	70
3.7	PYLO	73
3.7.1	STATIONS INFORMATION	73
3.7.2	MEASUREMENTS	75
3.7.3	PROCESSING	76
3.7.4	INVERSION	80
3.8	EPF	83
3.8.1	STATIONS INFORMATION	83
3.8.2	MEASUREMENTS	85
3.8.3	PROCESSING	86
3.8.4	INVERSION	90
3.9	PYAT	92
3.9.1	STATIONS INFORMATION	92
3.9.2	MEASUREMENTS	95
3.9.3	PROCESSING	96
3.9.4	INVERSION	101
4	DISCUSSIONS	103
4.1	RESULTS SYNTHESIS AND UNCERTAINTY ESTIMATION ATTEMPT	103
4.2	METHODOLOGICAL LEARNINGS	106
4.3	IS THERE ANY REFERENCE STATIONS?	107
4.4	WHAT ABOUT THE IMPACT ON KAPPA ESTIMATION?	109
5	CONCLUSIONS AND PERSPECTIVES	111
6	BIBLIOGRAPHY	ERREUR ! SIGNET NON DEFINI.

1 INTRODUCTION AND OBJECTIVES

1.1 CONTEXT AND OVERALL OBJECTIVES

Accelerometric station metadata are of a paramount importance for an optimal use of corresponding accelerograms into seismic hazard studies, for example GMPEs derivation. These metadata should give reliable information about the local site conditions in order to be able to evaluate (among other things) the site effects that affect the data. The French Accelerometric Permanent Network (RAP: Réseau Accélérométrique Permanent) still needs an important effort to optimize the quality of station metadata in order to reach the same level of quality that the one reached by neighbour countries, as Italy or Switzerland where an important effort was done over the last recent years.

Different approaches can be used to evaluate site conditions (Hollender et al. 2012). A first group includes the invasive approaches (cross-holes, down-doles, PS suspension logging...). A second group includes non-invasive approaches, especially the ones based on surface wave dispersion analysis. A third one is based on the use of accelerometric data themselves, for example within a Generalized Inversion Method (GIM) use (Drouet et al. 2010). All these approaches have their own benefits and drawbacks, and one of the SIGMA WP3 program is to evaluate the respective capabilities / limits of these methods, especially through the InterPacific sub-project that aims to compare invasive methods and non-invasive surface wave-based approaches and to propose a guideline for the use of these last methods.

The present work presents two main objectives:

- 1. The production of metadata for a first set of RAP stations.
- 2. A methodological effort, complementary to the InterPacific project that aims to i/ test the non-invasive approaches on sites that are not always favourable to the implementation of surface wave approaches, in a “productivity” context (one day per site); ii/ compare the possible results of surface wave methods to the GIM methods.

1.2 CHOICE OF INVESTIGATED STATIONS AND WORK ORGANIZATION

Concerning the choice of stations, we coordinated with SIGMA WP2. The objective was to focus on the French region that produced most accelerograms used within seismological studies. Among the Pyrenees stations, we first focused on the one that was used as “reference stations” within the previous work of Drouet et al. (2010): PYAS, PYLI, PYLL and PYLO. We completed this list with other important stations that produced a high amount of accelerograms: PYOR, PYLU, PYBB and PYAT. A ninth station was also investigated: EPF, which are a quite recent associated RAP station, operated by CEA/DASE/LDG (see Figure 1 and Figure 2).

It is also important to stress that this overall choice (exempt for a very few of them), led to a very difficult context for the surface wave methods implementation for both the acquisition itself but also for the processing:

- strong topography,
- difficult access to sites,
- a priori “rock stations” for which the amount of surface wave within the ambient vibration wave field is relatively low in comparison with soft sites.

Nevertheless, this complication was mandatory because we wanted to test the method in conditions in which it could be systematically applied in future developments. Developing a methodology that is only applicable in idealistic situations is useless.

This work was performed in coordination with the RAP working group on characterization of site conditions, led by Agathe ROULLE from BRGM and regional network operators:

- BRGM for PYLL, PYOR, PYLI, PYAS,
- OMP for PYLU, PYBB, PYLO, PYAT,
- LDG for EPF.

This work takes place within the SIGMAWP3 and CASHIMA program. It was led by CEA/DASE/LDG (coordination of Aline DECHAMP). The survey was performed over two weeks in September 2012 and involved over these two weeks: Aline DECHAMP, Vincent BOUTIN and Cédric GUYONNET-BENAIZE (CEA). They were helped over one week periods by Isabelle DOUSTE-BACQUE (ISTerre) and other punctual help. The acquisition material was provided by ISTerre (WARAN system developed by Marc WATHELET –ISTerre– for passive measurements, and standard Geode acquisition and 4,5 Hz geophones for MASW). The processing was then performed by Sylvette THOMASSIN (Résonance Ingénieurs-Conseils SA) with the Geopsy software (Wathelet 2008) with advices and quality control provided by Cécile CORNOU (ISTerre).

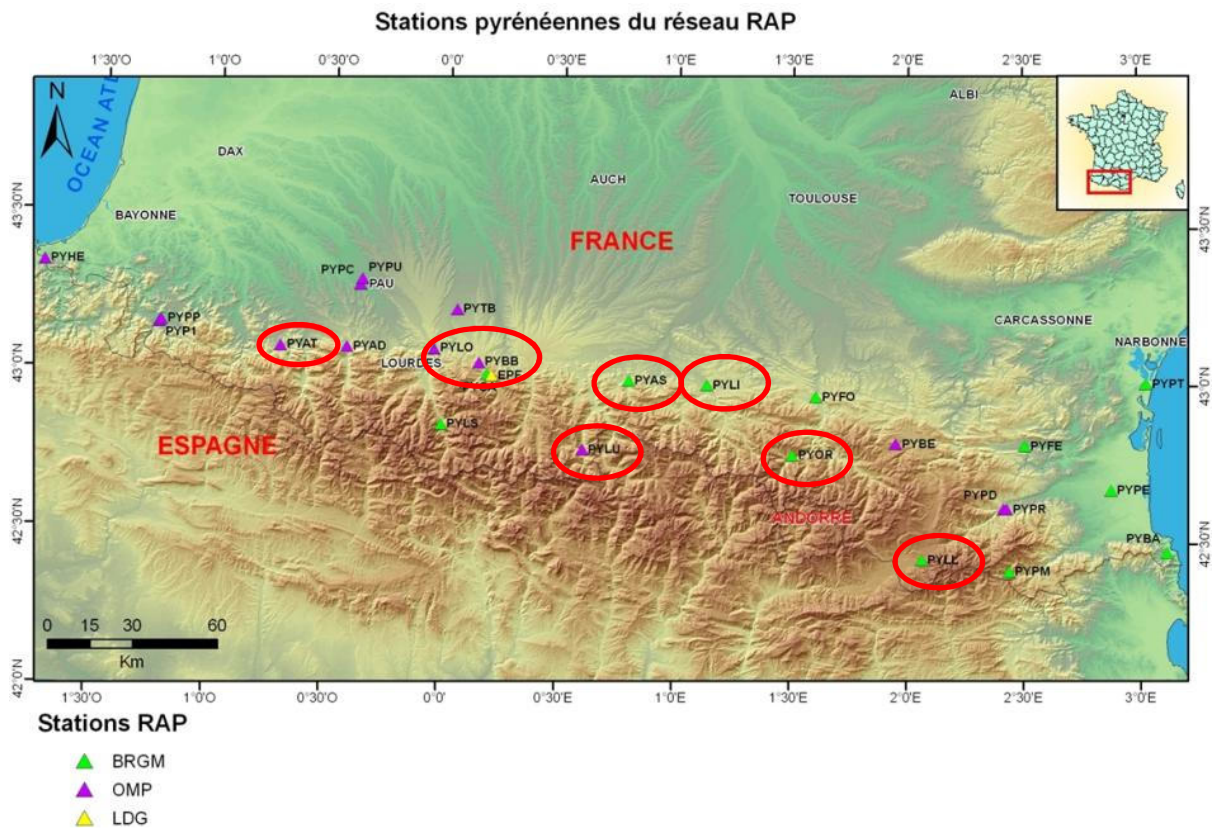


Figure 1: Pyrenean Accelerometric stations (RAP)

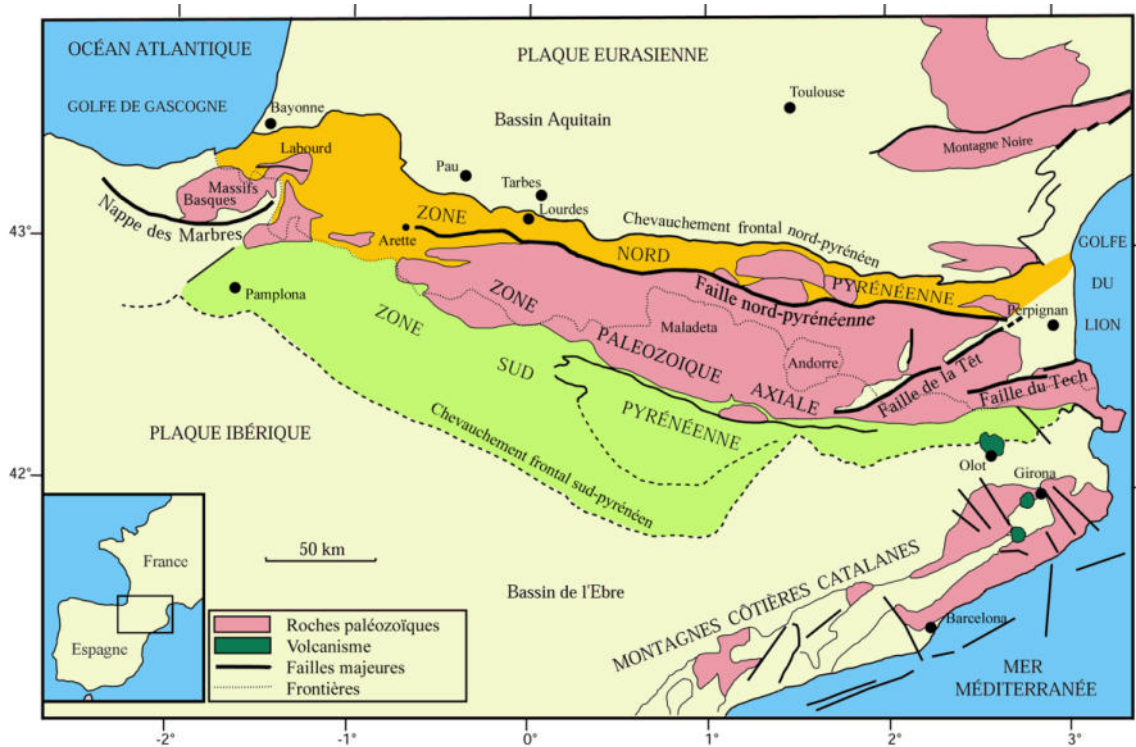


Figure 2: Pyrenean tectonic context (OMP Source).

2 ACQUISITION AND PROCESSING METHODOLOGY

The non-invasive methods based on surface wave dispersion analysis can be split in two groups: the passive ones that use ambient vibrations and the active ones that use the signal generated by an artificial source. We demonstrated in a previous work (Hollender et al. 2012) that we get more reliable results by mixing both approaches and doing a joint inversion of results of both approaches. So we tried to systematically use on each RAP site:

- Active method and especially MASW (Multi Analysis Surface waves). The MASW method consists of recording seismic data, especially surface waves (Rayleigh or Love) produced using active sources like a hammer striking. Waves are recorded by (vertical or horizontal) geophones, placed along line.
- Passive method, based on ambient vibrations array (AVA). The acquisition consists to deploy temporary, small aperture 3-component high sensitivity seismological 2D arrays to record the ambient vibrations. The geometry adopted for building these arrays is important and depends on the available number of sensors and site configuration. In the present work, we used circle geometries placing on sensor in the middle and 7 or 9 sensors on a circle. We measured consecutively 2 to 3 “circles” increasing the diameters in order to get a dispersion curve and a wide frequency range.

2.1 ACQUISITION

2.1.1 MASW

The MASW technique relies on the recording along a 1D linear profile of seismic signals produced by a 5 kg hammer. We used both 24 vertical geophones and 24 horizontal geophones (all with 4,5 Hz natural frequency) associated to a Geode acquisition system provided by ISTerre. We used a 5 kg hammer, hitting either vertically a metallic plate either horizontally wooden beam. On each we performed one or two profile in both horizontal and vertical polarisation, with an inter-geophone distance of 1 or 2 meters.

2.1.2 Ambient Vibration Array (AVA)

For passive measurements, we used the WARAN system developed by Marc Wathelet in ISTerre. With this system, all stations can communicate together through a WIFI system. Each station is also equipped by GPS sensors that allow time synchronisation but also real-time differential positioning. This give the capability to see the progressive constitution of the dispersion curves in near real time. The WARAN is a powerful tool with evident advantages among other kind of equipment but was still in a development phase and showed some limitations, especially due to the fact that it is not still rugged enough to be used over a two week period in quite difficult situations (for example rainy weather conditions).

The WARAN system allows using 10 stations. At the beginning of the survey, we used 10 sensors geometries but we should reduce to 8 sensors for last sites characterization due to technical problems. The WARAN acquisition stations were associated to Lennartz 5s 3 component velocimeters.

2.1.3 Topographic measurements

The locations of all measurement points were also determined with a Trimble GeoXH sensor, associated to a differential post-processing using online data provided by the French permanent GNSS network.

2.2 PROCESSING

2.2.1 MASW

For each site, MASW was process using the "linear FK" tool of the Geopsy software for each polarisation (leading to get DC curves of Rayleigh and Love waves). MASW processing generally allowed obtaining dispersion curves at high frequency (>15-20Hz most of time).

2.2.2 Ambient Vibration Arrays

2.2.2.1 *Quality check and H/V*

Data of passive measurements were analysed on different ways. We started the processing by checking the data quality with Fourier Spectra. Then we applied for each "single point" measurement a classical H/V analysis that allow to evaluate the spatial homogeneity of the investigated site, but also to get the fundamental resonance frequency of the site (when measureable) that could be used in joint inversion techniques.

2.2.2.2 *FK and HRFK*

The simultaneous waveform recordings of a group of spatially distributed stations are analysed in many narrow frequency bands for individual analysis windows cut from the overall recordings. For each

analysis windows and frequency band, a grid search is performed in the wavenumber domain by effectively find the propagation properties of the most coherent and/or powerful plane wave arrival in the analysis window. The apparent velocity equals the phase velocity of the surface wave at this particular frequency.

The vertical components of different array were processed using the FK and High-resolution FK analysis (Capon, 1969) using Geopsy software. The windows lengths depend of array aperture. For large aperture, we privileged large time windows because it gave better results.

The FK and HRFK lead to obtain Rayleigh waves dispersion curve in a frequency range that depends on the array geometry.

2.2.2.3 *Spatial Autocorrelation (SPAC)*

SPAC allows computing average spatial autocorrelation coefficients for any arbitrary array configurations. It relies on a stochastic ambient noise wave field stationary in both time and space. As application of the SPAC technique requires perfect circles arrays, it was difficult to achieve in Pyrenean sites. So in the report, we can see, on several sites, SPAC method did not work.

The SPAC approaches leads to auto-correlation curves that can be converted into dispersion curves.

2.3 INVERSION

The inversions were performed using the “Dinver” tool of the Geopsy package (Wathelet 2008). We tried to achieved on each stations a joint inversion of the different segments of Rayleigh wave dispersion curve produced by the different AVA array and vertical MASW survey, the autocorrelation curves when available, the Love dispersion curve at high frequency.

In order to estimate the uncertainties linked to the inversion, we applied the “acceptable misfit” approaches that consists to produce not only the “best estimate” velocity profile but also the one that are coherent with the DC curve within a $\pm 1 \sigma$ interval (sometimes in a $\pm 2 \sigma$ or $\pm 0,5 \sigma$ interval when needed).

The final output is then a set of velocity profiles, than we also derived in Vs30 values and Soil classes.

3 PRESENTATION OF SURVEYS, PROCESSING AND INVERSION FOR ALL INVESTIGATED STATIONS

3.1 PYLL

3.1.1 Stations information

3.1.1.1 PYLL choice

PYLL station is of the French Strong Motion Network (RAP) in Llo (Orientals Pyrenean). It has been retained in this project because it one of 4 Pyrenean stations which used as reference site in Generalized Inversion technic in France (Drouet et al., 2010) where PYLL station was considered as a rock site with Vs above 2000 m/s.

3.1.1.2 Geographic/Geologic information

Llo is located in Oriental Pyrenees department, next to the Spanish boundary and the “Faille de la Têt” tectonic structure. Main characteristic of the site is resumed in Table 1. On geological map, it is located on Precambrian substratum, especially Orthogenesis (Carança formation). On the field, bedrock appears massive but fractured at the surface. Topography is very important around PYLL station with big breaking slope. Little river is present too. PYLL station is set up in free field, in a little roughcast shelter (Figure 3 to Figure 6).

Table 1: main characteristic of PYLL station location

Station	City	Department	X Coord (Long)	Y Coord (Lat)	Network	Site	Slope
PYLL	Llo	Pyrénées-Atlantiques (64)	2.064732	42.453620	OMP - RAP	Pyrenean mountain (1400m)	Steep slope

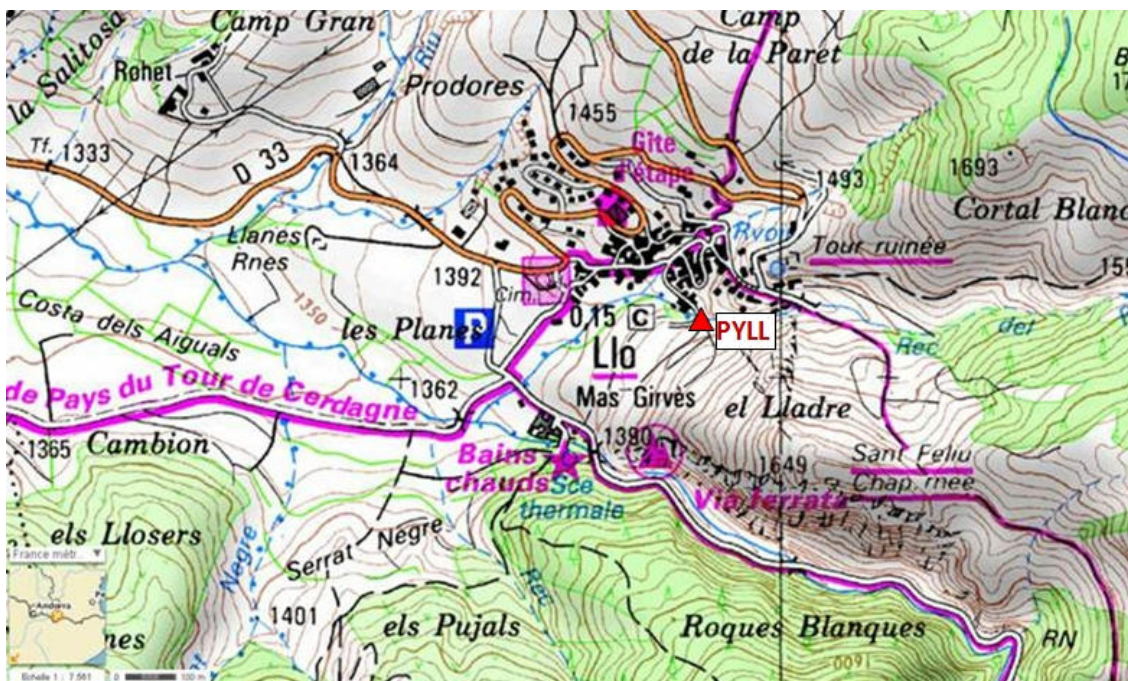


Figure 3 : PYLL location in Llo (IGN Geoportail source)



Figure 4: Steep slope on PYLL site



Figure 5: Picture of the site PYLL, during the measurement on the 4th September 2012.

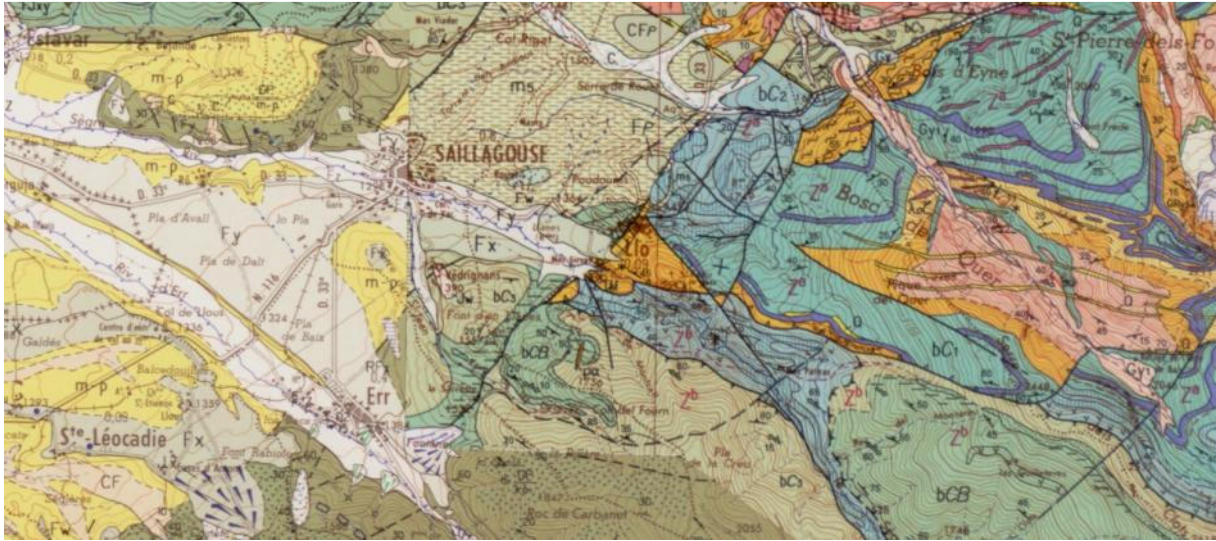


Figure 6: Extract of Saillagouse geological map (with Llo location)

3.1.2 Measurements

The measurement survey was performed on 4th September 2012. For Ambient Vibration Array method, one geometry with 2 circles of 20 and 60 m around a central station (near real PYLL station) was performed (10 sensors). For the second method, MASW, one 34.5 m profile was done, with Rayleigh and Love waves recording. Location of investigation is showed at Figure 7. Parameters of these 2 arrays and MASW investigation are presented in Table 2.

Table 2: PYLL recording parameters, 04th September 2012

Measurments	Numbers of Sensors	Beginning (TU)	End (TU)	Noise/ environnement	Topography	Weather conditions
Array R = 10m	10	09:10:00	10:02:00	little river in the array	slope	wind
Array R = 40m	10	11:18:00	12:30:00	little river in the array	Steep slope	wind
MASW N240E 34.5m, Dx = 1.5m	24 géophones (H and V)	14:00:00	16:00:00	Wind ++	slope	wind

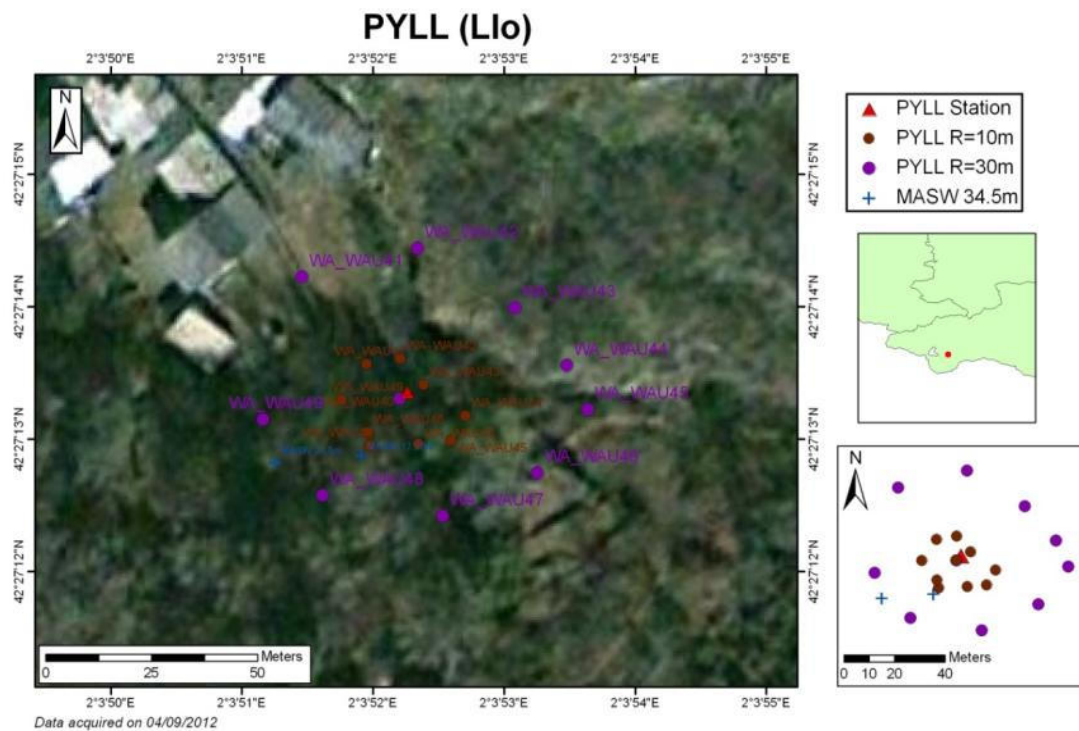


Figure 7: location of the arrays, the MASW shots and the PYLL Station.

3.1.3 Processing

3.1.3.1 H/V

The Fourier spectra amplitudes computed on the three component records of ambient vibrations at each PYLL array receiver are shown in Figure 8. The corresponding H/V curves are displayed in Figure 9. Most of the H/V curves are flat. The other curves show large H/V amplitude over a broad frequency band.

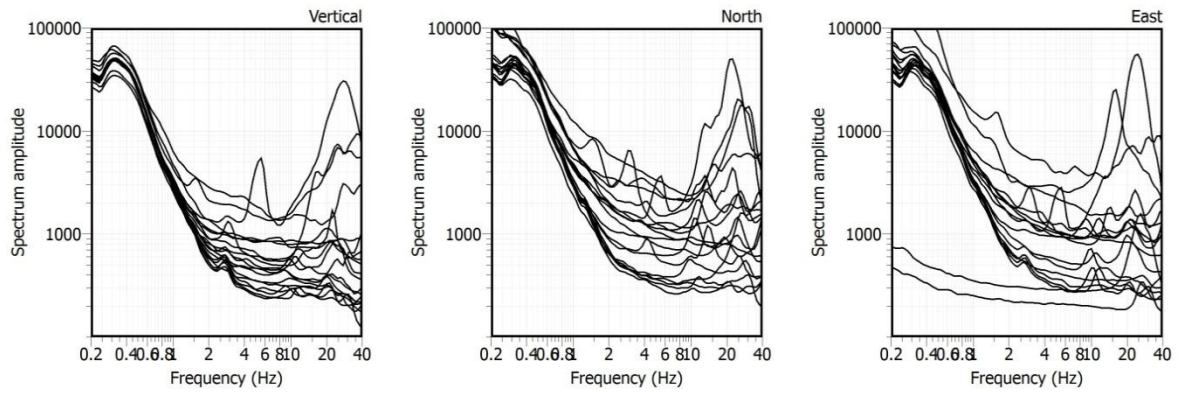


Figure 8: Amplitude of the Fourier spectra computed on 3-Recordings of ambient vibrations at each PYLL array receiver.

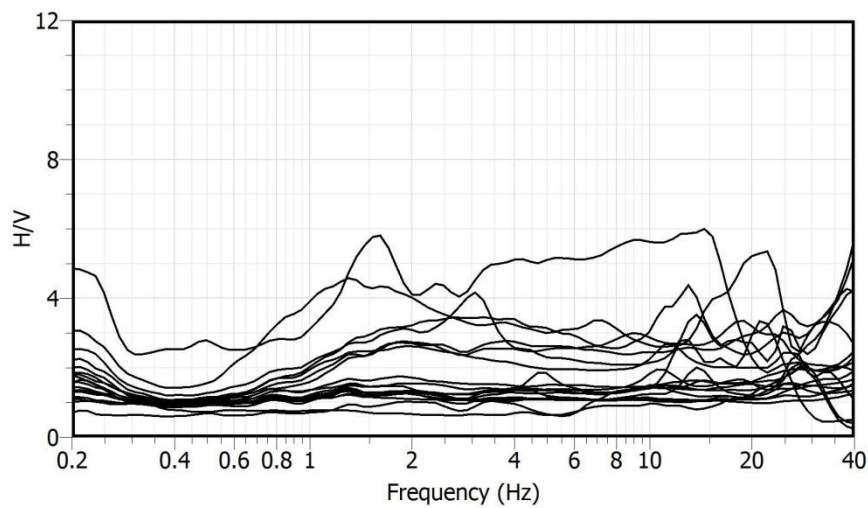


Figure 9: H/V amplitude at each PYLL array receiver.

3.1.3.2 AMV

The parameters used for FK and HRFK analysis at PYLL site are described in Table 3.

Table 3: PYLL FK and HFRK analysis parameters: array radius (Array), windows length according to the centre period of the frequency band T (Windows length), minimum and maximum (central) frequencies (Fmin and Fmax), number of frequency sample (Step), anti-aliasing limits kmin and kmax, fk grid resolution (Grid step), maximum search radius for the fk grid (Grid size), minimum velocity and half-bandwidth for the frequency band (Band width).

Array	Windows length	Fmin Hz	Fmax Hz	Step	Kmin rad/m	Kmax rad/m	Grid step rad/m	Grid size rad/m	Vmin m/s	Band width
FK										
10 m	70 T	20	40	30	0.2393	1.9634	0.0598	2.500	100	0.1
30 m	200 T	10	40	50	0.0799	0.5063	0.0200	1.013	150	0.1
HFRK										
10 m	150 T	20	40	100	0.2393	1.9634	0.0120	3.927	50	0.03
30 m	200 T	13	30	100	0.0799	0.5063	0.0040	1.013	150	0.03

FK

The histogram distributions of phase velocities estimation of Rayleigh waves derived from the ensemble of the wave-propagation estimates obtained for each individual time-frequency cell using the FK method are shown in Figure 10 for PYLL arrays.

It was not possible to derive Rayleigh dispersion curve from the FK analysis.

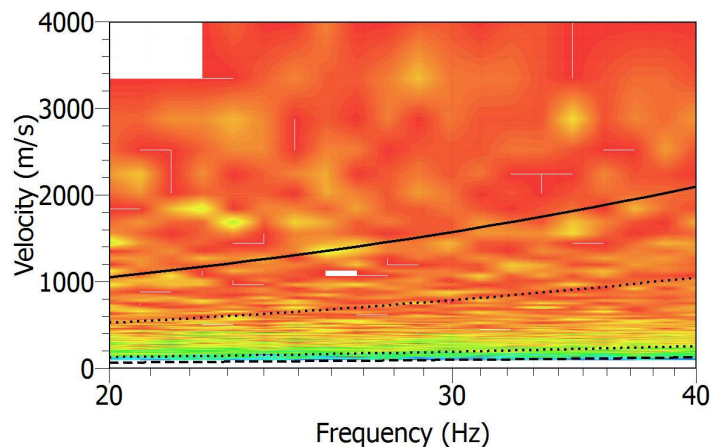


Figure 10: Results for the 10 m (top) and 30 m (bottom) radius arrays at PYLL site (vertical component): histogram distributions of phase velocities derived from the ensemble of the wave-propagation estimates obtained for each individual time-frequency cell using the FK method (color scale: red and magenta colors indicate min and max values, respectively). The anti-aliasing limits for each array configuration are also shown: thick line ($k_{min}/2$), dotted lines (k_{min} and $k_{max}/2$) and dashed line (k_{max}).

HRFK

The resulting estimation of Rayleigh waves phase velocities are shown in Figure 11 for PYLL arrays. It was not possible to derive Rayleigh dispersion curve from the HRFK analysis.

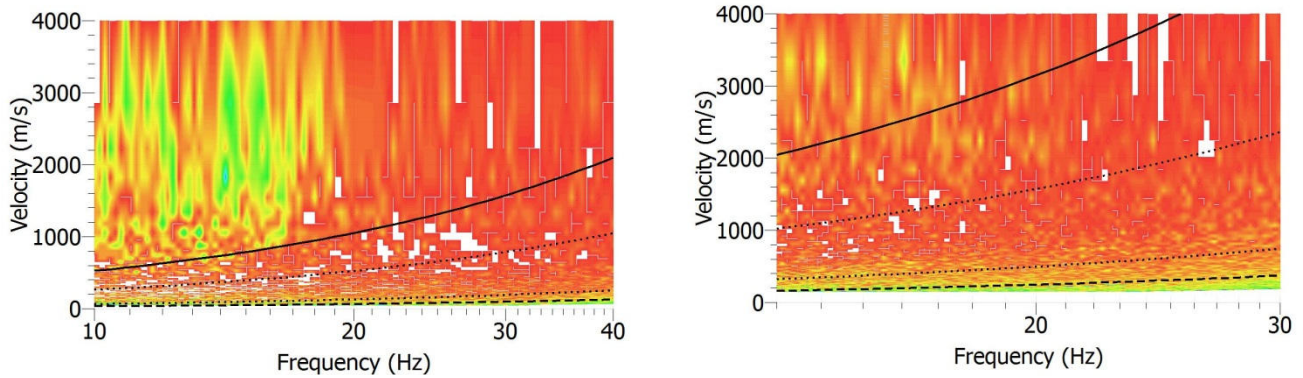


Figure 11: Results for the 10 m (left) and 30 m (right) radius arrays at PYLL site (vertical component): histogram distributions of phase velocities derived from the ensemble of the wave-propagation estimates obtained for each individual time-frequency cell using the HRFK method (color scale: red and magenta colors indicate min and max values, respectively). The anti-aliasing limits for each array configuration are also shown: thick line ($k_{min}/2$), dotted lines (k_{min} and $k_{max}/2$) and dashed line (k_{max}).

SPAC

The parameters used for the SPAC analysis for the 30 m array at PYLL site are described in Table 4. The computed spatial autocorrelation coefficients are displayed for each ring in the Figure 12. These autocorrelation coefficients don't lead to estimate reliable dispersion curve.

Table 4: PYLL SPAC analysis parameters: array radius (Array), windows length according to the centre period of the frequency band T (Windows length), minimum and maximum (central) frequencies (F_{min} and F_{max}), number of frequency sample (Step), number of rings, minimum and maximum radius of rings (R_{min} and R_{max}) and number of pairs of sensors in each ring.

Array	Windows length	Fmin Hz	Fmax Hz	Step	Nimber of rings	Rmin m	Rmax m	Number of pairs
30 m	100 T	10	30	30	4	11.22	28.83	12
						30.47	44.21	12
						45.6	53.05	7
						58.51	71.50	14

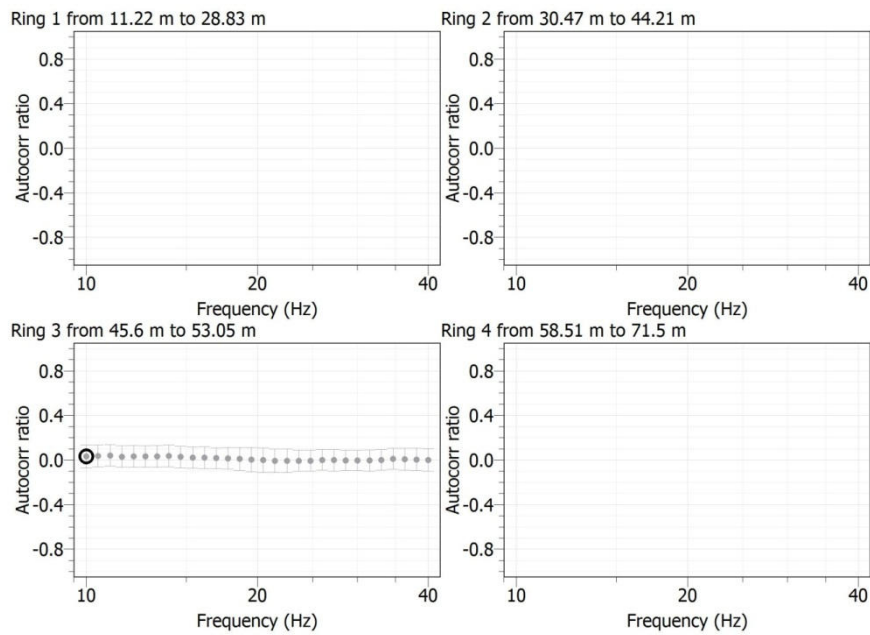


Figure 12: Spatial autocorrelation curves computed for each ring of the 30 m array radius at PYLL site.

3.1.3.3 MASW

The MASW measurements have been done along one profile. The length of the profile is 34.5 m and the distance between two geophones is 1.5 m (see Table 2). The shots were located at both ends (offsets-2 m and 37.5 m) and in the centre (offset 17.25 m) of the profile. For the analysis the minimum and maximum distances between source – receiver are 2 m and 37 m respectively. The duration of the processing time windows is 2 s. The lowest frequency limit to manually pick the dispersion curve is set to 20 Hz and the minimum wavelength limit is 17 m. The results are shown in Figure 13.

For the PYLL site, only four dispersion curves were manually picked:

- Two curves in the vertical direction (profile ZZ-1 offset 36.5 m and profile ZZ-2 offset 36.5 m)
- Two curves in the horizontal direction (profile NS offset 36.5 m and profile SN offset 36.5 m)

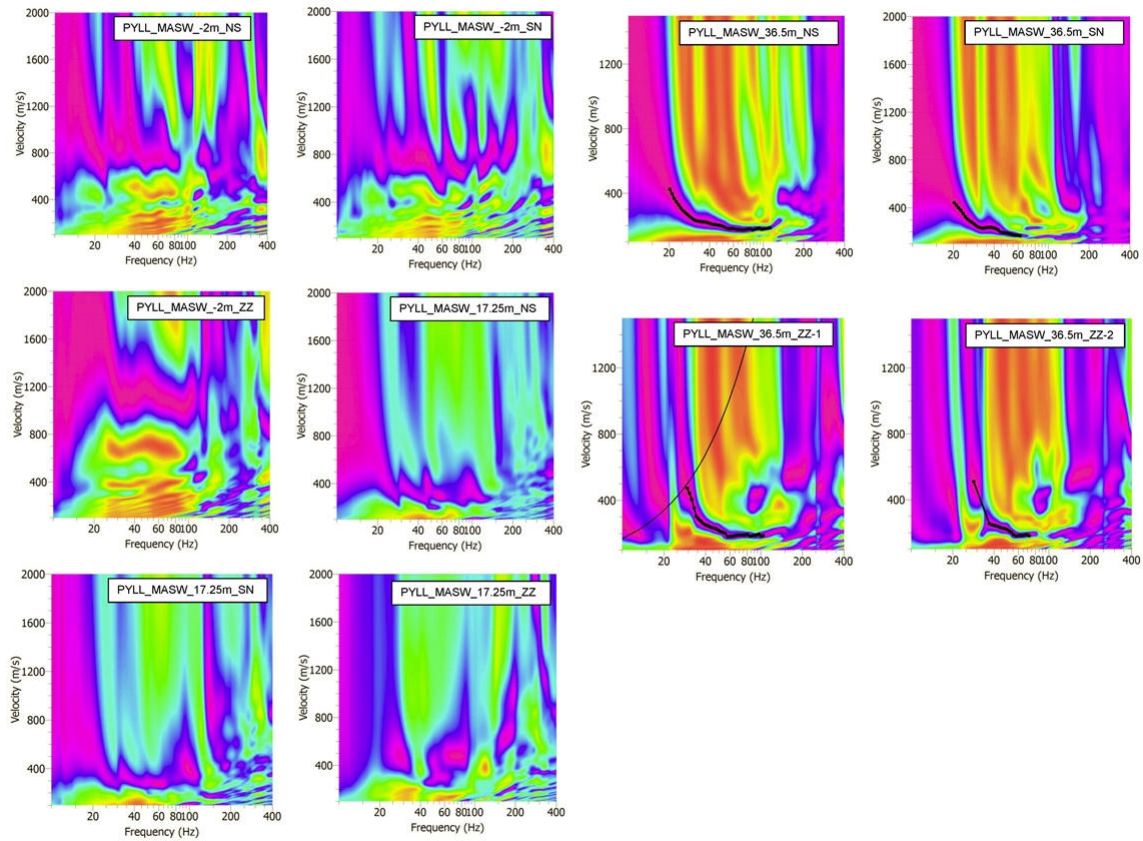


Figure 13: Histogram distributions of phase velocities derived from MASW analysis at PYLL site. The dispersion curves, manually picked, are shown in black dots.

3.1.4 Inversion

Figure 14 shows all dispersion curves derived from AVA and MASW analysis. These curves have been averaged and resampled in order to be inverted (Figure 15). The minimum and maximum wavelengths are 1.5 m and 20 m respectively. The parameter space for the S-wave velocity profile is defined by the 5-layered soil model described in Table 5.

Poisson's ratio ranges between 0.2 and 0.5 for each layer and density is set to 2000 kg/m^3 . The V_p profile is defined by a gradient soil model (5 layers): V_p velocity ranges between 200 and 5000 m/s, bedrock depth is linked to V_s profile.

The results for the "acceptable models" with misfit equal to two sigma are displayed in Figure 16. The investigation depth is very shallow (10 m) because Rayleigh and Love wave dispersion curves are based only on MASW analysis. The V_s profile is thus probably truncated at 10 m deep.

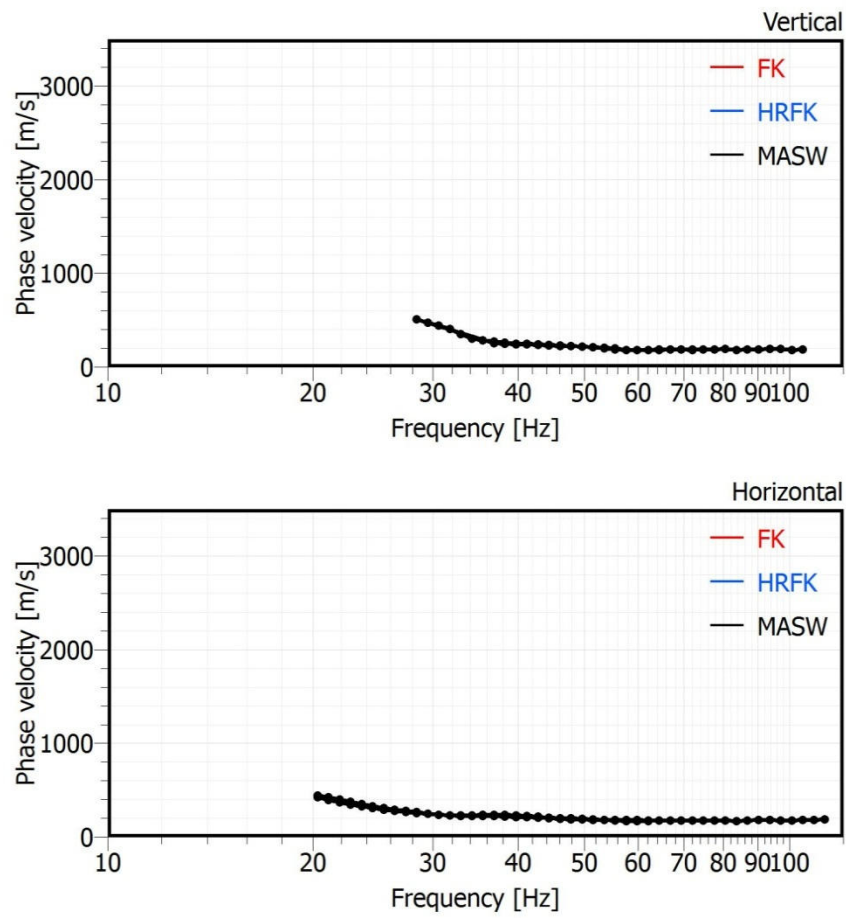


Figure 14: Dispersion curves derived from AVA and MASW analysis at PYLL site.

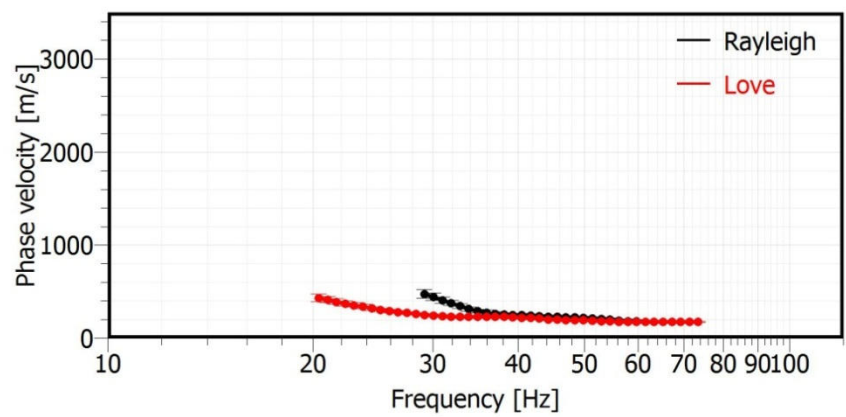


Figure 15: Rayleigh and Love dispersion curves used for the inversion process at PYLL site.

Table 5: Soil parameterization for the 5-layered model of the parameter space at PYLL site.

	Bottom depth (m)		Vs (m/s)	
	Min	Max	Min	Max
Layer 1	0.18	0.73	150	3500
Layer 2	0.73	1.77	150	3500
Layer 3	1.77	3.75	150	3500
Layer 4	3.75	7.52	150	3500
Layer 5	7.52	10	150	3500
Half-space	> 10		150	3500

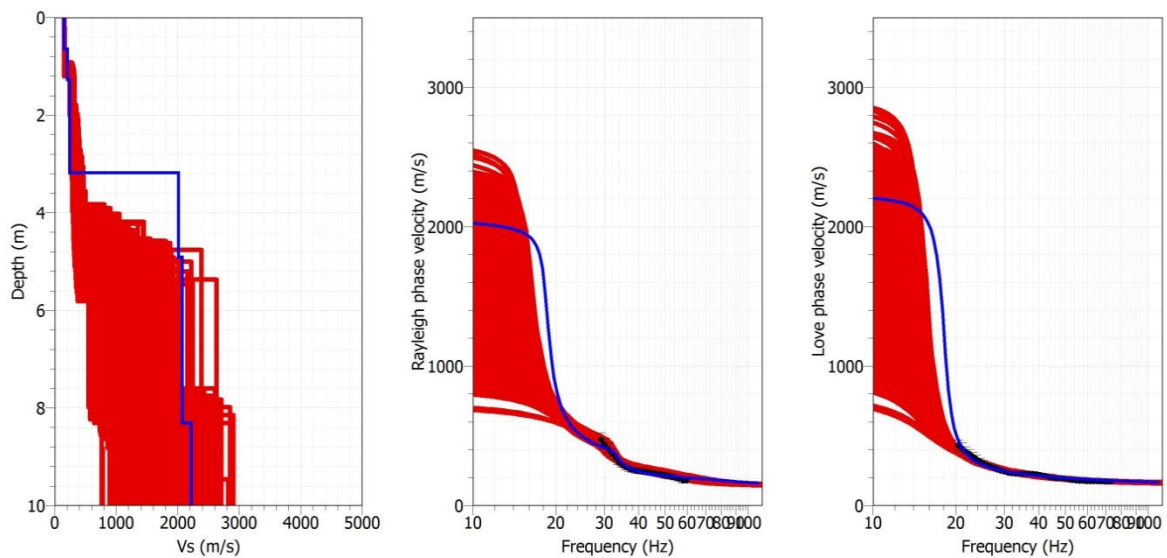


Figure 16: Results for PYLL site: inverted S-wave velocity profile (left) and dispersion curve (right) for the "acceptable models" with misfit equal to two sigma. The Rayleigh and Love waves dispersion curve derived from AVA and MASW analysis are displayed in black dots. Result for the best estimate model (from "classical" inversion) is also shown in blue.

For PYLL site the investigation depth is too shallow (about 10 m) to be able to calculate accurate Vs30. See the section 4.1 for a final estimation of Vs30 and associated uncertainties.

3.2 PYOR

3.2.1 Stations information

3.2.1.1 PYOR choice

PYOR station is one of the French Strong Motion Network (RAP) in Orus (Ariege department). It has been retained in this project because it has recorded the most of seismic events during last years. It is located along main Pyrenean fault segment. But we have no geotechnical or geophysical information about it (just uniform velocity profile extract from Lavergne relations). PYOR station is considered as a rock site with a steep slope under station.

3.2.1.2 Geographic/Geologic information

Orus is located in Ariège department, next to the Nord-Pyrenean Fault. Main characteristic of the site is resumed in Table 6.

Table 6: main characteristics of PYOR station location

Station	City	Department	X Coord (Long)	Y Coord (Lat)	Network	Site	Slope
PYOR	Orus	Ariège (09)	1.507411	42.782801	OMP - RAP	Pyrenean mountain (1065m)	slope

On geological map, PYOR station is set up on massive magmatic rocks (anatexites migmatites) Migmatites, which present high velocities. On the field, bedrock not appears directly at outcrop. Topography is marked around PYOR station with an important breaking slope. Site is quiet but GPS using is difficult at the top of PYOR station because of many trees and forest. PYOR sensor is set up in a little water tower. (Figure 17 to Figure 19).

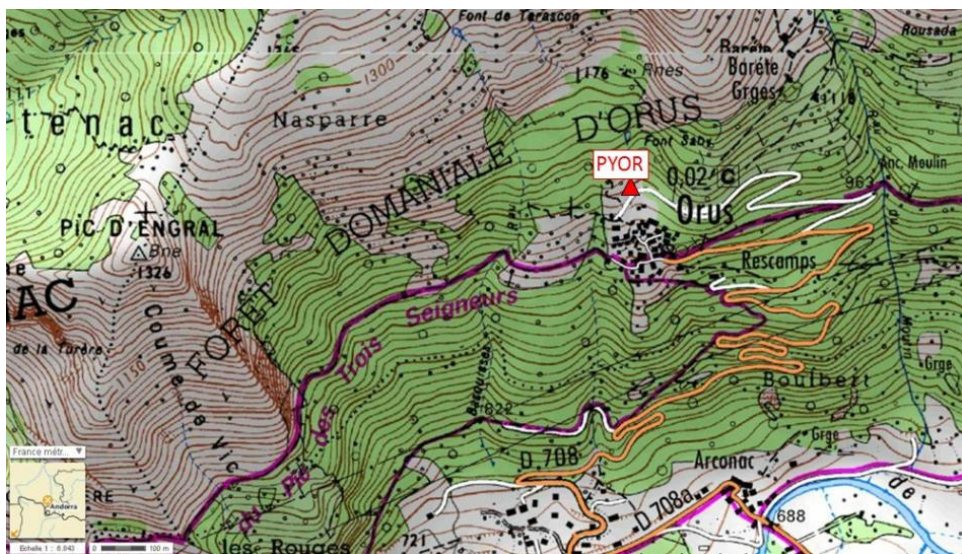


Figure 17 : PYOR location in Orus (IGN Geoportail source)



Figure 18: Picture of PYOR site, during the measurement on the 5th September 2012.

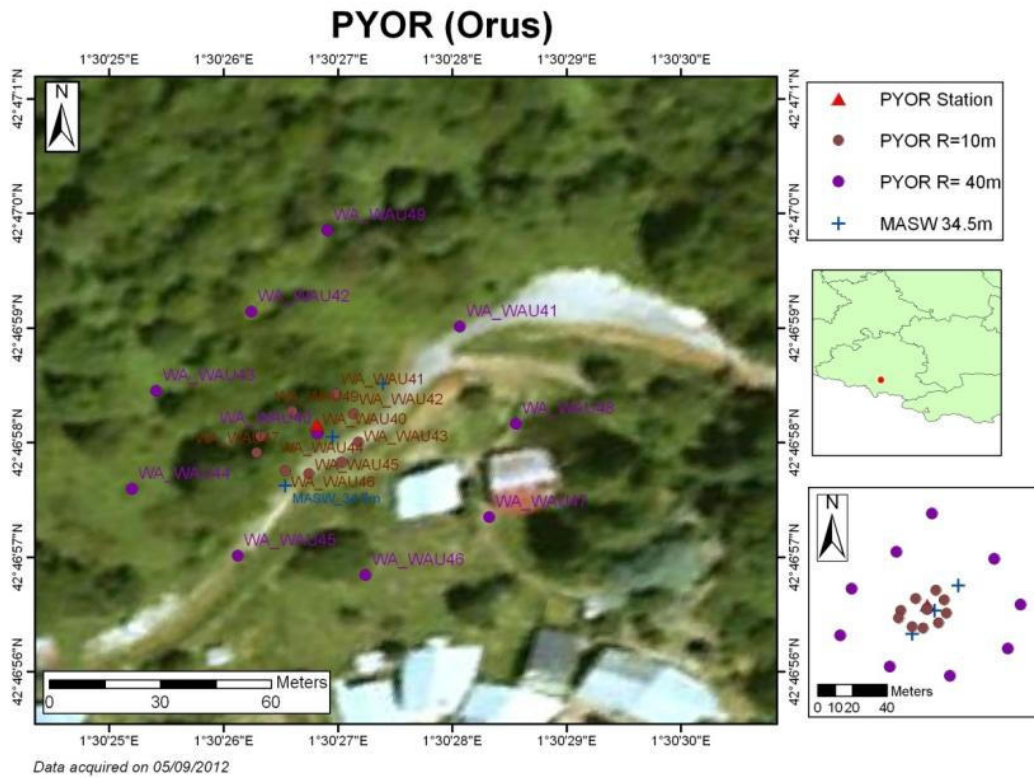


Figure 20: location of the arrays, the MASW shots and PYOR Station.

3.2.3 Processing

3.2.3.1 H/V

The Fourier spectra amplitudes computed on the three component records of ambient vibrations at each PYOR array receiver are shown in Figure 21. The corresponding H/V curves are displayed in Figure 22. Most H/V curves exhibit a low amplitude peak at 4 Hz.

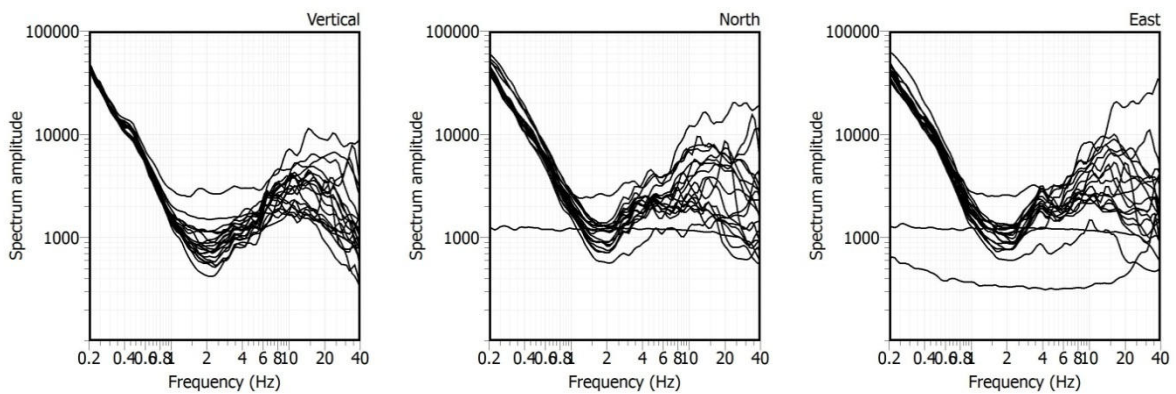


Figure 21: Amplitude of the Fourier spectra computed on 3-C recordings of ambient vibrations at each PYOR array receiver.

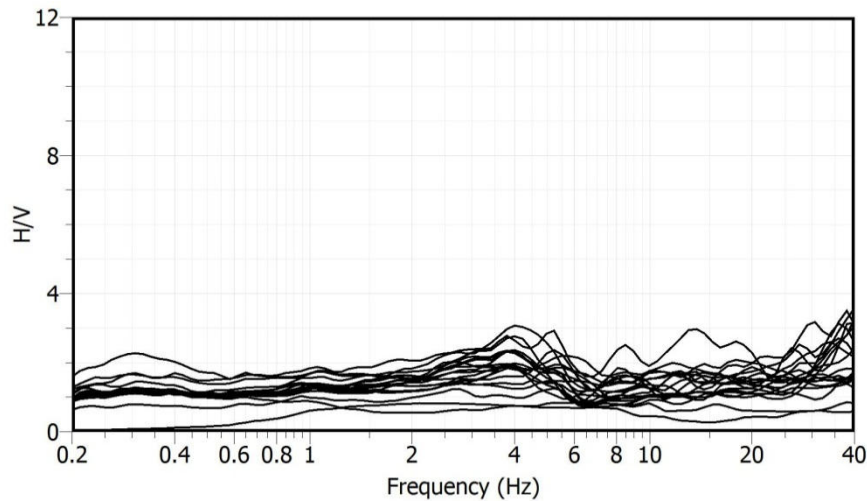


Figure 22: H/V amplitude at each PYOR array receiver

3.2.3.2 AMV

The parameters used for FK and HRFK analysis at PYOR site are described in Table 8.

Table 8: PYOR FK and HRFK analysis parameters: array radius (Array), windows length according to the centre period of the frequency band T (Windows length), minimum and maximum (central) frequencies (Fmin and Fmax), number of frequency sample (Step), anti-aliasing limits kmin and kmax, fk grid resolution (Grid step), maximum search radius for the fk grid (Grid size), minimum velocity and half-bandwidth for the frequency band (Band width).

Array	Windows length	Fmin Hz	Fmax Hz	Step	Kmin rad/m	Kmax rad/m	Grid step rad/m	Grid size rad/m	Vmin m/s	Band width
FK										
10 m	70 T	8	20	5	0.2535	1.6535	0.0634	3.307	150	0.1
40 m	150 T	5.5	9	40	0.0566	0.4389	0.0141	0.878	150	0.1
HRFK										
10 m	150 T	8	30	20	0.2535	1.6535	0.0127	3.307	50	0.03
40 m	200 T	5.5	10	50	0.0566	0.4389	0.0028	0.878	150	0.03

FK

The histogram distributions of phase velocities estimation of Rayleigh waves derived from the ensemble of the wave-propagation estimates obtained for each individual time-frequency cell using the FK method are shown in Figure 23 for PYOR arrays.

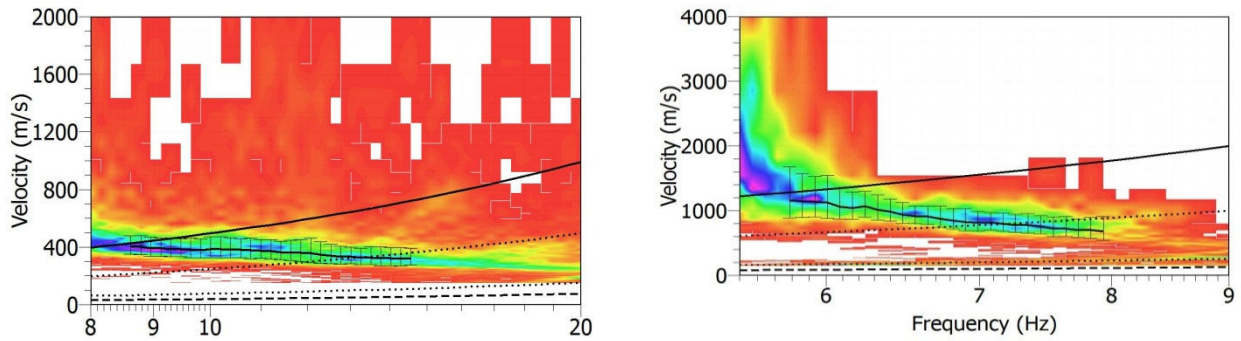


Figure 23: Results for the 10 m (left) and 40 m (right) radius arrays at PYOR site (vertical component): histogram distributions of phase velocities derived from the ensemble of the wave-propagation estimates obtained for each individual time-frequency cell using the FK method (color scale: red and magenta colors indicate min and max values, respectively). The anti-aliasing limits for each array configuration are also shown: thick line ($k_{min}/2$), dotted lines (k_{min} and $k_{max}/2$) and dashed line (k_{max}).

HRFK

The resulting estimation of Rayleigh waves phase velocities are shown in Figure 24 for PYOR arrays.

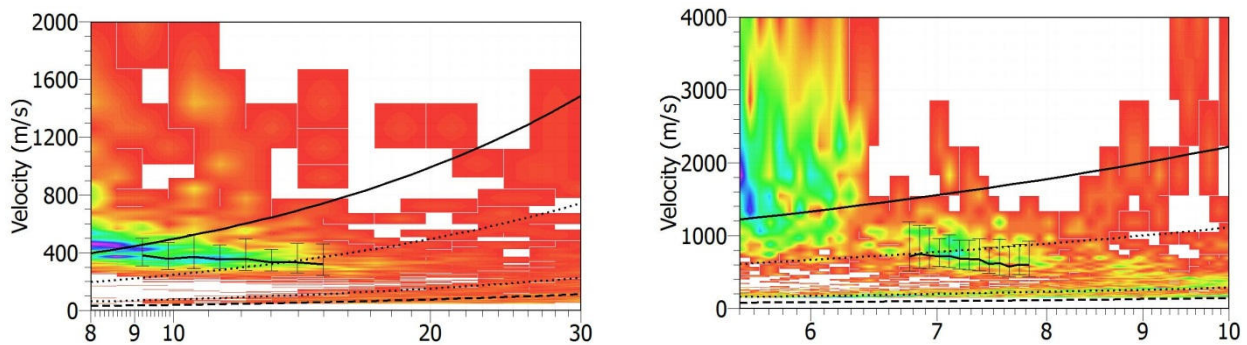


Figure 24: Results for the 10 m (left) and 40 m (right) radius arrays at PYOR site (vertical component): histogram distributions of phase velocities derived from the ensemble of the wave-propagation estimates obtained for each individual time-frequency cell using the HRFK method (color scale: red and magenta colors indicate min and max values, respectively). The anti-aliasing limits for each array configuration are also shown: thick line ($k_{min}/2$), dotted lines (k_{min} and $k_{max}/2$) and dashed line (k_{max}).

SPAC

The parameters used for the SPAC analysis for the 40 m array at PYOR site are described in Table 9. The computed spatial autocorrelation coefficients are displayed for each ring in theFigure 25. These autocorrelation coefficients don't lead to estimate reliable dispersion curve.

Table 9: PYOR SPAC analysis parameters: array radius (Array), windows length according to the centre period of the frequency band T (Windows length), minimum and maximum (central) frequencies (Fmin and Fmax), number of frequency sample (Step), number of rings, minimum and maximum radius of rings (Rmin and Rmax) and number of pairs of sensors in each ring.

Array	Windows length	Fmin Hz	Fmax Hz	Step	Nimber of rings	Rmin m	Rmax m	Number of pairs
40 m	200 T	2	10	30	3	25.86 45.90 70.52	42.29 65.47 98.18	13 14 18

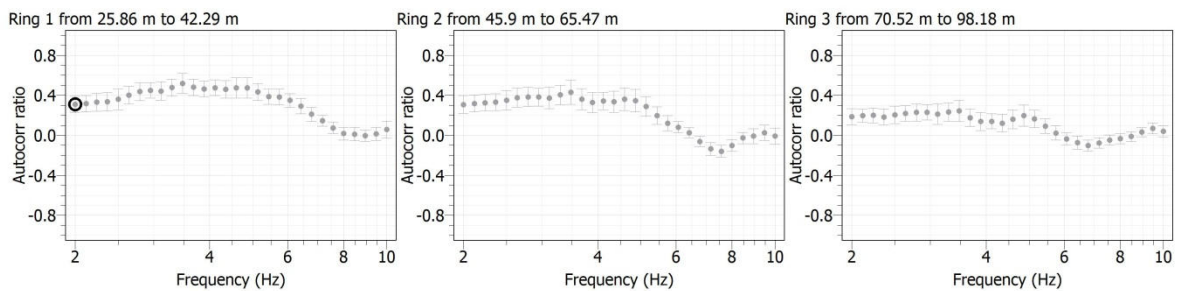


Figure 25: Spatial autocorrelation curves computed for each ring of the 40 m array radius at PYOR site.

MASW

The MASW measurements have been done along one profile. The length of the profile is 34.5 m and the distance between two geophones is 1.5 m (see Table 7). The shots were located at both ends (offsets -2 m and 37.5 m) and in the centre (offset 17.25 m) of the profile. For the analysis the minimum and maximum distances between source – receiver are 2 m and 37 m respectively. The duration of the processing time windows is 1 s. The lowest frequency limit to manually pick the dispersion curve is set to 10 Hz and the minimum wavelength limit is 17 m. The results are shown in Figure 26. For the PYOR site, seven dispersion curves were manually picked.

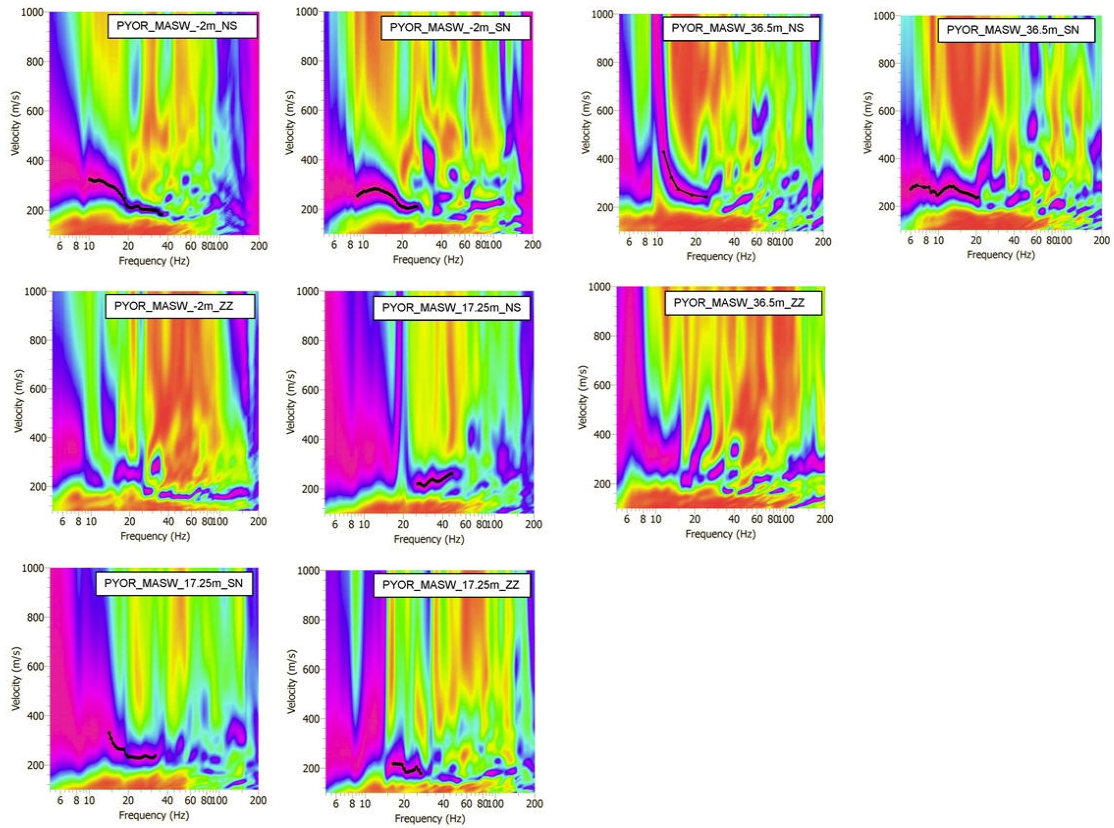


Figure 26: Histogram distributions of phase velocities derived from MASW analysis at PYOR site. The dispersion curves, manually picked, are shown in black dots.

3.2.4 Inversion

Figure 27 shows all dispersion curves derived from AVA and MASW analysis. These curves have been averaged and resampled in order to be inverted (Figure 28). The minimum and maximum wavelengths are 6.5 m and 200 m respectively. The parameter space for the S-wave velocity profile is defined by the 5-layered soil model described in Table 10. Poisson's ratio ranges between 0.2 and 0.5 for each layer and density is set to 2000 kg/m³. The Vp profile is defined by a gradient soil model (5 layers): Vp velocity ranges between 200 and 5000 m/s, bedrock depth is linked to Vs profile.

The results for the "acceptable models" with misfit equal to two sigma are displayed in Figure 29.

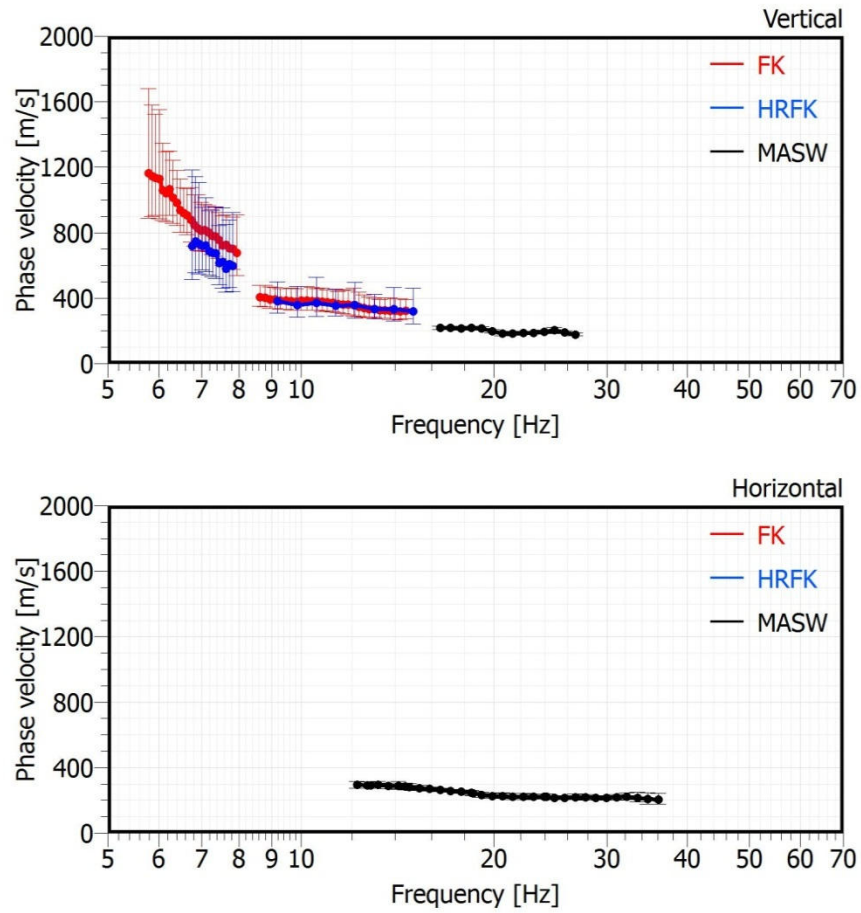


Figure 27: Dispersion curves derived from AVA and MASW analysis at PYOR site.

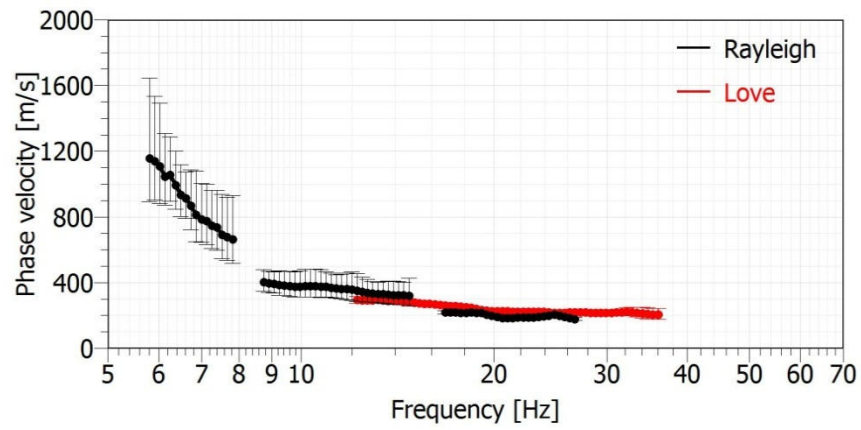


Figure 28: Rayleigh and Love dispersion curves used for the inversion process at PYOR site.

Table 10: Soil parameterization for the 5-layered model of the parameter space at PYOR site.

	Bottom depth (m)		Vs (m/s)	
	Min	Max	Min	Max
Layer 1	0.81	3.63	150	3500
Layer 2	3.63	10.57	150	3500
Layer 3	10.57	27.70	150	3500
Layer 4	27.70	70	150	3500
Layer 5	70	100	150	3500
Half-space	> 100		150	3500

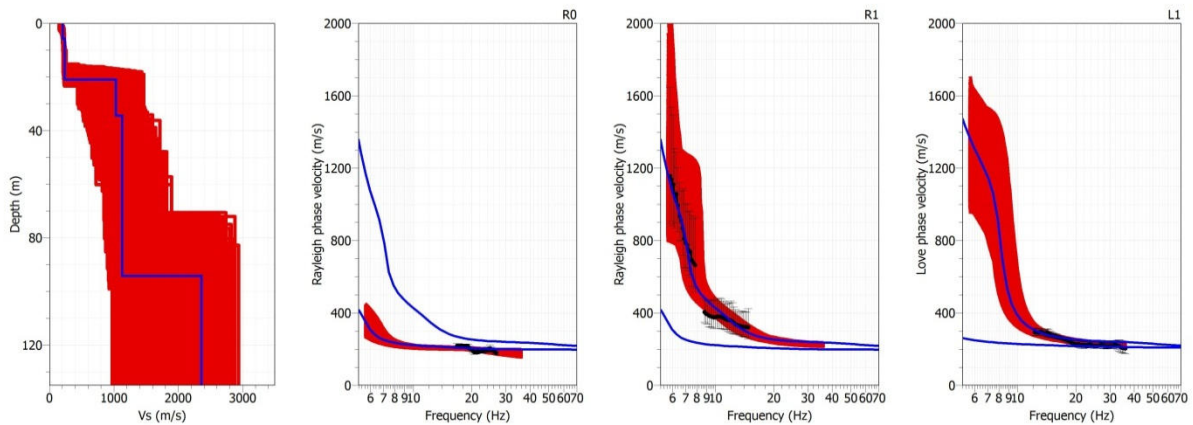


Figure 29: Results for PYOR site: inverted S-wave velocity profile (left) and dispersion curve (right) for the "acceptable models" with misfit equal to two sigma. The Rayleigh and Love waves dispersion curve derived from AVA and MASW analysis are displayed in black dots. Result for the best estimate model (from "classical" inversion) is also shown in blue.

Among the solution shown in Figure 29, one thousand soil profiles having a misfit equal to two sigma were randomly selected in order to compute statistic for Vs30. The associated distribution displayed in Figure 30. See the section 4.1 for a final estimation of Vs30 and associated uncertainties.

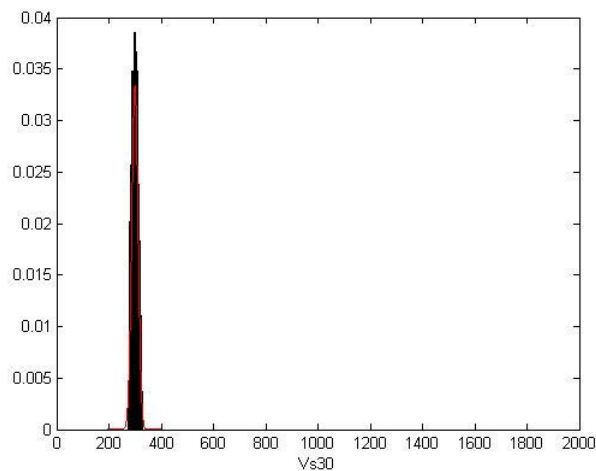


Figure 30: Distribution of Vs30 at PYOR site. The distribution is computed from 1000 soil profiles randomly selected and having a equal to two sigma. The theoretical normal distribution is displayed in red.

3.3 PYLI

3.3.1 Stations information

3.3.1.1 PYLI choice

PYLI station is one of the French Strong Motion Network (RAP) in Saint-Lizier (Ariege department). It has been retained in this project because it is used as a reference site in Generalized Inversion Technic (Drouet, 2010), and it records a lot of events compared other Pyrenean stations. Before our campaign investigation, PYLI station is considered as a rock site with a steep slope under station.

3.3.1.2 Geographic/Geologic information

Saint-Lizier is located in Ariège department, next to the Nord-Pyrenean Fault. Main characteristic of the site is resumed in Table 11.

Table 11: main characteristics of PYLI station location.

Station	City	Department	X Coord (Long)	Y Coord (Lat)	Network	Site	Slope
PYLI	Orus	Ariege (09)	1.135826	43.001478	OMP - BRGM	Edge of Pyrenean chain	Slope in the town

On geological map, PYLI station is set up on alluvion, but we supposed that marlstone or limestone bedrock formation is shallow. All around PYLI station Topography is marked and historical documents show that town has been built on different natural or anthropic carriers or karts. So, soils conditions are not homogeneous at the scale of measurements (Figure 31 to Figure 33).

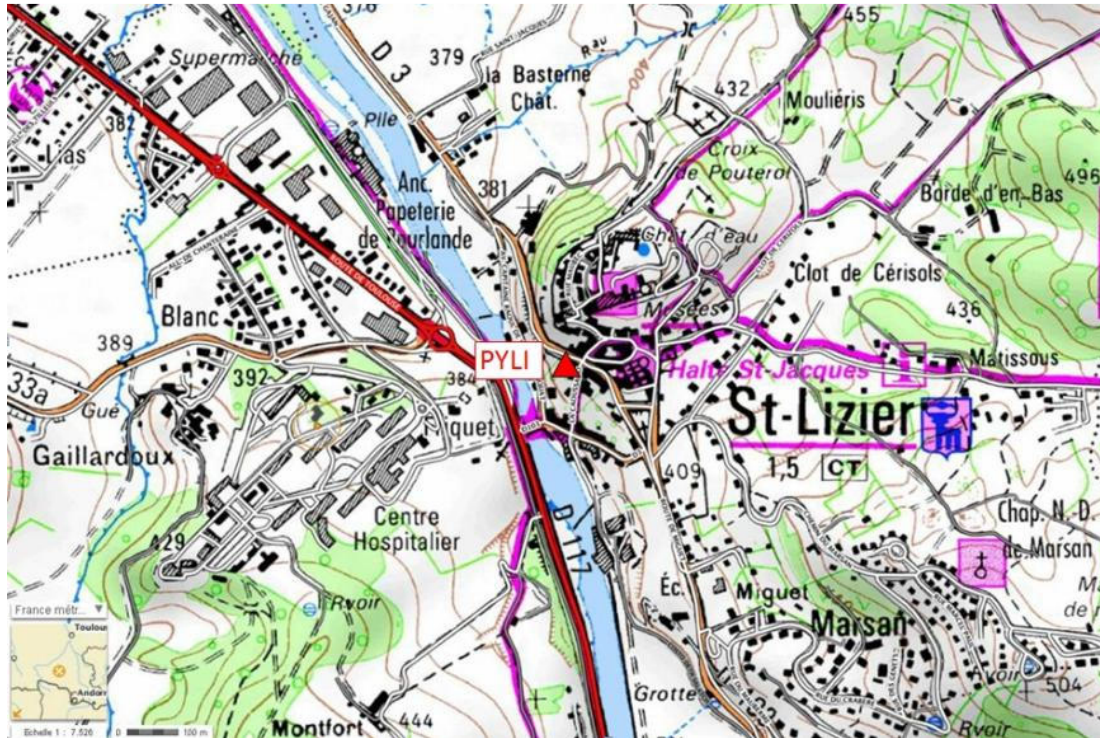


Figure 31 : PYLI location in Saint-Lizier (IGN Geoportail source).



Figure 32: Picture of PYLI site, during the measurement on the 6th September 2012.

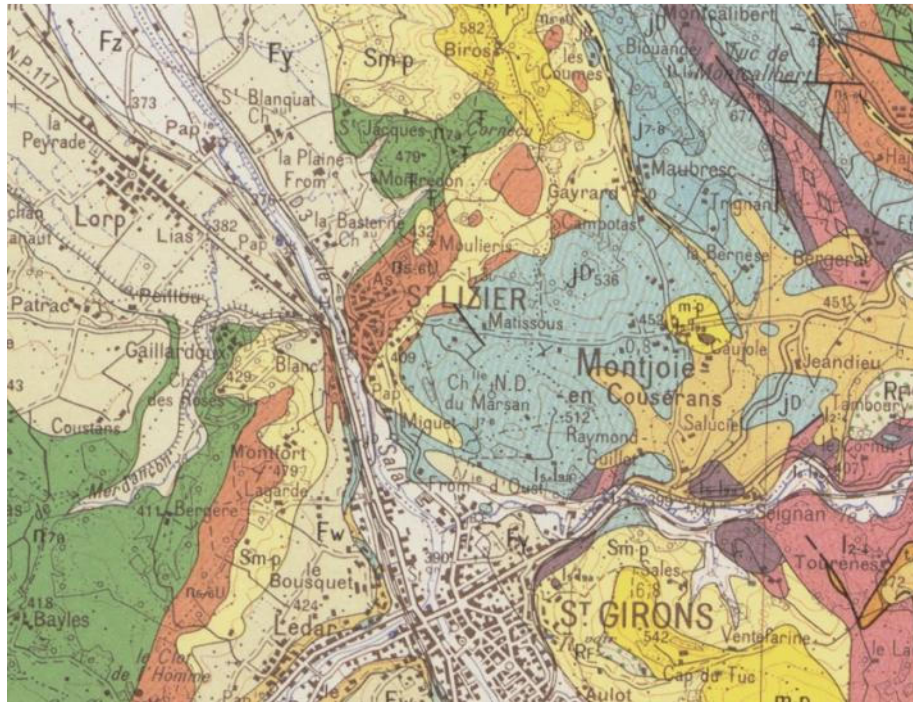


Figure 33: Extract of Saint-Girons geological map (with Saint-Lizier location on delta deposits like grave, sand,... and marlstone or limestone)

3.3.2 Measurements

The acquisition survey was performed on 6th September 2012. For Ambient Vibration Array method, one configuration with 3 circles of 10, 40m and 120m around a central station (near real PYLI station) was performed (10 sensors). For the second method, MASW, two profiles were done (34.5 m and 46 m). Parameters of these 3 arrays and MASW investigation are presented in Table 12. Location of investigation is showed at Figure 34.

Table 12: PYLI recording parameters, 06th September 2012

Measurments	Numbers of Sensors	Beginning (TU)	End (TU)	Noise/ environnement	Topography	Weather conditions
Array R = 3m	10	12:29:00	13:10:00	Mid-urban	flat	good
Array R = 20m	10	10:00:00	11:08:00	urban	Steep slope	good
Array R = 60m	10	14:00:00	16:15:00		Steep slope	
MASW N10°E 46m, Dx = 2m	24 geophones (H and V)	10:30:00	11:30:00	urban	Steep slope	good
MASW N120°E34.5m, Dx =1.5m	24 vertical geophones(V)	15:24:00	16:15:00	urban	flat	good

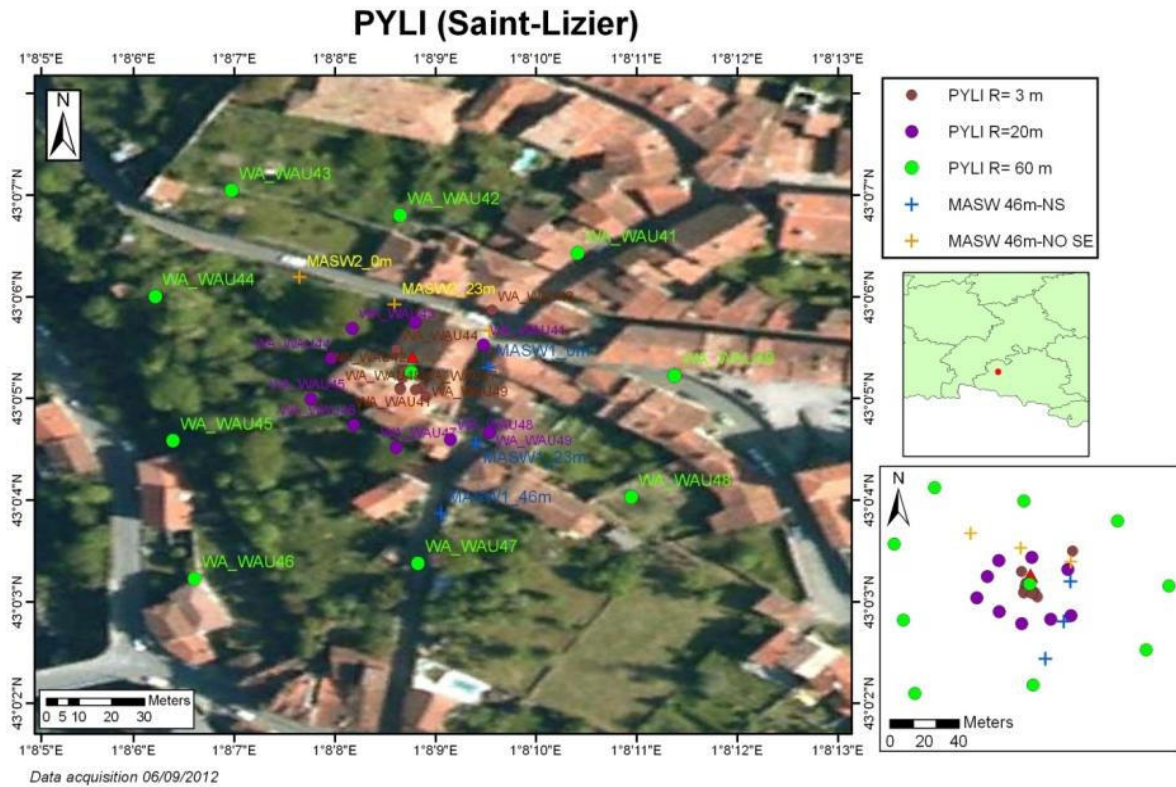


Figure 34: location of the arrays, the MASW shots and PYLI Station

3.3.3 Processing

3.3.3.1 H/V

The Fourier spectra amplitudes computed on the three component records of ambient vibrations at each PYLI array receiver are shown in Figure 35. The corresponding H/V curves are displayed in Figure 36. Most H/V curves are flat below 20 Hz. Only three curves exhibit a clear H/V peak between 10 and 16 Hz.

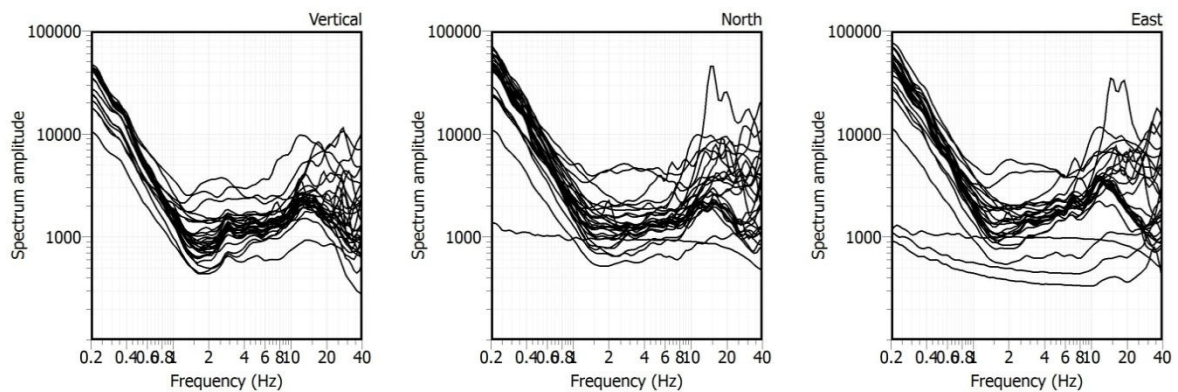


Figure 35: Amplitude of the Fourier spectra computed on 3-C recordings of ambient vibrations at each PYLI array receiver

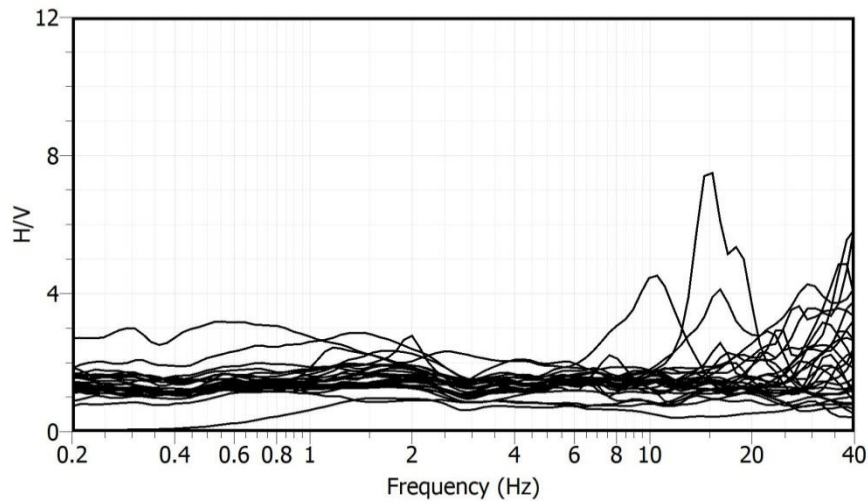


Figure 36: H/V amplitude at each PYLI array receiver

3.3.3.2 AMV

The parameters used for FK and HRFK analysis at PYLI site are described in Table 13.

Table 13: PYLI FK and HRFK analysis parameters: array radius (Array), windows length according to the centre period of the frequency band T (Windows length), minimum and maximum (central) frequencies (Fmin and Fmax), number of frequency sample (Step), anti-aliasing limits kmin and kmax, fk grid resolution (Grid step), maximum search radius for the fk grid (Grid size), minimum velocity and half-bandwidth for the frequency band (Band width).

Array	Windows length	Fmin Hz	Fmax Hz	Step	Kmin rad/m	Kmax rad/m	Grid step rad/m	Grid size rad/m	Vmin m/s	Band width
FK										
3 m	70 T	20	40	20	0.5831	2.2100	0.1458	4.4420	150	0.1
20 m	70 T	15	35	20	0.1203	0.6530	0.0301	1.3060	150	0.1
60 m	150 T	5	20	30	0.3999	0.0917	0.0104	0.4060	150	0.1
HRFK										
3 m	150 T	20	40	50	0.5831	2.2100	0.0292	4.4420	50	0.03
20 m	150 T	20	30	30	0.1203	0.6530	0.0060	1.3060	150	0.03
60 m	200 T	8	15	50	0.3999	0.0917	0.0210	0.4060	150	0.02

FK

The histogram distributions of phase velocities estimation of Rayleigh waves derived from the ensemble of the wave-propagation estimates obtained for each individual time-frequency cell using the FK method are shown in Figure 37 for PYLI arrays.

Rayleigh dispersion curves were determined for the 20 m and 60 m radius arrays. It was not possible to derived dispersion curve from the 3 m radius array.

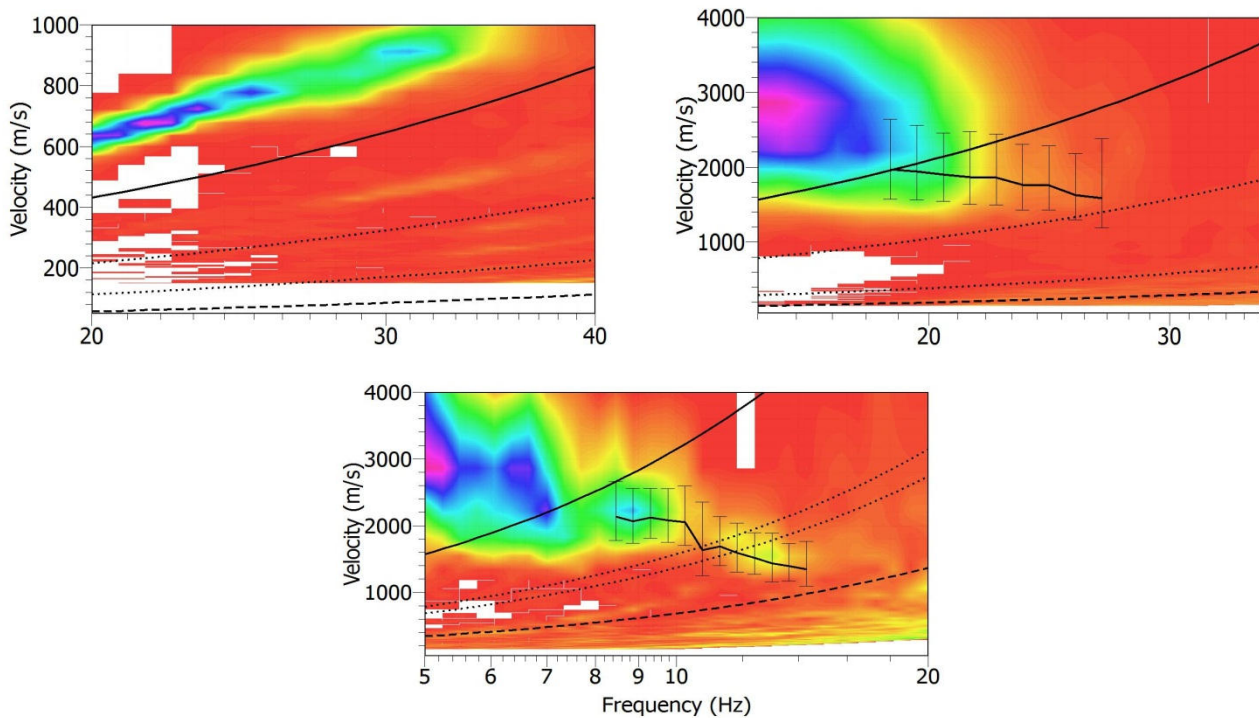


Figure 37: Results for the 3 m (top-left), 20 m (top-right) and 60 m (bottom) radius arrays at PYLI site (vertical component): histogram distributions of phase velocities derived from the ensemble of the wave-propagation estimates obtained for each individual time-frequency cell using the FK method (color scale: red and magenta colors indicate min and max values, respectively). The anti-aliasing limits for each array configuration are also shown: thick line ($k_{min}/2$), dotted lines (k_{min} and $k_{max}/2$) and dashed line (k_{max}).

HRFK

The resulting estimation of Rayleigh waves phase velocities are shown in Figure 38 for PYLI arrays.

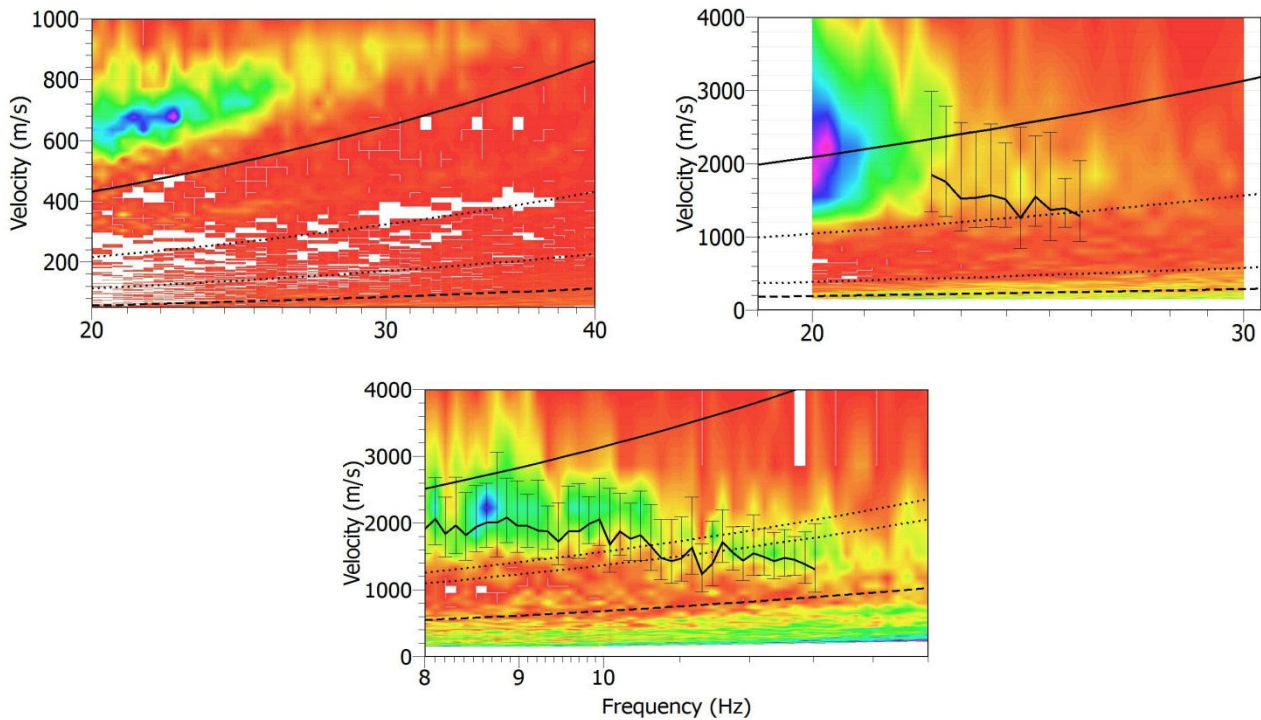


Figure 38: Results for the 3 m (top-left), 20 m (top-right) and 60 m (bottom) radius arrays at PYLI site (vertical component): histogram distributions of phase velocities derived from the ensemble of the wave-propagation estimates obtained for each individual time-frequency cell using the HRFK method (color scale: red and magenta colors indicate min and max values, respectively). The anti-aliasing limits for each array configuration are also shown: thick line ($k_{min}/2$), dotted lines (k_{min} and $k_{max}/2$) and dashed line (k_{max}).

Rayleigh dispersion curves were determined for the 20 m and 60 m radius arrays. It was not possible to derived dispersion curve from the 3 m radius array.

SPAC

The parameters used for the SPAC analysis for the 60 m array at PYLI site are described in Table 14. The computed spatial autocorrelation coefficients are displayed for each ring in the Figure 39. These autocorrelation coefficients don't lead to estimate reliable dispersion curve.

Table 14: PYLISPAC analysis parameters: array radius (Array), windows length according to the centre period of the frequency band T (Windows length), minimum and maximum (central) frequencies (Fmin and Fmax), number of frequency sample (Step), number of rings, minimum and maximum radius of rings (Rmin and Rmax) and number of pairs of sensors in each ring.

Array	Windows length	Fmin Hz	Fmax Hz	Step	Nimber of rings	Rmin m	Rmax m	Number of pairs
60 m	100 T	5	40	50	2	38.64 100.91	92.51 150.55	20 16

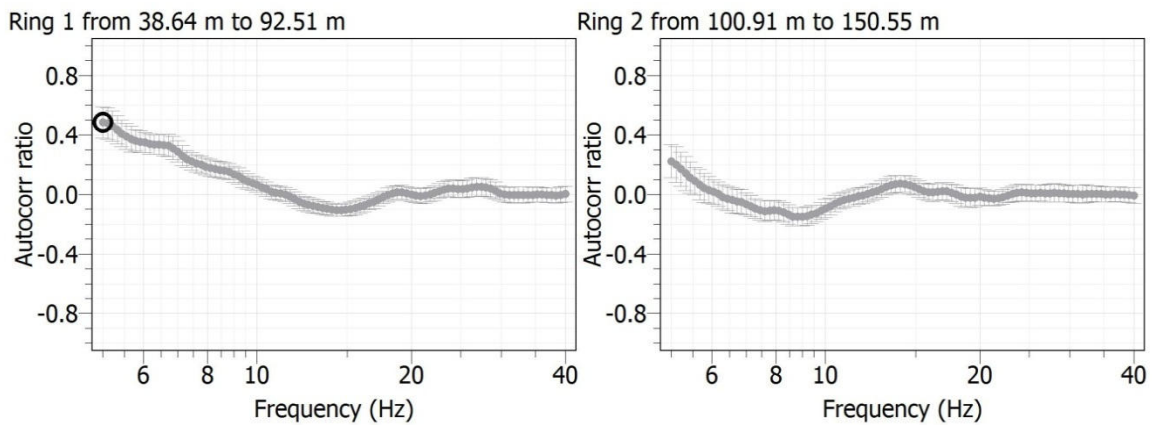


Figure 39: Spatial autocorrelation curves computed for each ring of the 30 m array radius at PYLI site.

MASW

The MASW measurements have been done along two profiles. The lengths of the profiles are 46 m (profile 1) and 34.5 m (profile 2) (see Table 12). For the profile 1, the distance between two geophones is 2 m. The shots were located at both ends (offsets -2 m and 48 m) and in the centre (offset 23 m) of the profile. For the analysis the minimum and maximum distances between source – receiver are 2 m and 48 m respectively. For the profile 2, the length of the profile is 34.5 m and the distance between two geophones is 1.5 m. The shots were located at both ends (offsets -2 m and 37.5 m) and in the centre (offset 17.25 m) of the profile. For the analysis the minimum and maximum distances between source – receiver are 2 m and 37 m respectively

The duration of the processing time windows is 1 s. The lowest frequency limit to manually pick the dispersion curve is set to 30 Hz and the minimum wavelength limit is 23 m. The results are shown in Figure 40. For the PYLI site, only four dispersion curves were manually picked.

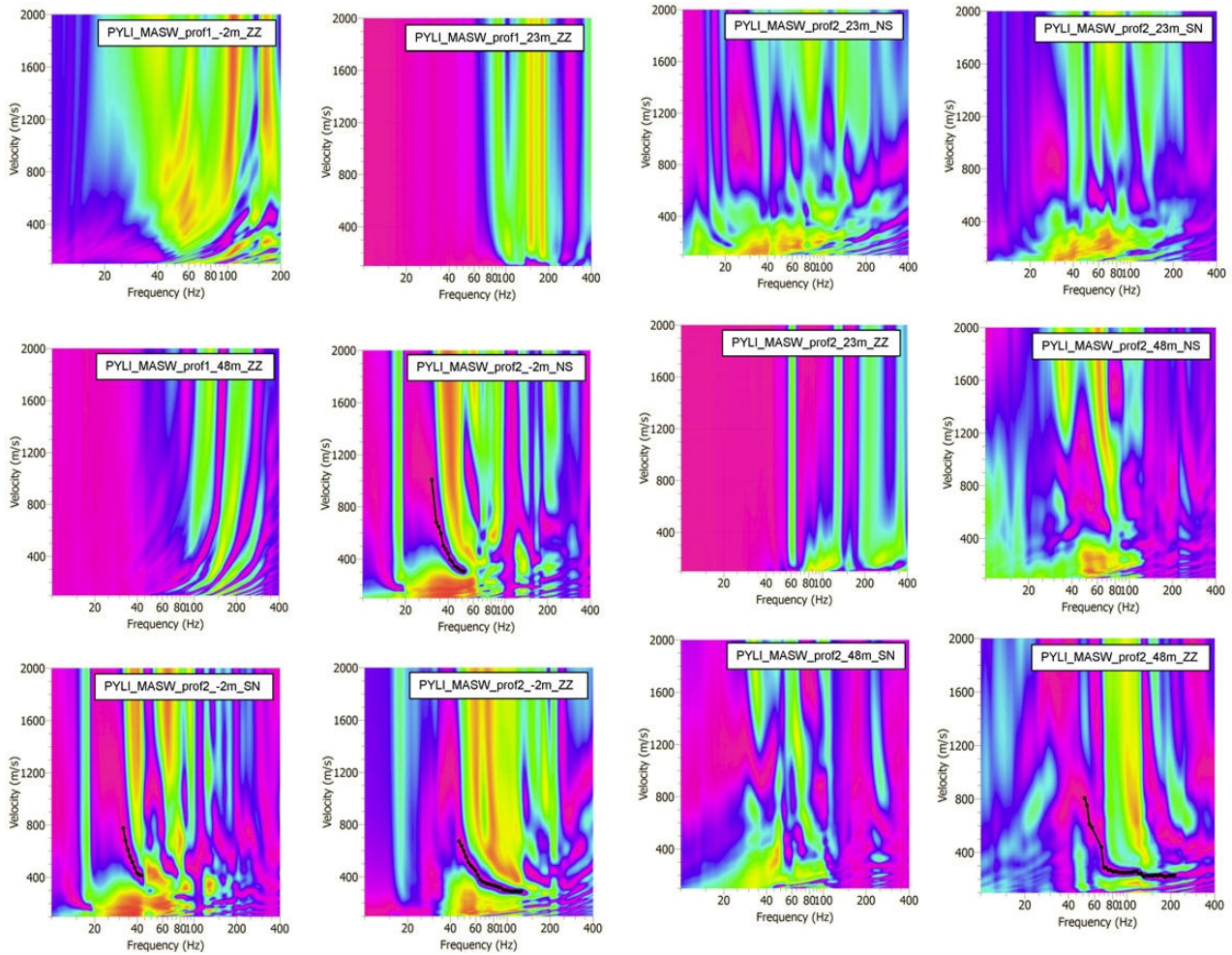


Figure 40: Histogram distributions of phase velocities derived from MASW analysis at PYLI site. The dispersion curves, manually picked, are shown in black dots.

3.3.4 Inversion

Figure 41 shows all dispersion curves derived from AVA and MASW analysis. These curves have been averaged and resampled in order to be inverted (Figure 42). The minimum and maximum wavelengths are 1 m and 252 m respectively. The parameter space for the S-wave velocity profile is defined by the 5-layered soil model described in Table 15. Poisson's ratio ranges between 0.2 and 0.5 for each layer and density is set to 2000 kg/m³. The Vp profile is defined by a gradient soil model (5 layers): Vp velocity ranges between 200 and 5000 m/s, bedrock depth is linked to Vs profile. The results for the "acceptable models" with misfit equal to one sigma are displayed in Figure 43.

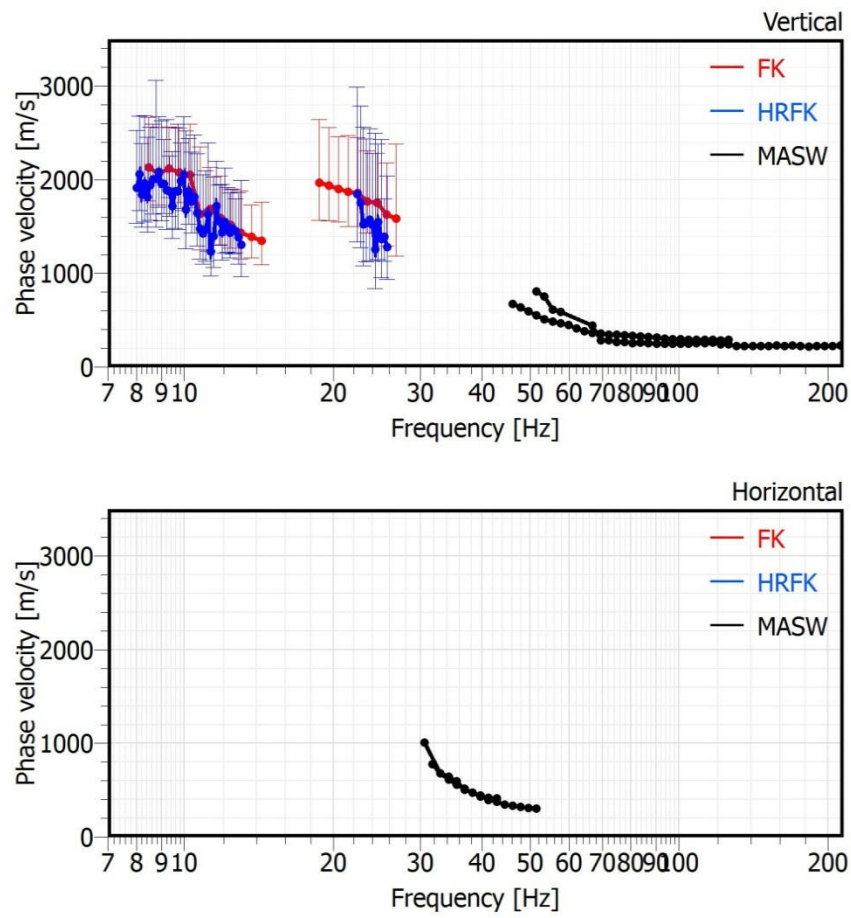


Figure 41: Dispersion curves derived from AVA and MASW analysis at PYLI site.

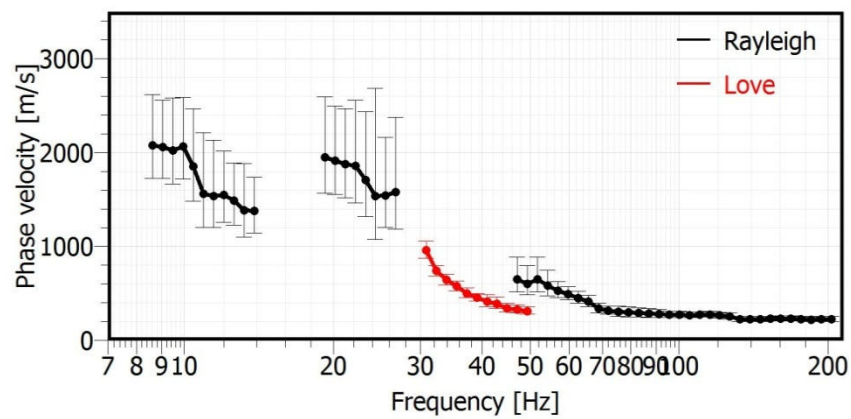


Figure 42: Rayleigh and Love dispersion curves used for the inversion process at PYLI site.

Table 15: Soil parameterization for the 5-layered model of the parameter space at PYLI site.

	Bottom depth (m)		Vs (m/s)	
	Min	Max	Min	Max
Layer 1	0.12	0.80	150	3500
Layer 2	0.80	3.83	150	3500
Layer 3	3.83	17.29	150	3500
Layer 4	17.29	77.14	150	5000
Layer 5	77.14	126.00	150	5000
Half-space	>126		150	5000

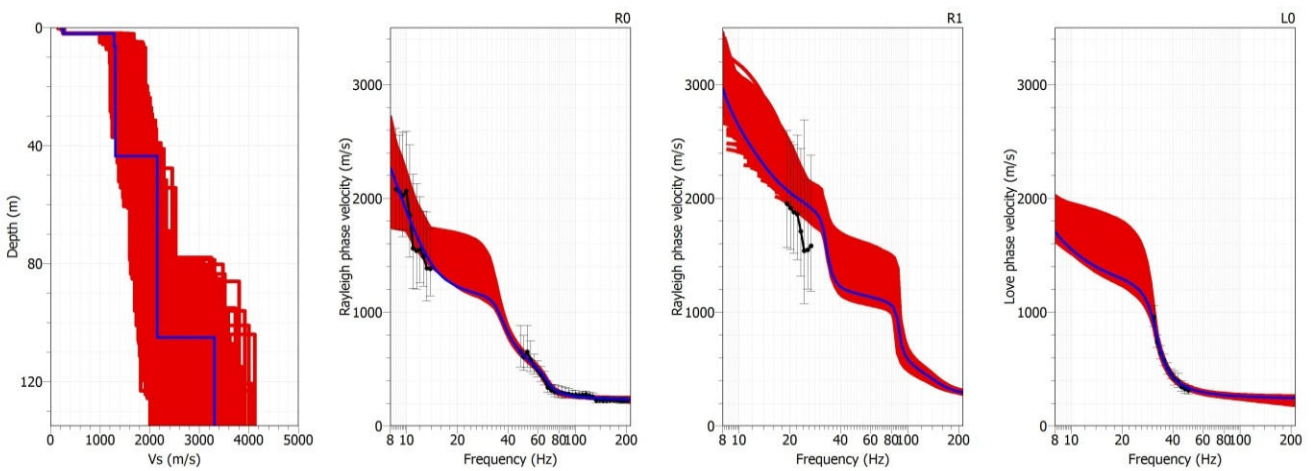


Figure 43: Results for PYLI site: inverted S-wave velocity profile (left) and dispersion curve (right) for the "acceptable models" with misfit equal to one sigma. The Rayleigh and Love waves dispersion curve derived from AVA and MASW analysis are displayed in black dots. Result for the best estimate model (from "classical" inversion) is also shown in blue.

Among the solution shown in Figure 43, one thousand soil profiles having a misfit equal to one sigma were randomly selected in order to compute statistic for Vs30. The associated distribution is displayed in Figure 44. See the section 4.1 for a final estimation of Vs30 and associated uncertainties.

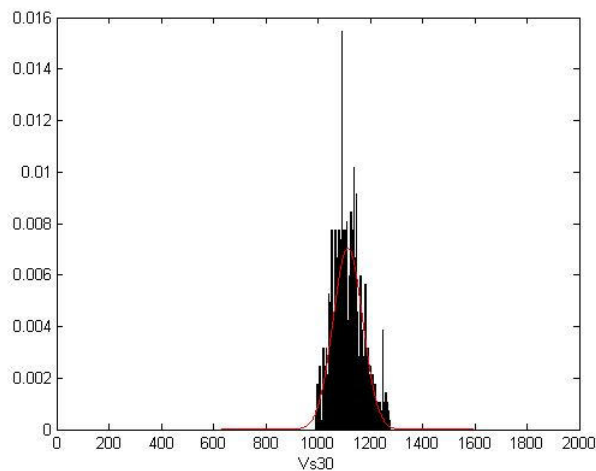


Figure 44: Distribution of Vs30 at PYLI site. The distribution is computed from 1000 soil profiles randomly selected and having a misfit equal to one sigma. The theoretical normal distribution is displayed in red.

3.4 PYAS

3.4.1 Stations information

3.4.1.1 PYAS choice

PYAS station is one of the French Strong Motion Network (RAP) in Aspet (Haute-Garonne department). PYAS station is from part reference site used by Drouet (Drouet, 2010) in Generalized Inversion Technic. As PYLI, PYLI or PYLL, it records a lot of events compared with other Pyrenean stations.

3.4.1.2 Geographic/Geologic information

Aspet is located in Haute-Garonne department, in the north part of Pyrenean chain. Main characteristic of the site is resumed in Table 16.

Table 16: PYAS characteristics.

Station	City	Department	X Coord (Long)	Y Coord (Lat)	Network	Site	Slope
PYAS	Aspet	Haute-Garonne(31)	0.797255	43.011958	BRGM	Edge of Pyrenean chain	Flat

As Aspet geological map is not available, we have not precise information about formations. On the field, PYAS station is set up quaternary origin sediments deposits. We don't have precise idea of the depth. On the west part of site, limestone cliff is presents, so we supposed, bedrock limit is shallow (Figure 45 to Figure 46).



Figure 45 : PYAS location in Aspet (IGN Geoportail source)



Figure 46: Picture of PYAS site, during the measurement on the 7th September 2012.

3.4.2 Measurements

The measurement survey was performed on 07th September 2012. For Ambient Vibration Array method, one configuration with 3 circles of 20, 60m and 100m around a central station (near real PYAS station) was performed (10, then 8 sensors because of technical problems). For the second method, MASW, two profiles were recorded (34.5 m and 46 m). Parameters of these 3 arrays and MASW investigation are presented in Table 17. Location of investigation is showed at Figure 47.

Table 17: PYAS recording parameters, 07th September 2012

Measurments	Numbers of Sensors	Beginning (TU)	End (TU)	Noise/ environnement	Topography	Weather conditions
Array R = 5m	10	10:37:00	11:20:00	Mid-urban	flat	good
Array R = 30m	8	13:58:00	14:58:00	Mid-urban	flat	good
Array R = 50m	8	15:44:00	16:45:00	Mid-urban	flat, with a river at the middle of the array	
MASW N10°E 46m, Dx = 2m	24 vertical geophones V)	11:20:00	11:30:00	Mid-urban	flat	good
MASW N120°E 24m, Dx =1m	24 vertical geophones(V)	11:30:00	12:30:00	Mid-urban	flat	good

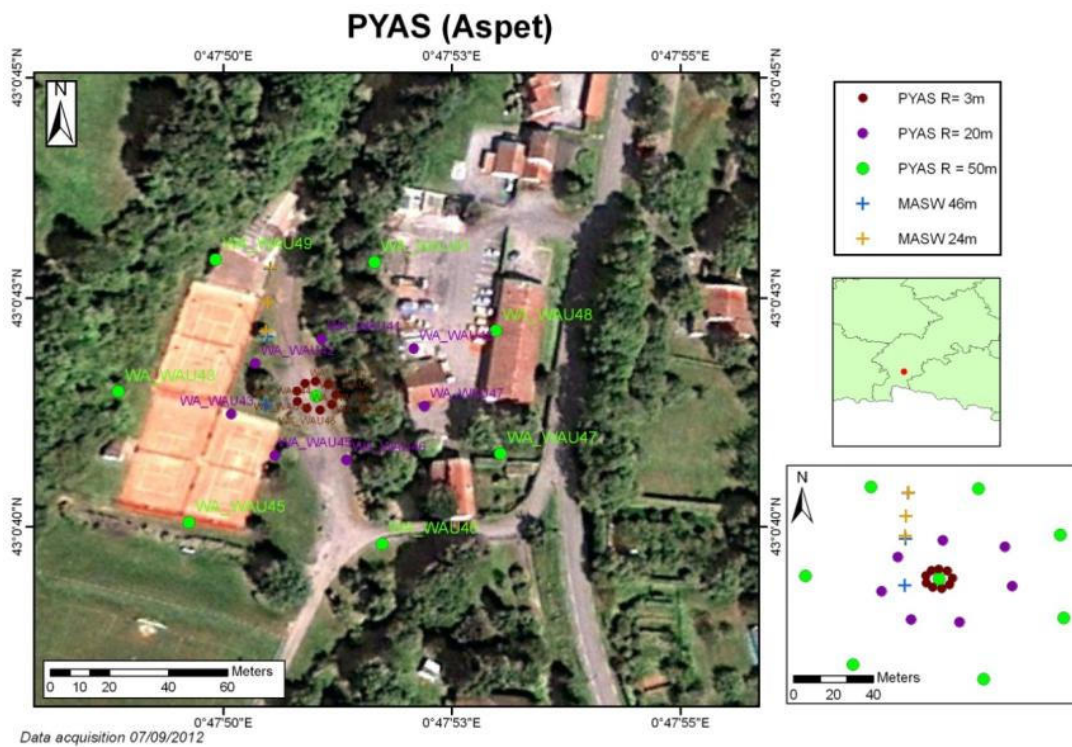


Figure 47: location of the arrays, the MASW shots and PYAS Station.

3.4.3 Processing

3.4.3.1 H/V

The Fourier spectra amplitudes computed on the three component records of ambient vibrations at each PYAS array receiver are shown in Figure 48. The corresponding H/V curves are displayed in Figure 49. Most H/V curves exhibit a clear H/V peak between 8 and 20 Hz.

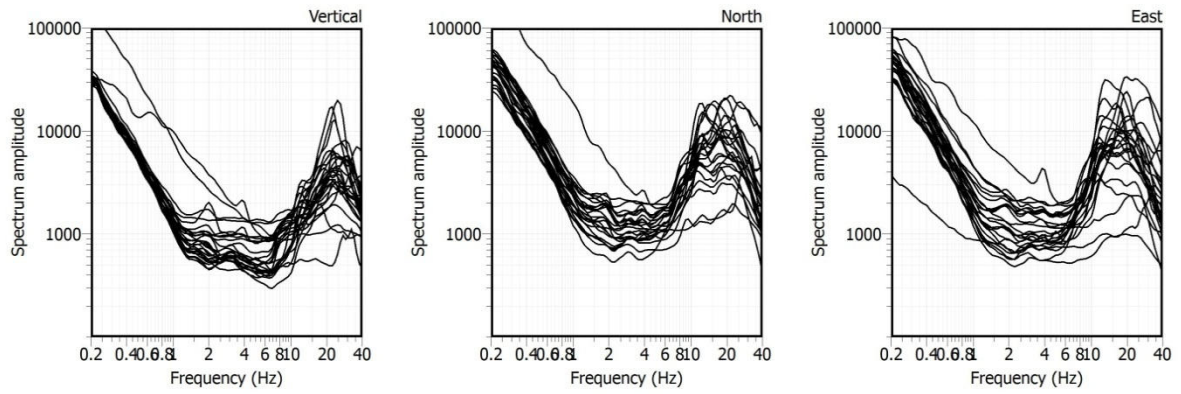


Figure 48: Amplitude of the Fourier spectra computed on 3-C recordings of ambient vibrations at each PYAS array receiver.

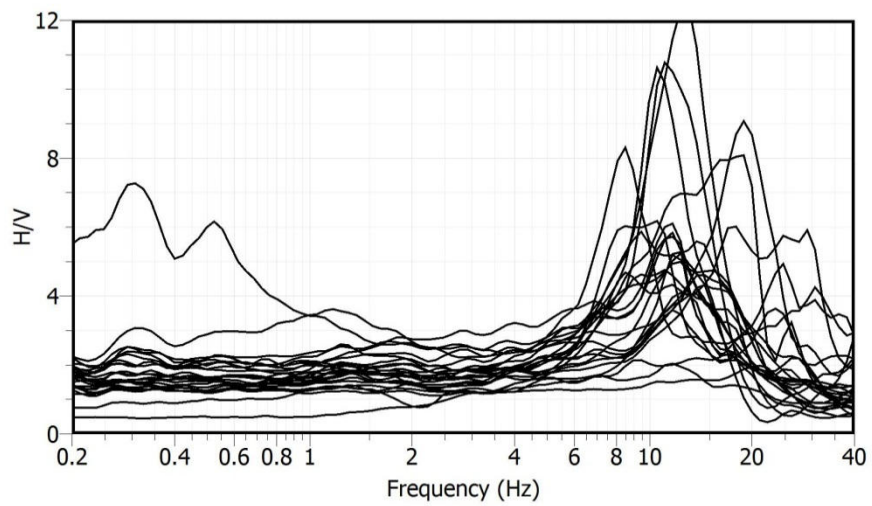


Figure 49: H/V amplitude at each PYAS array receiver.

3.4.3.2 AMV

The parameters used for FK and HRFK analysis at PYAS site are described in Table 18.

Table 18: PYAS FK and HFRK analysis parameters: array radius (Array), windows length according to the centre period of the frequency band T (Windows length), minimum and maximum (central) frequencies (Fmin and Fmax), number of frequency sample (Step), anti-aliasing limits kmin and kmax, fk grid resolution (Grid step), maximum search radius for the fk grid (Grid size), minimum velocity and half-bandwidth for the frequency band (Band width).

Array	Windows length	Fmin Hz	Fmax Hz	Step	Kmin rad/m	Kmax rad/m	Grid step rad/m	Grid size rad/m	Vmin m/s	Band width
FK										
5 m	70 T	20	40	50	0.4821	3.5203	0.1205	7.041	150	0.1
30 m	150 T	15	25	50	0.1148	0.6070	0.0287	1.214	150	0.1
50 m	200 T	10	20	40	0.0470	0.1145	0.0118	0.2290	150	0.1
HRFK										
5 m	100 T	22	40	30	0.4821	3.5203	0.0241	7.041	50	0.05
30 m	100 T	17	20	50	0.1148	0.6070	0.0057	1.214	150	0.03
50 m	200 T	7	20	40	0.0470	0.1145	0.0024	0.2290	150	0.02

FK

The histogram distributions of phase velocities estimation of Rayleigh waves derived from the ensemble of the wave-propagation estimates obtained for each individual time-frequency cell using the FK method are shown in Figure 50 for PYAS arrays.

Rayleigh dispersion curves were determined for the 5 m and 50 m radius arrays. It was not possible to derived dispersion curve from the 30 m radius array.

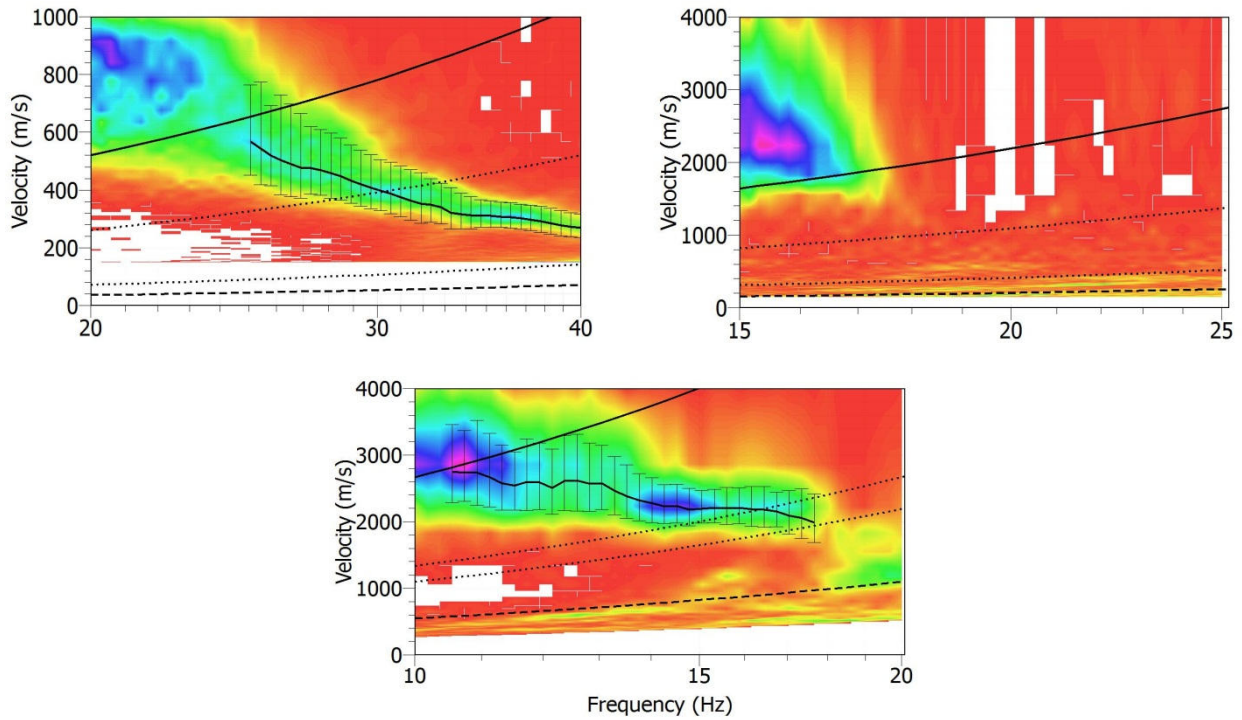


Figure 50: Results for the 5 m (top-left), 30 m (top-right) and 50 m (bottom) radius arrays at PYAS site (vertical component): histogram distributions of phase velocities derived from the ensemble of the wave-propagation estimates obtained for each individual time-frequency cell using the FK method (color scale: red and magenta colors indicate min and max values, respectively). The anti-aliasing limits for each array configuration are also shown: thick line ($k_{min}/2$), dotted lines (k_{min} and $k_{max}/2$) and dashed line (k_{max}).

HRFK

The resulting estimation of Rayleigh waves phase velocities are shown in Figure 51 for PYAS arrays.

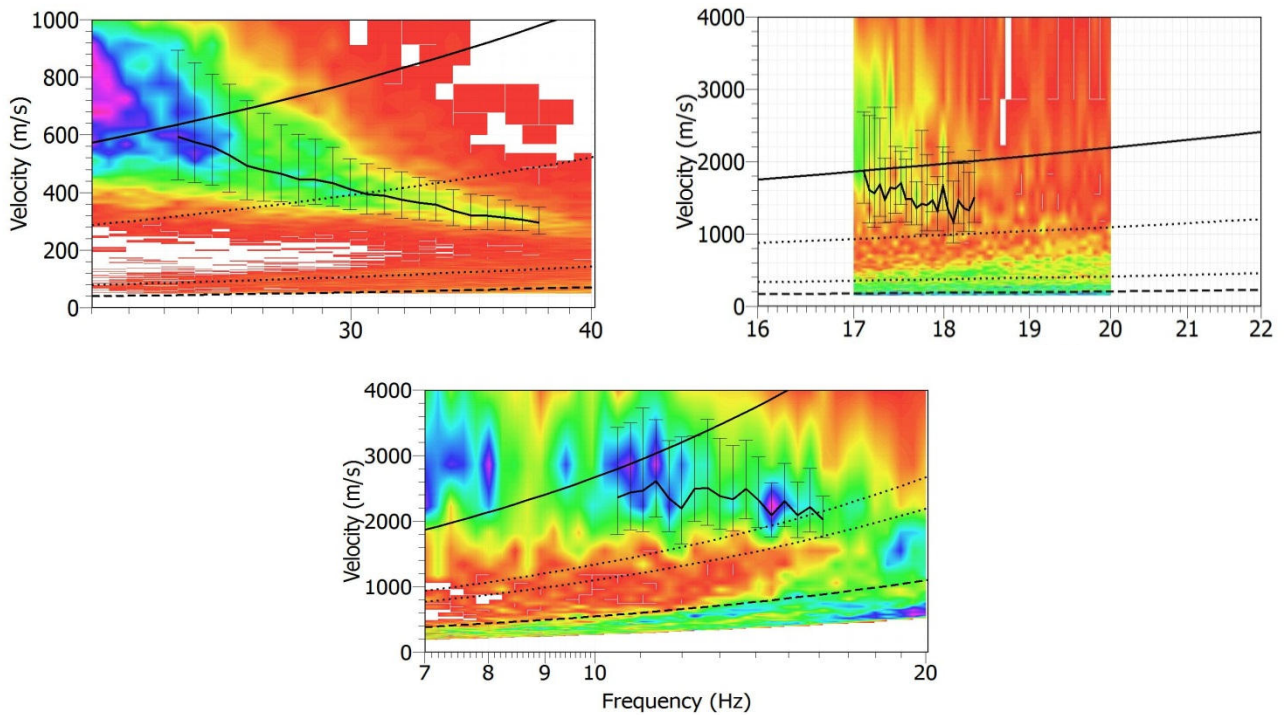


Figure 51: Results for the 5 m (top-left), 30 m (top-right) and 50 m (bottom) radius arrays at PYAS site (vertical component): histogram distributions of phase velocities derived from the ensemble of the wave-propagation estimates obtained for each individual time-frequency cell using the HRFK method (color scale: red and magenta colors indicate min and max values, respectively). The anti-aliasing limits for each array configuration are also shown: thick line ($k_{min}/2$), dotted lines (k_{min} and $k_{max}/2$) and dashed line (k_{max}).

SPAC

The parameters used for the SPAC analysis for the 50 m array at PYAS site are described in Table 19. The computed spatial autocorrelation coefficients are displayed for each ring in the Figure 52. These autocorrelation coefficients don't lead to estimate reliable dispersion curve.

Table 19: PYAS SPAC analysis parameters: array radius (Array), windows length according to the centre period of the frequency band T (Windows length), minimum and maximum (central) frequencies (F_{min} and F_{max}), number of frequency sample (Step), number of rings, minimum and maximum radius of rings (R_{min} and R_{max}) and number of pairs of sensors in each ring.

Array	Windows length	Fmin Hz	Fmax Hz	Step	Number of rings	Rmin m	Rmax m	Number of pairs
50 m	200 T	2	15	100	4	41.43	49.50	5
						50.01	62.35	9
						75.75	94.78	6
						91.51	122.33	11

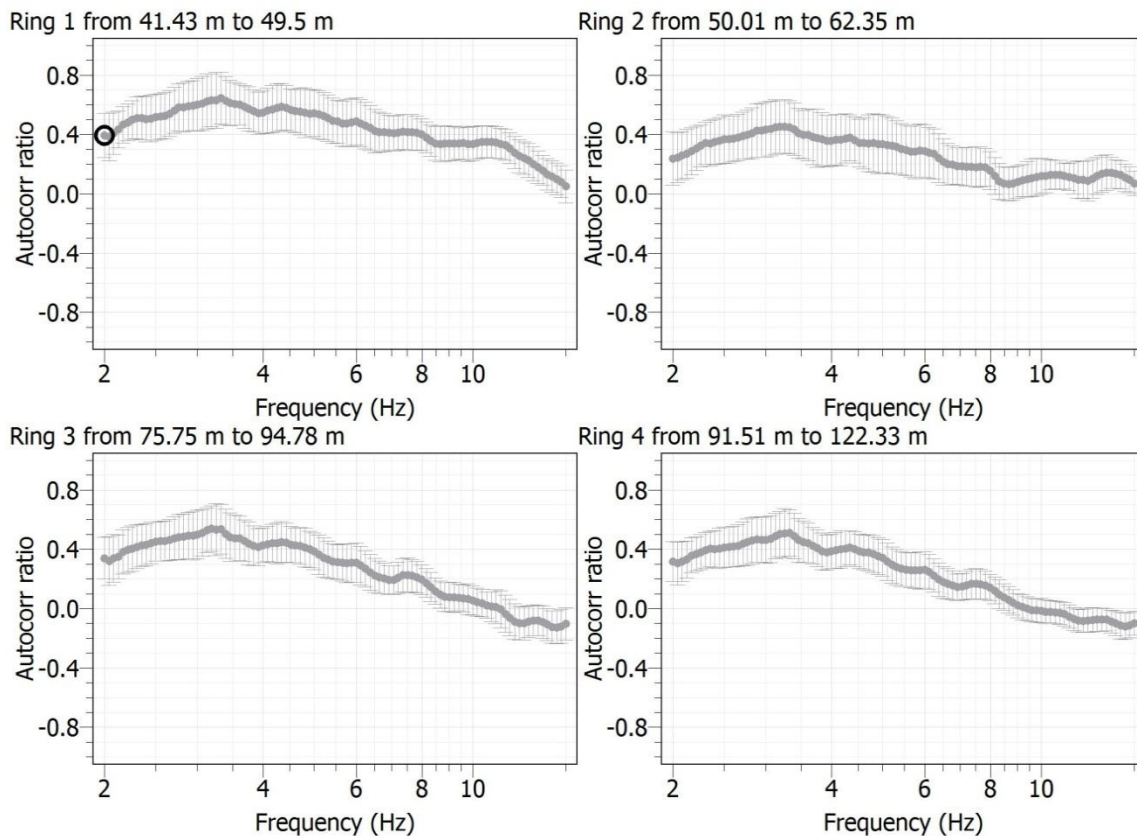


Figure 52: Spatial autocorrelation curves computed for each ring of the 50 m array radius at PYAS site.

3.4.3.3 MASW

The MASW measurements have been done along two profiles. The lengths of the profiles are 46 m (profile 1) and 24 m (profile 2) (see Table 17). For the profile 1, the distance between two geophones is 2 m. The shots were located at both ends (offsets -2 m and 48 m) and in the centre (offset 23 m) of the profile. For the analysis the minimum and maximum distances between source – receiver are 2 m and 48 m respectively. For the profile 2, the length of the profile is 24 m and the distance between two geophones is 1 m. The shots were located at both ends (offsets -2 m and 26 m) and in the centre (offset 11.5 m) of the profile. For the analysis the minimum and maximum distances between source – receiver are 2 m and 12 to 26 m respectively.

The duration of the processing time windows is 1 s. The lowest frequency limit to manually pick the dispersion curve is between 12 and 20 Hz and the minimum wavelength limits are 23 m for the profile 1 and 12 m for the profile 2. The results are shown in Figure 53. For the PYAS site, fourteen dispersion curves were manually picked.

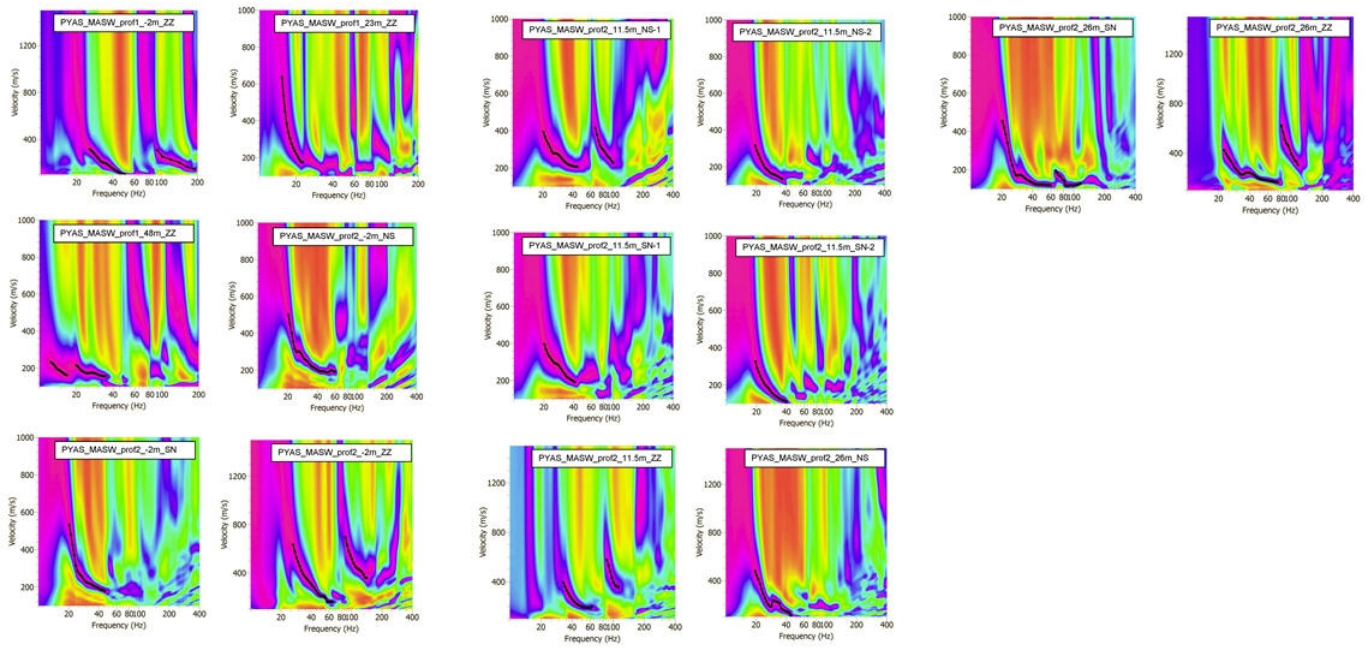


Figure 53: Histogram distributions of phase velocities derived from MASW analysis at PYAS site. The dispersion curves, manually picked, are shown in black dots.

3.4.4 Inversion

Figure 54 shows all dispersion curves derived from AVA and MASW analysis. These curves have been averaged and resampled in order to be inverted (Figure 55). The minimum and maximum wavelengths are 2 m and 260 m respectively. The parameter space for the S-wave velocity profile is defined by the 5-layered soil model described in Table 20. Poisson's ratio ranges between 0.2 and 0.5 for each layer and density is set to 2000 kg/m³. The Vp profile is defined by a gradient soil model (5 layers): Vp velocity ranges between 200 and 5000 m/s, bedrock depth is linked to Vs profile. The results for the "acceptable models" with misfit equal to one sigma are displayed in Figure 56.

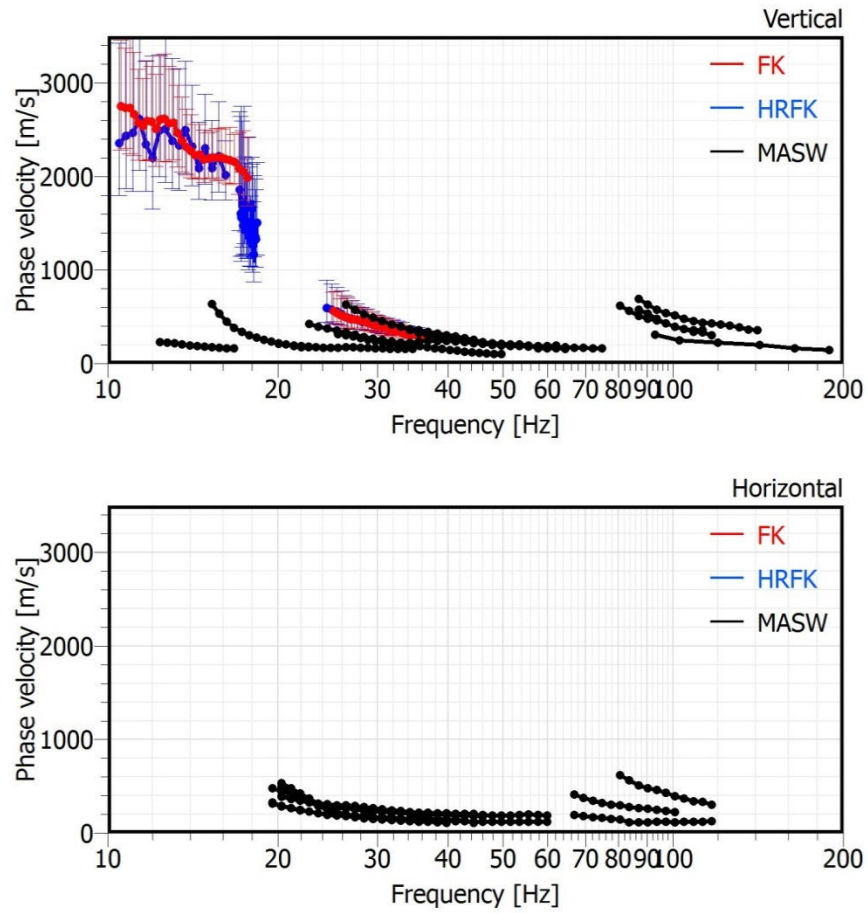


Figure 54: Dispersion curves derived from AVA and MASW analysis at PYAS site.

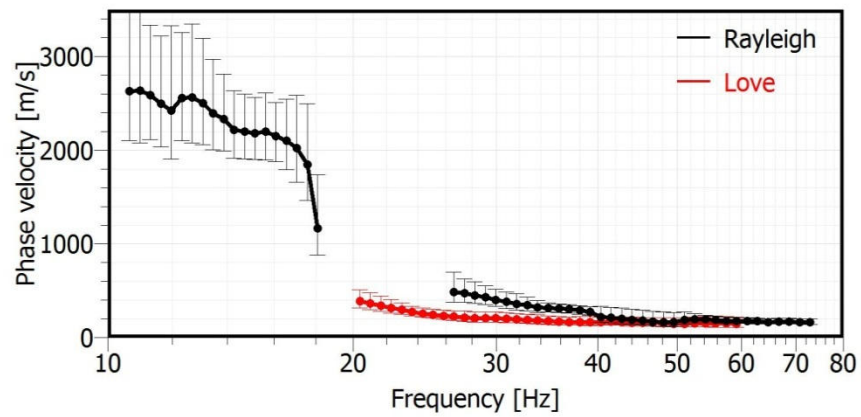


Figure 55: Rayleigh and Love dispersion curves used for the inversion process at PYAS site.

Table 20: Soil parameterization for the 5-layered model of the parameter space at PYAS site.

	Bottom depth (m)		Vs (m/s)	
	Min	Max	Min	Max
Layer 1	0.25	1.43	150	3500
Layer 2	1.43	5.80	150	3500
Layer 3	5.80	22.06	150	3500
Layer 4	22.06	82.43	150	5000
Layer 5	82.43	130	150	5000
Half-space	> 130		150	5000

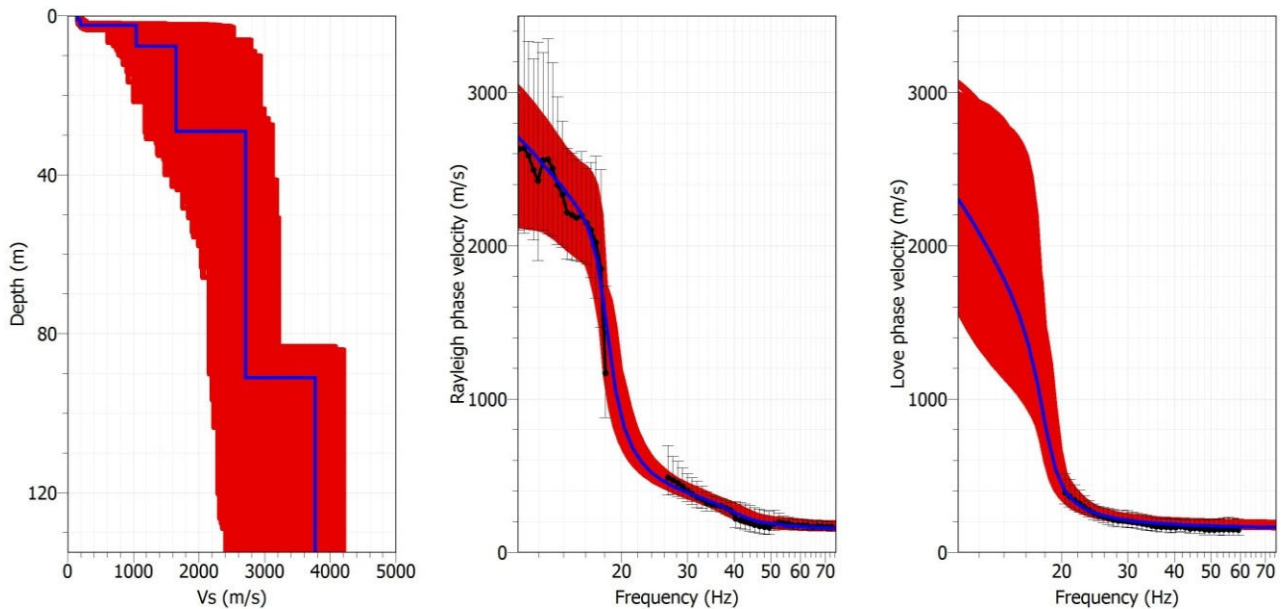


Figure 56: Results for PYAS site: inverted S-wave velocity profile (left) and dispersion curve (right) for the "acceptable models" with misfit equal to one sigma. The Rayleigh and Love waves dispersion curve derived from AVA and MASW analysis are displayed in black dots. Result for the best estimate model (from "classical" inversion) is also shown in blue.

Among the solution shown in Figure 56, one thousand soil profiles having a misfit equal to one sigma were randomly selected in order to compute statistic for Vs30. The associated distribution displayed in Figure 57. See the section 4.1 for a final estimation of Vs30 and associated uncertainties.

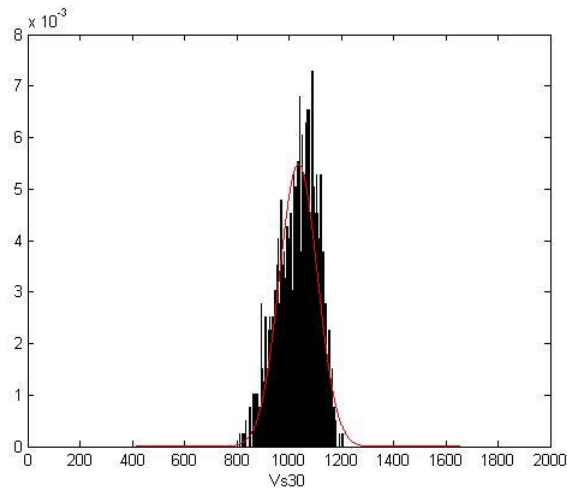


Figure 57: Distribution of Vs30 at PYAS site. The distribution is computed from 1000 soil profiles randomly selected and having a misfit equal to one sigma. The theoretical normal distribution is displayed in red.

3.5 PYLU

3.5.1 Stations information

3.5.1.1 PYLU choice

PYLU station is one of the French Strong Motion Network (RAP) in Bagnères-de Luchon (Haute-Garonne department). Contrary to other investigated stations, PYLU station is set up on alluvial sediments. Several boreholes located next to PYLU station show different depth of quaternary deposits and schist. One of aims of measurement is to estimate bedrock depth.

3.5.1.2 Geographic/Geologic information

Bagnères-de-Luchon is located in Haute-Garonne department, in the south of Pyrenean chain. Main characteristic of the site is resumed in Table 21.

Table 21: PYLU characteristics.

Station	City	Department	X Coord (Long)	Y Coord (Lat)	Network	Site	Slope
PYLU	Bagnères-de-luchon	Haute-Garonne(31)	0.600254	42.789855	OMP	In the high Pyrenean chain	Flat

PYLU station is set up on alluvial plain, composed of sediments. Sensor is installed on Football site, especially in the change room. Campaign measurements were performed on flat slope, but thickness of sediments deposits seems variable according to data boreholes (Figure 58 to Figure 60).

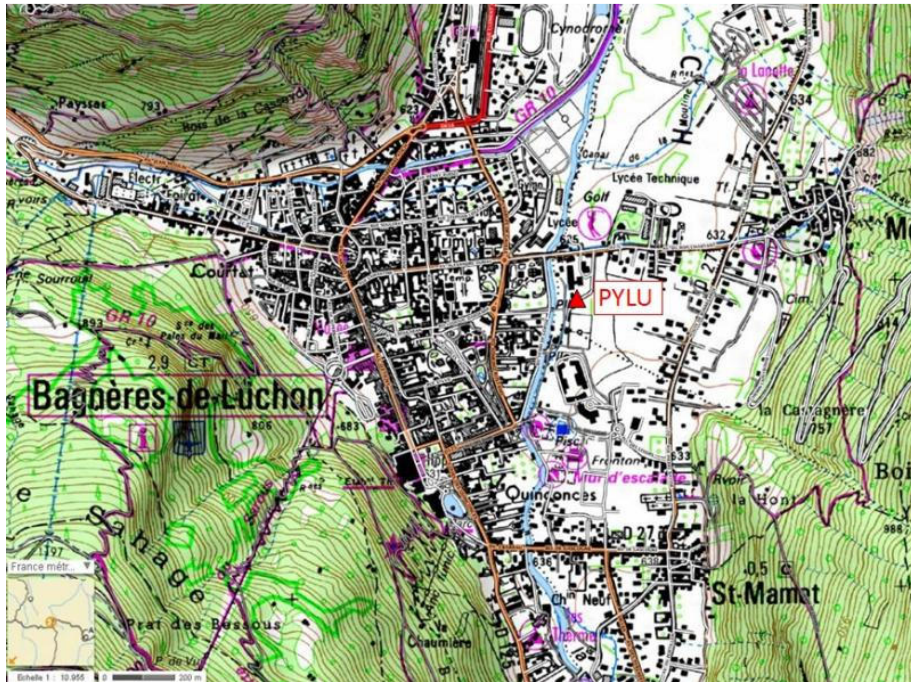


Figure 58 : PYLU location in Bagnères-de-Luchon (IGN Geoportail source)



Figure 59: Picture of PYLU site, during the measurement on the 8th September 2012.



Figure 60: Extract of Bagnères-de-Luchon geological map (with PYLU location on alluvial plain deposits, next to scree cone).

3.5.2 Measurements

The measurement survey was performed on 8th September 2012. For Ambient Vibration Array method, one configuration with 3 circles of 20, 60m and 100m around a central station (near real PYLU station) was performed (10, then 8 sensors because of technical problems). For the second method, MASW, two profiles were recorded (34.5 m and 46 m). Parameters of these 3 arrays and MASW investigation are presented in Table 22. Location of investigation is showed at Figure 61.

Table 22: PYLU recording parameters, 08th September 2012

Measurments	Numbers of Sensors	Beginning (TU)	End (TU)	Noise/ environnement	Topography	Weather conditions
Array R = 10m	10	11:00:00	13:00:00	No urban	flat	good
Array R = 30m	10	12:25:00	14:00:00	Mid-urban	flat	good
Array R = 80m	10	15:39:00	16:20:00	urban	flat	good
MASW N05°E 46m, Dx = 2m	24 geophones H and V)	11:20:00	11:30:00	no-urban	flat	good

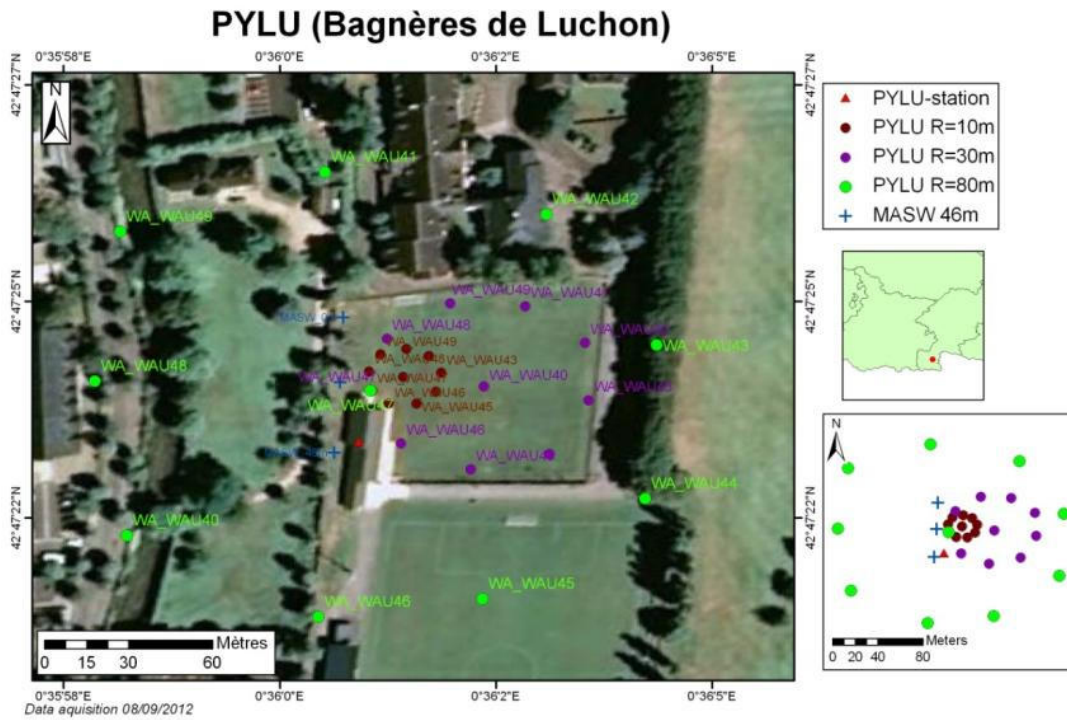


Figure 61: location of the arrays, the MASW shots and PYLU Station.

3.5.3 Processing

3.5.3.1 H/V

The Fourier spectra amplitudes computed on the three component records of ambient vibrations at each PYLU array receiver are shown in Figure 62. The corresponding H/V curves are displayed in Figure 63. Most H/V curves exhibit broad peak with large amplitude below 1 Hz.

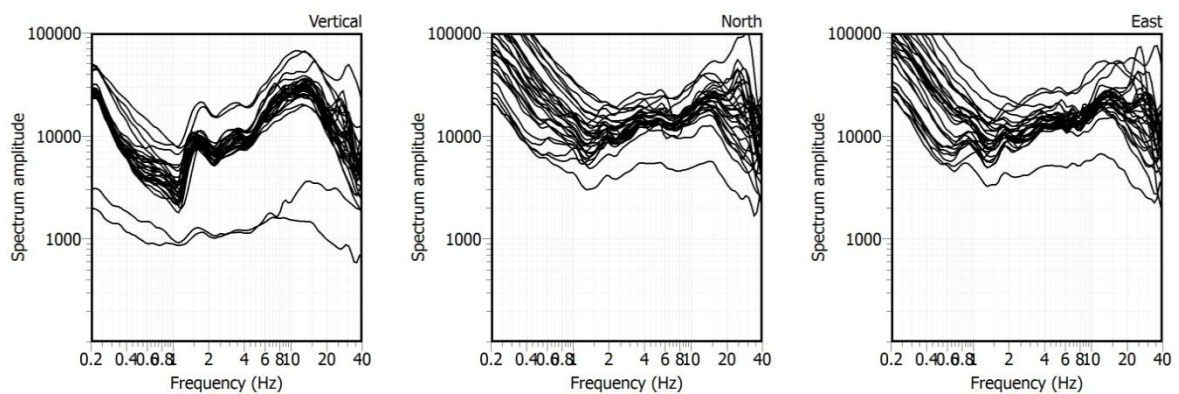


Figure 62: Amplitude of the Fourier spectra computed on 3-C recordings of ambient vibrations at each PYLU array receiver.

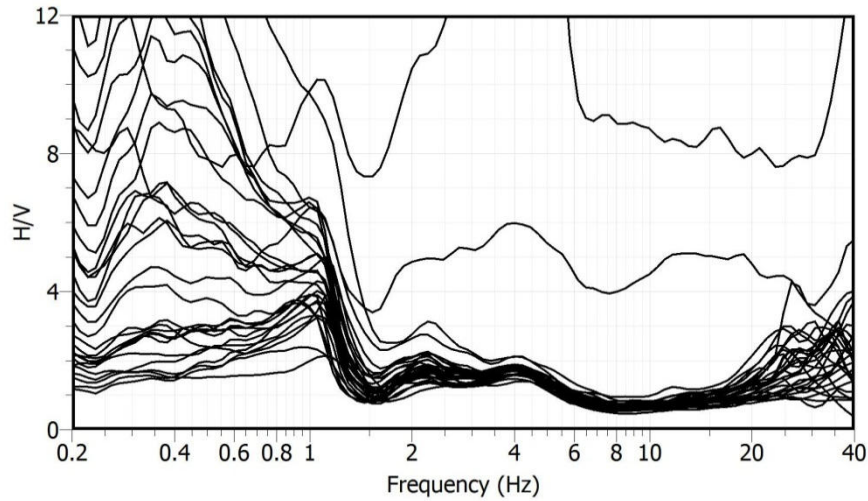


Figure 63: H/V amplitude at each PYLU array receiver.

3.5.3.2 AMV

The parameters used for FK and HRFK analysis at PYLU site are described in Table 23.

Table 23: PYLU FK and HRFK analysis parameters: array radius (Array), windows length according to the centre period of the frequency band T (Windows length), minimum and maximum (central) frequencies (Fmin and Fmax), number of frequency sample (Step), anti-aliasing limits kmin and kmax, fk grid resolution (Grid step), maximum search radius for the fk grid (Grid size), minimum velocity and half-bandwidth for the frequency band (Band width).

Array	Windows length	Fmin Hz	Fmax Hz	Step	Kmin rad/m	Kmax rad/m	Grid step rad/m	Grid size rad/m	Vmin m/s	Band width
FK										
10 m	70 T	8	25	40	0.2378	1.6922	0.0595	3.384	150	0.1
30 m	100 T	4	18	40	0.0795	0.5421	0.0199	1.084	150	0.1
80 m	200 T	2	8	40	0.0296	0.1712	0.0740	0.3430	150	0.1
HRFK										
10 m	100 T	10	25	50	0.2378	1.6922	0.0119	3.384	50	0.03
30 m	100 T	4	18	40	0.0795	0.5421	0.0040	1.084	150	0.1
80 m	200 T	2	10	50	0.0296	0.1712	0.0015	0.3430	150	0.1

FK

The histogram distributions of phase velocities estimation of Rayleigh waves derived from the ensemble of the wave-propagation estimates obtained for each individual time-frequency cell using the FK method are shown in Figure 64 for PYLU arrays.

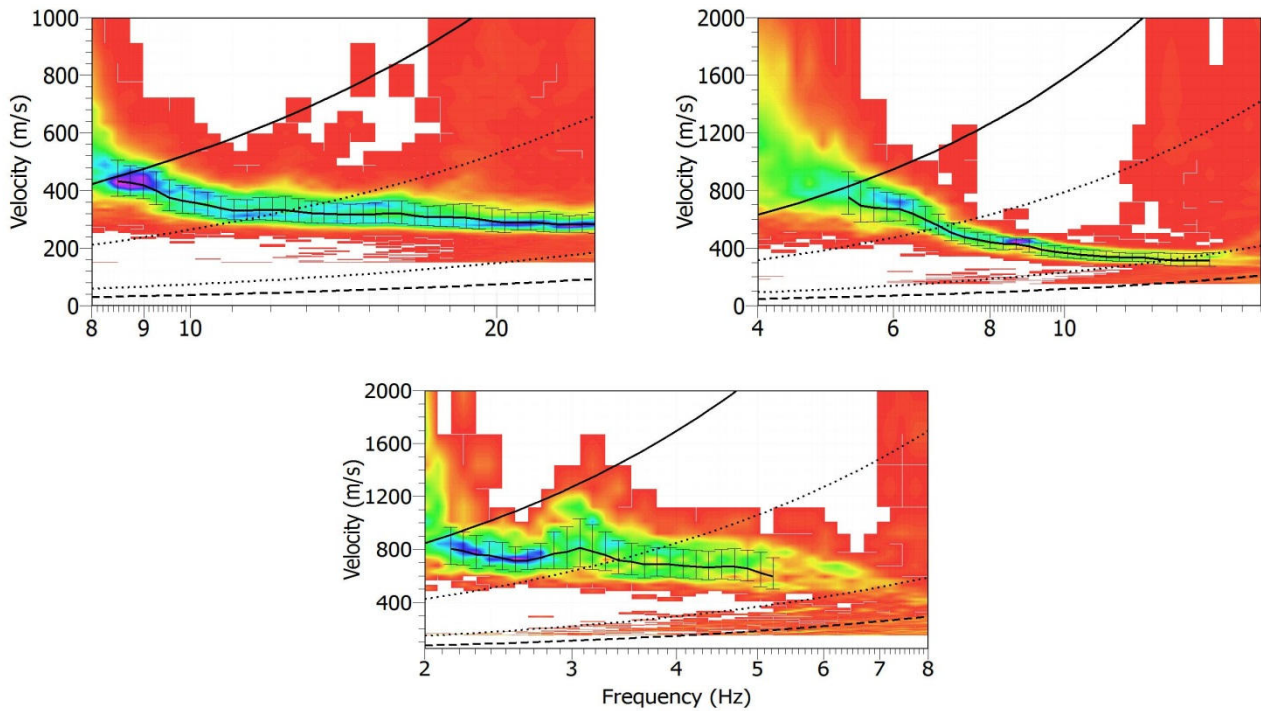


Figure 64: Results for the 10 m (top-left), 30 m (top-right) and 80 m (bottom) radius arrays at PYLU site (vertical component): histogram distributions of phase velocities derived from the ensemble of the wave-propagation estimates obtained for each individual time-frequency cell using the FK method (color scale: red and magenta colors indicate min and max values, respectively). The anti-aliasing limits for each array configuration are also shown: thick line ($k_{min}/2$), dotted lines (k_{min} and $k_{max}/2$) and dashed line (k_{max}).

HRFK

The resulting estimation of Rayleigh waves phase velocities are shown in Figure 65 for PYLU arrays.

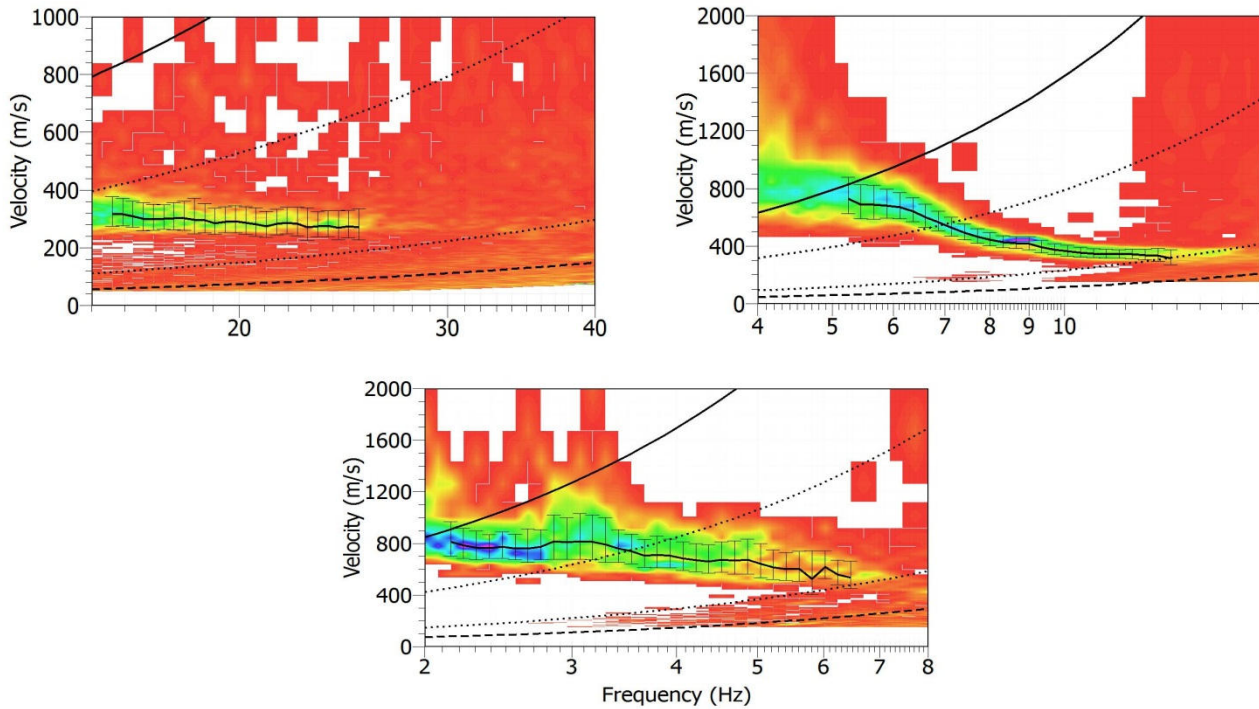


Figure 65: Results for the 10 m (top-left), 30 m (top-right) and 80 m (bottom) radius arrays at PYLU site (vertical component): histogram distributions of phase velocities derived from the ensemble of the wave-propagation estimates obtained for each individual time-frequency cell using the HRFK method (color scale: red and magenta colors indicate min and max values, respectively). The anti-aliasing limits for each array configuration are also shown: thick line ($k_{min}/2$), dotted lines (k_{min} and $k_{max}/2$) and dashed line (k_{max}).

SPAC

The parameters used for the SPAC analysis for the 80 m array at PYLU site are described in Table 24. The computed spatial autocorrelation coefficients are displayed for each ring in the Figure 66 and the corresponding phase velocities are shown in Figure 67. These autocorrelation coefficients lead to estimate Rayleigh dispersion curve between 1.5 and 1.8 Hz.

Table 24: PYLU SPAC analysis parameters: array radius (Array), windows length according to the centre period of the frequency band T (Windows length), minimum and maximum (central) frequencies (Fmin and Fmax), number of frequency sample (Step), number of rings, minimum and maximum radius of rings (Rmin and Rmax) and number of pairs of sensors in each ring.

Array	Windows length	Fmin	Fmax	Step	Number of rings	Rmin	Rmax	Number of pairs
		Hz	Hz			m	m	
80 m	200 T	2	10	50	5	106.09 138.00 160.42	126.58 157.82 199.12	8 8 11

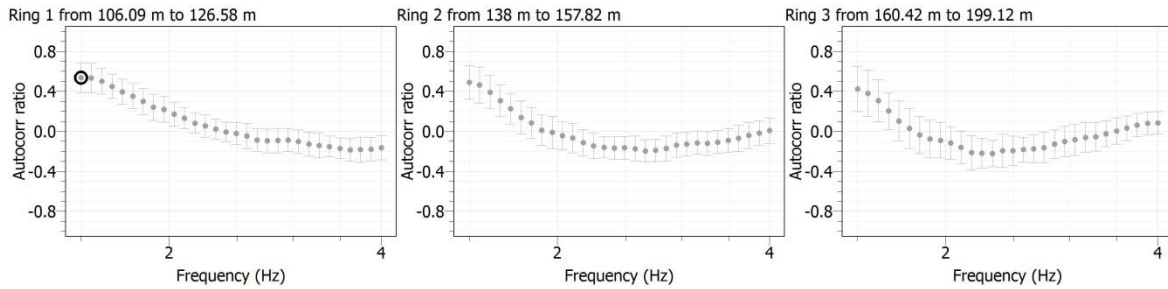


Figure 66: Spatial autocorrelation curves computed for each ring of the 80 m array radius at PYLU site.

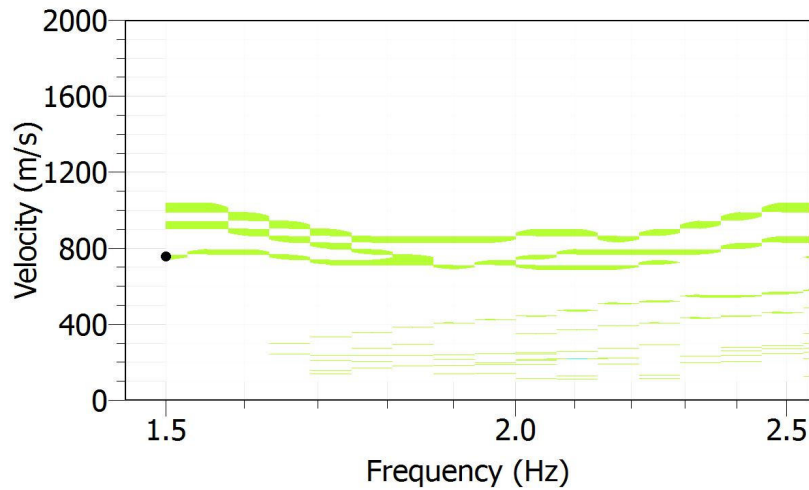


Figure 67: Phase velocities estimated with SPAC for the 80 m array radius at PYLU site.

3.5.3.3 MASW

The MASW measurements have been done along one profile. The length of the profile is 46 m and the distance between two geophones is 2 m (see Table 22). The shots were located at both ends (offsets -2 m and 48 m) and in the centre (offset 23 m) of the profile. For the analysis the minimum and maximum distances between source – receiver are 2 m and 48 m respectively. The duration of the processing time windows is 1 s. The lowest frequency limit to manually pick the dispersion curve is set to 20 Hz and the minimum wavelength limit is 23 m. The results are shown in Figure 68. For the PYLU site, nine dispersion curves were manually picked.

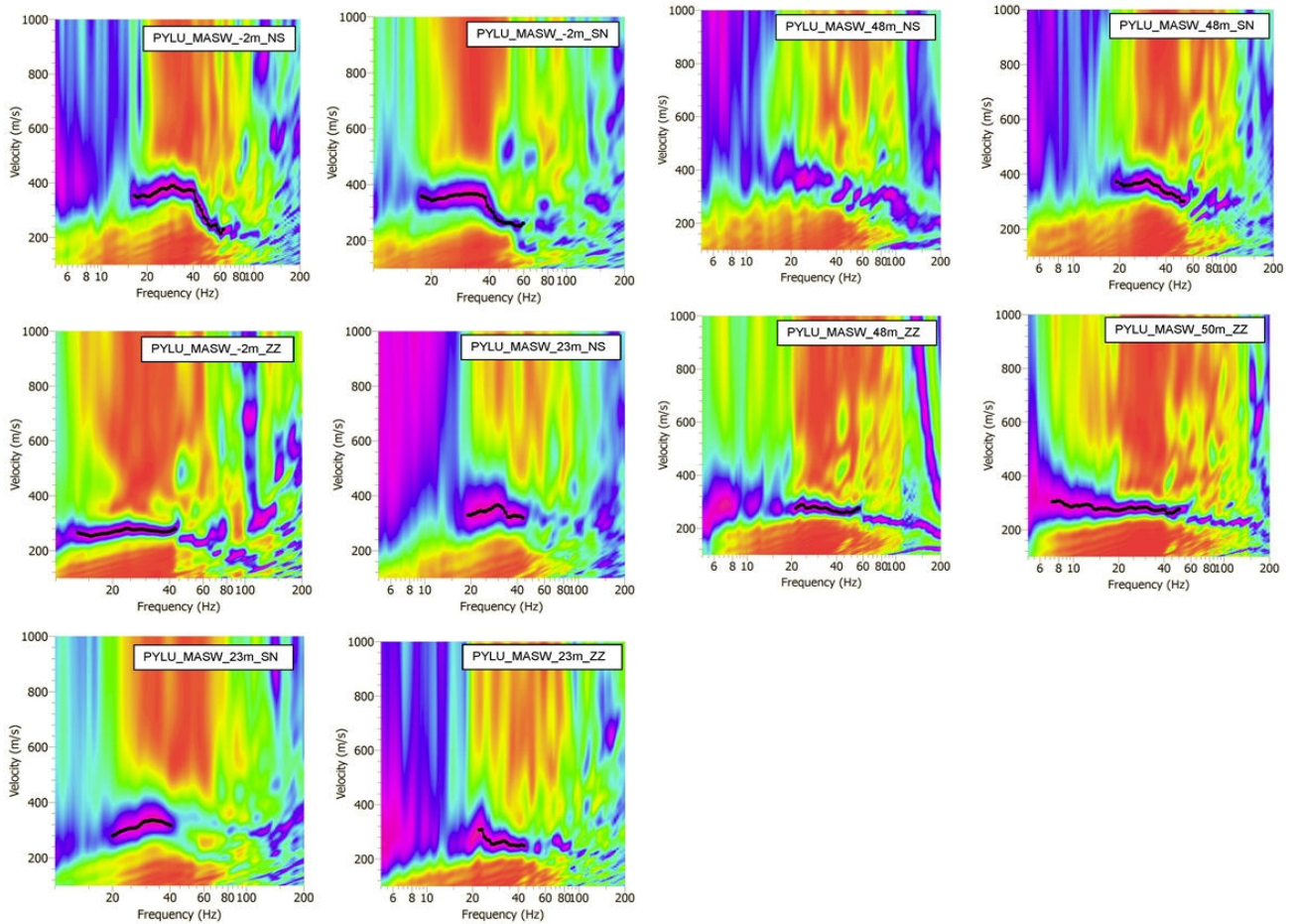


Figure 68: Histogram distributions of phase velocities derived from MASW analysis at PYLU site. The dispersion curves, manually picked, are shown in black dots.

3.5.4 Inversion

Figure 69 shows all dispersion curves derived from AVA, SPAC and MASW analysis. These curves have been averaged and resampled in order to be inverted (Figure 70). The minimum and maximum wavelengths are 6 m and 626 m respectively. The parameter space for the S-wave velocity profile is defined by the 5-layered soil model described in Table 25. Poisson's ratio ranges between 0.2 and 0.5 for each layer and density is set to 2000 kg/m³. The Vp profile is defined by a gradient soil model (5 layers): Vp velocity ranges between 200 and 5000 m/s, bedrock depth is linked to Vs profile. The results for the "acceptable models" with misfit equal to one sigma are displayed in Figure 71.

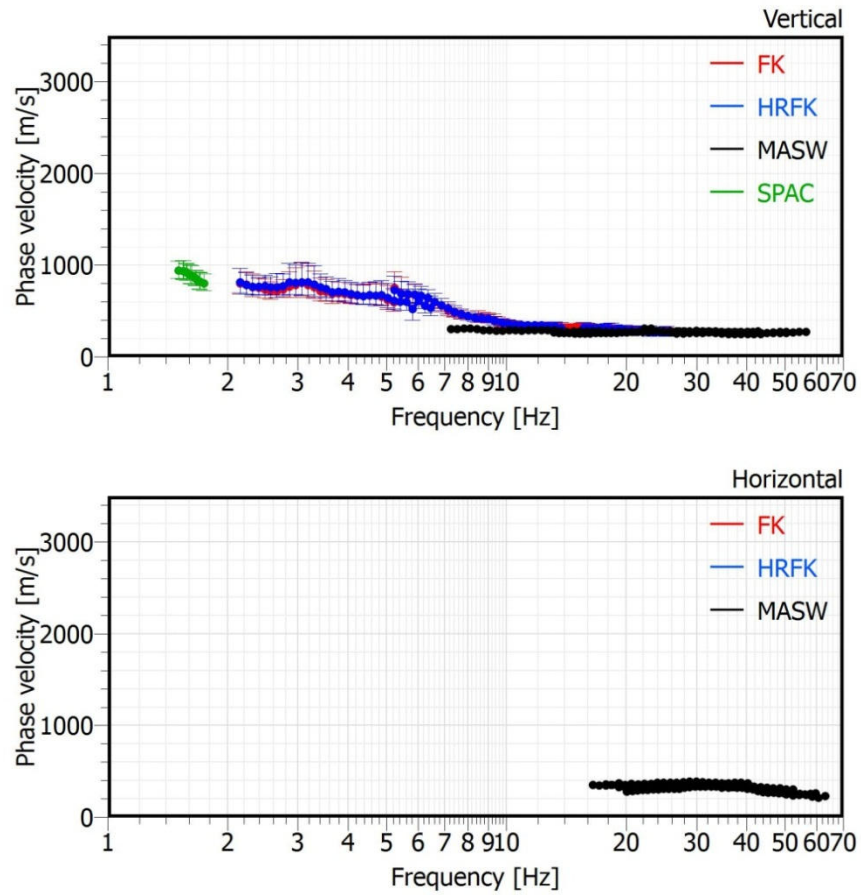


Figure 69: Dispersion curves derived from AVA, SPAC and MASW analysis at PYLU site.

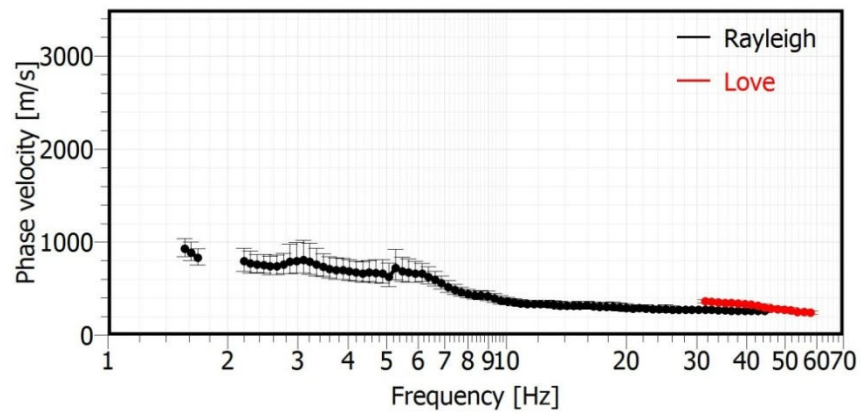


Figure 70: Rayleigh and Love dispersion curves used for the inversion process at PYLU site.

Table 25: Soil parameterization for the 5-layered model of the parameter space at PYLU site.

	Bottom depth (m)		Vs (m/s)	
	Min	Max	Min	Max
Layer 1	0.75	4.12	150	3500
Layer 2	4.12	15.90	150	3500
Layer 3	15.90	57	150	3500
Layer 4	57	201	150	3500
Layer 5	201	313	150	3500
Half-space	> 313		150	3500

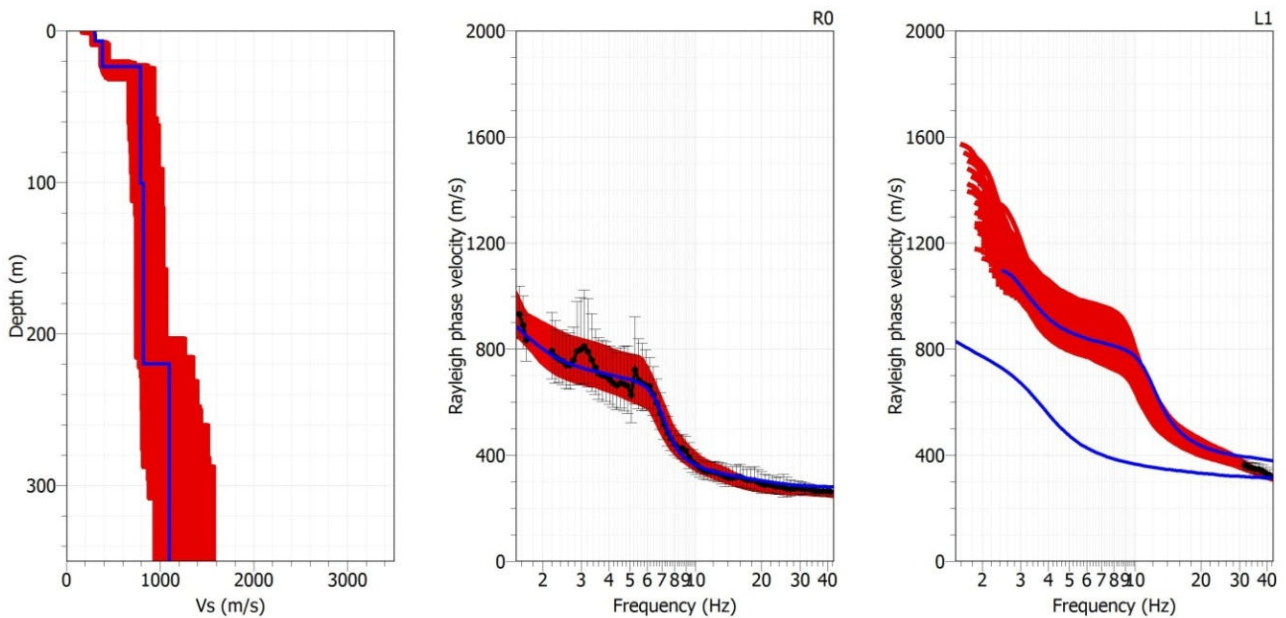


Figure 71 Results for PYLU site: inverted S-wave velocity profile (left) and dispersion curve (right) for the "acceptable models" with misfit equal to one sigma. The Rayleigh and Love waves dispersion curve derived from AVA and MASW analysis are displayed in black dots. Result for the best estimate model (from "classical" inversion) is also shown in blue.

Among the solution shown in Figure 56, one thousand soil profiles having a misfit equal to one sigma were randomly selected in order to compute statistic for Vs30. The associated distribution is displayed in Figure 72. See the section 4.1 for a final estimation of Vs30 and associated uncertainties.

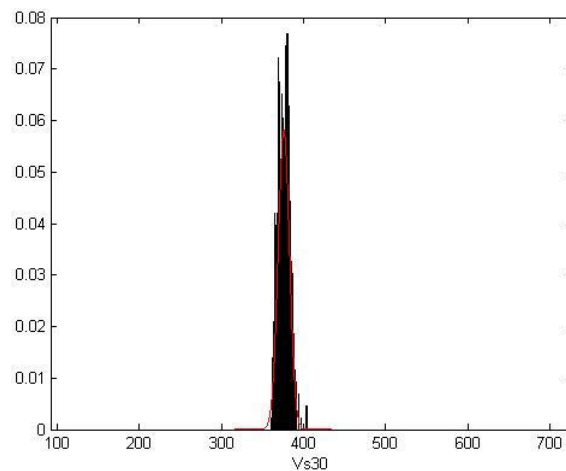


Figure 72: Distribution of Vs30 at PYLU site. The distribution is computed from 1000 soil profiles randomly selected and having a misfit equal to one sigma. The theoretical normal distribution is displayed in red.

3.6 PYBB

3.6.1 Stations information

3.6.1.1 PYBB choice

PYBB station is one of the French Strong Motion Network (RAP) in Bagnères-de-Bigorre (Hautes-Pyrénées department). A few years ago, PYBB, and more generally Bagnères-de-Bigorre city had been studied as pilot site effect. So, in the present study, we have selected PYBB to completed site characterisation and particularly previous MASW investigation.

3.6.1.2 Geographic/Geologic information

Bagnères-de-Bigorre is located in Haute-Pyrénées department, in the south of Pyrenean chain. Main characteristic of the site is resumed in Table 26.

Table 26: PYBB characteristics

Station	City	Department	X Coord (Long)	Y Coord (Lat)	Network	Site	Slope
PYBB	Bagnères-de-Bigorre	Haute-Pyrénées (65)	0.148778	43.058575	OMP	In the high Pyrenean chain	Weak slope

PYBB station is set up on mid-cretaceous limestone formation, on alternately flysch and limestone-marlstone. Sensor is fixed on concrete stone, in a little house. Campaign measurements were performed on parking and in camps around (Figure 73 to Figure 75).

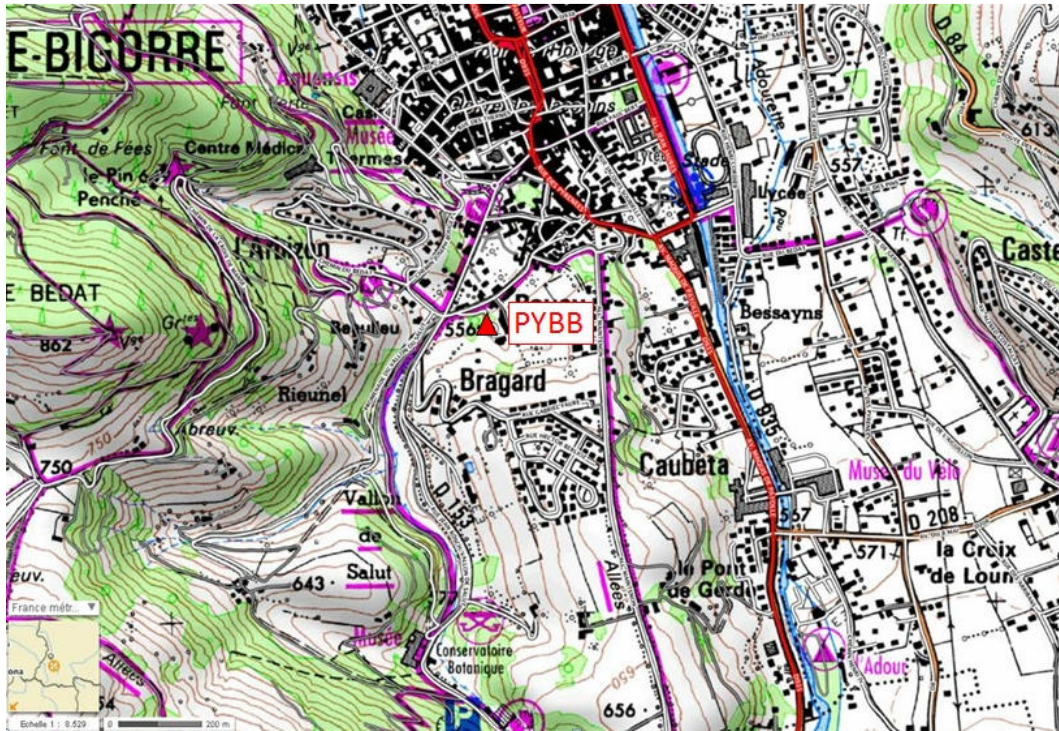


Figure 73 : PYBB location in Bagnères-de-Luchon (IGN Geoportail source).



Figure 74: Picture of PYBB site (and accelerometer installation), during the measurement on the 10th September 2012.

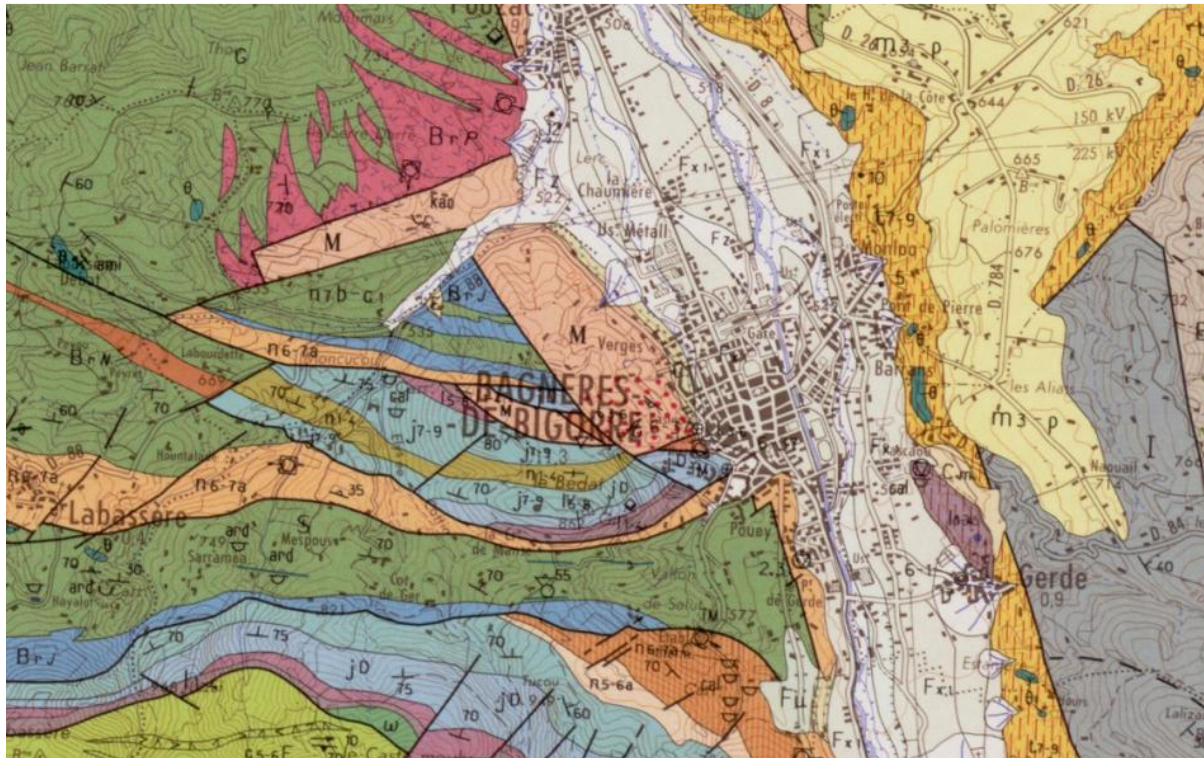


Figure 75: Extract of Bagnères- de- Bigorre geological map (with PYBB location on plain deposits, next to scree cone).

3.6.2 Measurements

The measurement survey was performed on 8th September 2012. For Ambient Vibration Array method, one configuration with 3 circles of 20, 60m and 100m around a central station (near real PYLI station) was performed (10, then 8 sensors because of technical problems). Parameters of these 3 arrays and MASW investigation are presented in Table 27.

Table 27: PYBB recording parameters, 10th September 2012

Measurments	Numbers of Sensors	Beginning (TU)	End (TU)	Noise/ environnement	Topography	Weather conditions
Array R = 25m	10	11:00:00	11:58:00	No urban	flat	good
Array R = 50m	10	13:20:00	15:00:00	No urban	Flat slope	good
Array R = 80m	8	17:00:00	17:50:00	Mid-urban	Steep slope	good

Location of investigation is showed at Figure 76. All coordinates are available in Appendix.

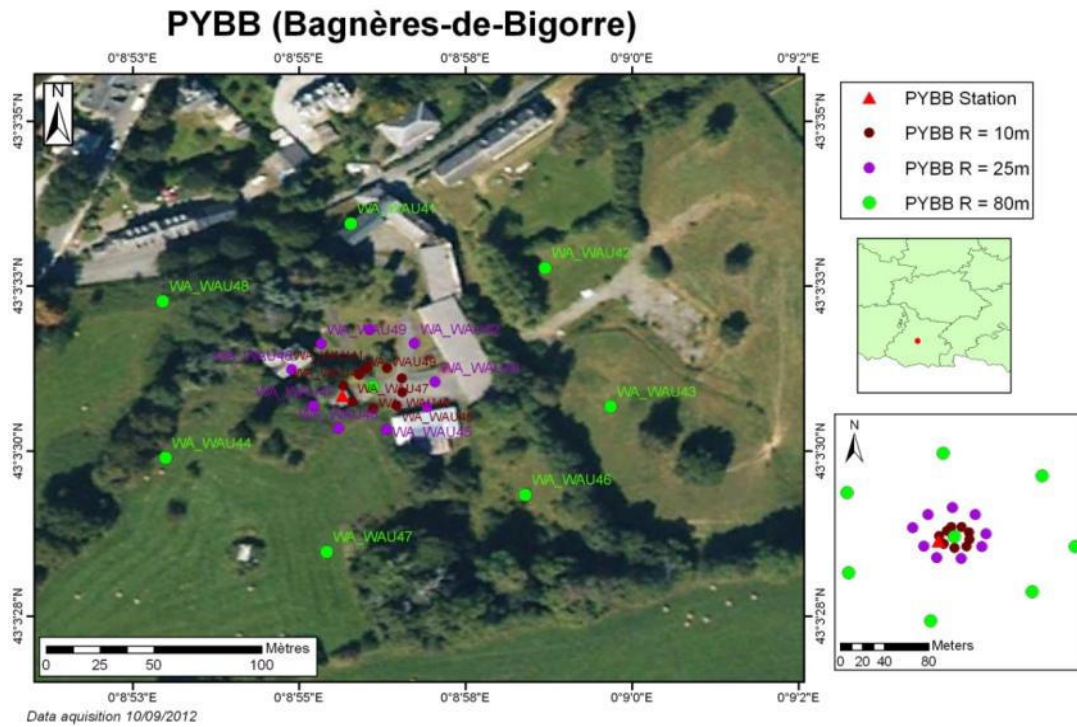


Figure 76: location of the arrays, the MASW shots and PYBB Station.

3.6.3 Processing

3.6.3.1 H/V

The Fourier spectra amplitudes computed on the three component records of ambient vibrations at each PYBB array receiver are shown in Figure 77. The corresponding H/V curves are displayed in Figure 78. H/V curves exhibit one clear peak with peak frequency varying from 6 Hz to 15 Hz.

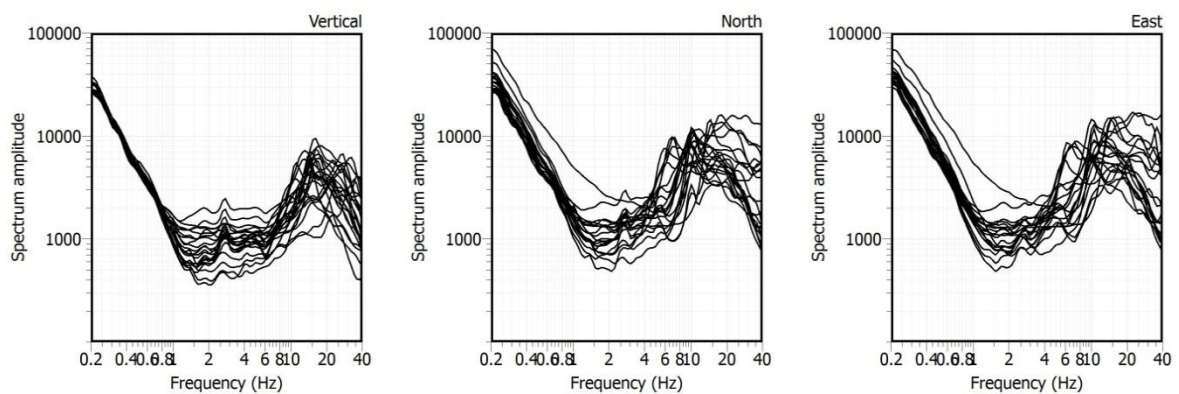


Figure 77: Amplitude of the Fourier spectra computed on 3-C recordings of ambient vibrations at each PYBB array receiver

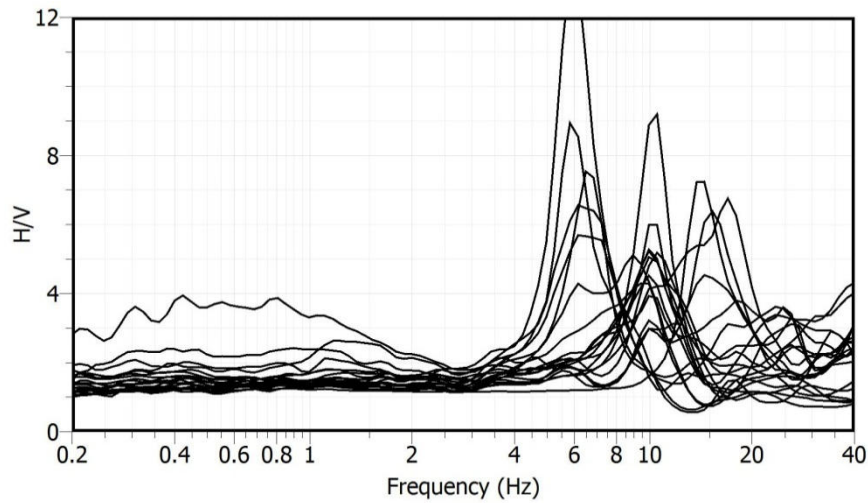


Figure 78: H/V amplitude at each PYBB array receiver.

3.6.3.2 AMV

The parameters used for FK and HRFK analysis at PYBB site are described in Table 28.

Table 28: PYBB FK and HRFK analysis parameters: array radius (Array), windows length according to the centre period of the frequency band T (Windows length), minimum and maximum (central) frequencies (Fmin and Fmax), number of frequency sample (Step), anti-aliasing limits kmin and kmax, fk grid resolution (Grid step), maximum search radius for the fk grid (Grid size), minimum velocity and half-bandwidth for the frequency band (Band width).

Array	Windows length	Fmin Hz	Fmax Hz	Step	Kmin rad/m	Kmax rad/m	Grid step rad/m	Grid size rad/m	Vmin m/s	Band width
FK										
10 m	70 T	10	40	50	0.2445	1.4058	0.0930	1.407	150	0.1
25 m	100 T	10	30	50	0.1018	0.3538	0.0284	0.7110	150	0.1
80 m	150 T	6	13	50	0.0320	0.0080	0.0092	0.1520	150	0.1
HRFK										
10 m	70 T	15	30	40	0.2445	1.4058	0.0186	1.407	150	0.1
25 m	200 T	12	20	100	0.1018	0.3538	0.0057	0.7110	150	0.02
80 m	150 T	5	15	20	0.0320	0.0080	0.0018	0.1520	150	0.1

FK

The histogram distributions of phase velocities estimation of Rayleigh waves derived from the ensemble of the wave-propagation estimates obtained for each individual time-frequency cell using the FK method are shown in Figure 79 for PYBB arrays.

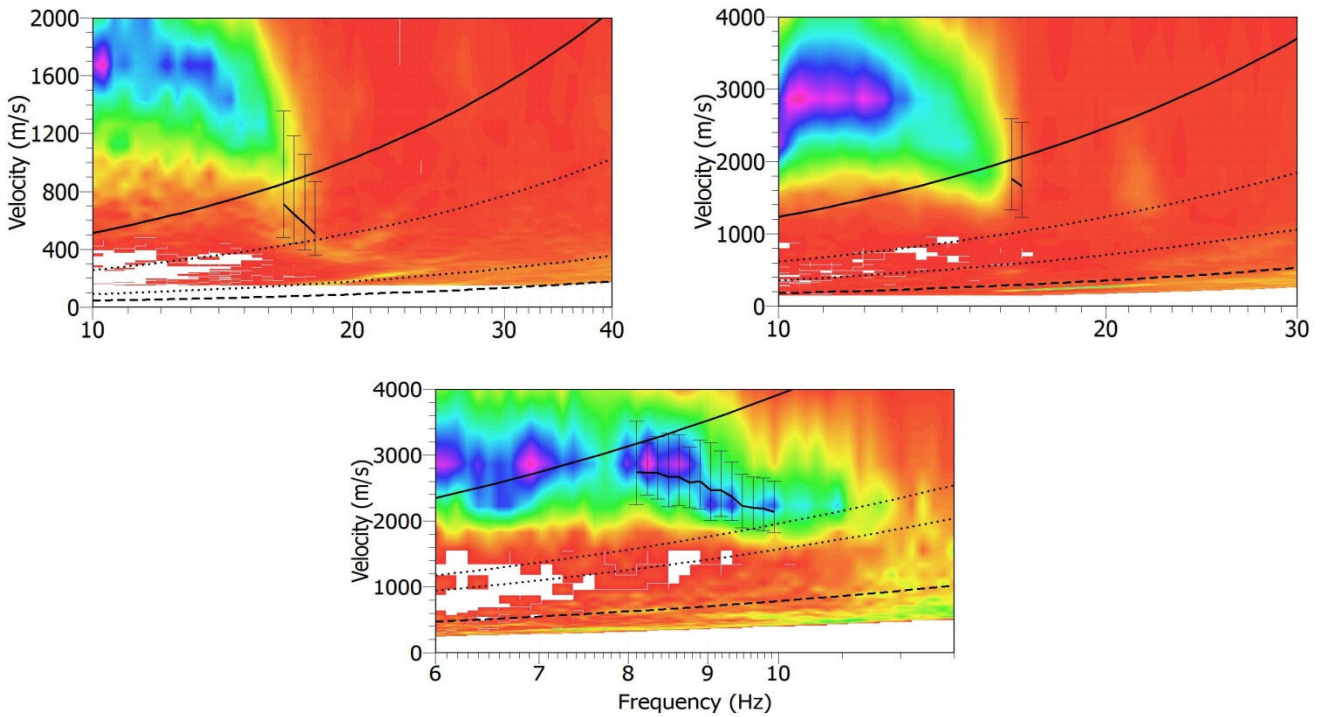


Figure 79: Results for the 10 m (top-left), 25m (top-right) and 80 m (bottom) radius arrays at PYBB site (vertical component): histogram distributions of phase velocities derived from the ensemble of the wave-propagation estimates obtained for each individual time-frequency cell using the FK method (color scale: red and magenta colors indicate min and max values, respectively). The anti-aliasing limits for each array configuration are also shown: thick line ($k_{min}/2$), dotted lines (k_{min} and $k_{max}/2$) and dashed line (k_{max}).

HRFK

The resulting estimation of Rayleigh waves phase velocities are shown in Figure 80 for PYBB arrays.

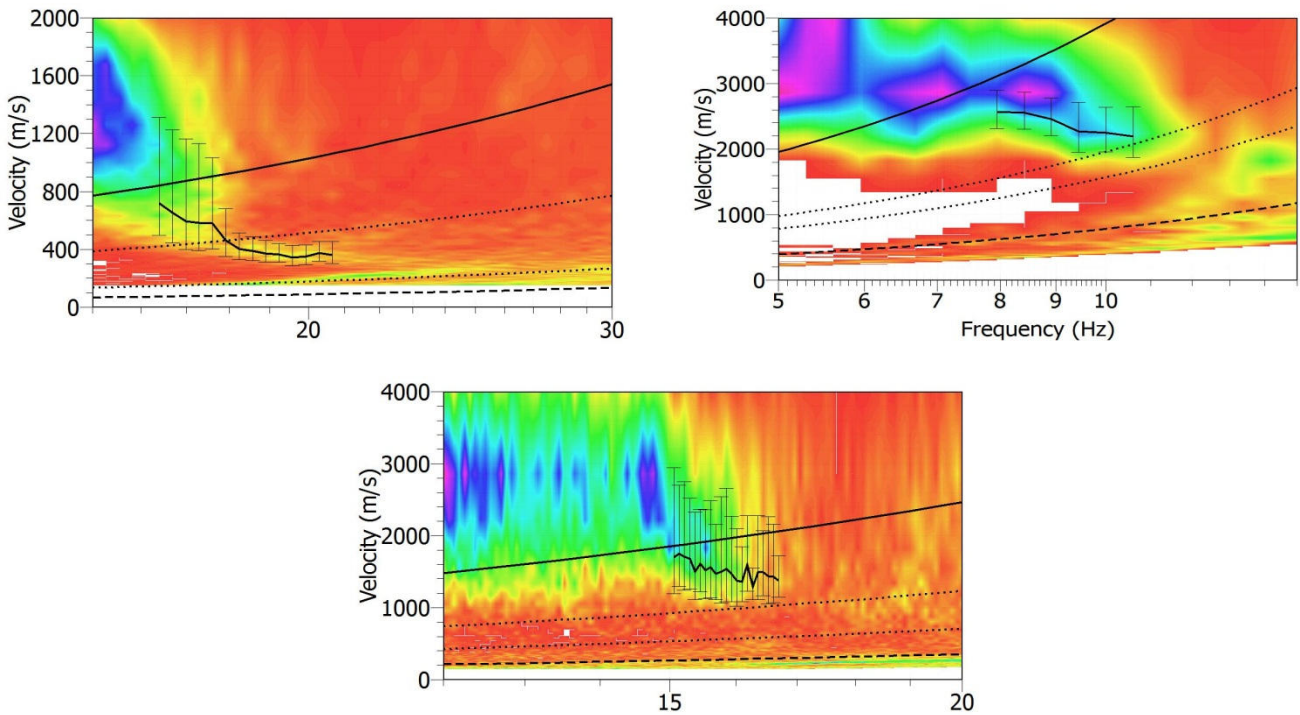


Figure 80: Results for the 10 m (top), 25 m (middle) and 80 m (bottom) radius arrays at PYBB site (vertical component): histogram distributions of phase velocities derived from the ensemble of the wave-propagation estimates obtained for each individual time-frequency cell using the HRFK method (color scale: red and magenta colors indicate min and max values, respectively). The anti-aliasing limits for each array configuration are also shown: thick line ($k_{min}/2$), dotted lines (k_{min} and $k_{max}/2$) and dashed line (k_{max}).

SPAC

The parameters used for the SPAC analysis for the 80 m array at PYBB site are described in Table 29. The computed spatial autocorrelation coefficients are displayed for each ring in the Figure 81. These autocorrelation coefficients don't lead to estimate reliable dispersion curve.

Table 29: PYBB SPAC analysis parameters: array radius (Array), windows length according to the centre period of the frequency band T (Windows length), minimum and maximum (central) frequencies (F_{min} and F_{max}), number of frequency sample (Step), number of rings, minimum and maximum radius of rings (R_{min} and R_{max}) and number of pairs of sensors in each ring.

Array	Windows length	F_{min} Hz	F_{max} Hz	Step	Number of rings	R_{min} m	R_{max} m	Number of pairs
80 m	150 T	5	20	30	2	54.99	103.26	11
						105.76	199.69	10

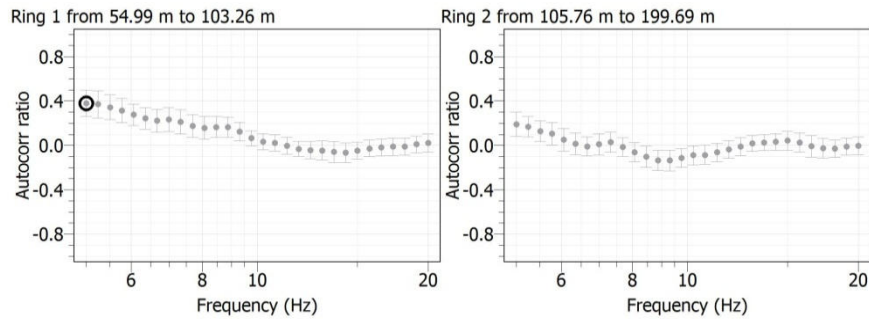


Figure 81: Spatial autocorrelation curves computed for each ring of the 80 m array radius at PYBB site.

3.6.3.3 MASW

The result of the MASW measurements is shown in Figure 82.

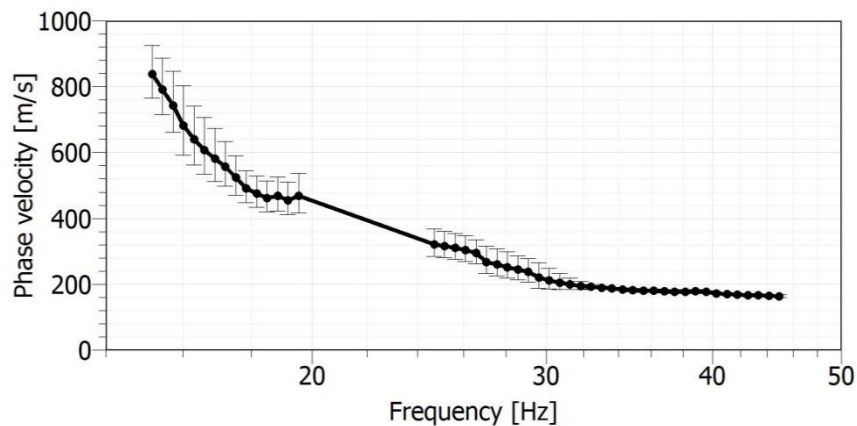


Figure 82: Dispersion curve derived from MASW analysis at PYBB site.

3.6.4 Inversion

Figure 83 shows all dispersion curves derived from AVA and MASW analysis. These curves have been averaged and resampled in order to be inverted (Figure 84). The minimum and maximum wavelengths are 4 m and 338 m respectively. The parameter space for the S-wave velocity profile is defined by the 5-layered soil model described in Table 30. Poisson's ratio ranges between 0.2 and 0.5 for each layer and density is set to 2000 kg/m³. The Vp profile is defined by a gradient soil model (5 layers): Vp velocity ranges between 200 and 7000 m/s, bedrock depth is linked to Vs profile. The results for the "acceptable models" with misfit equal to one sigma are displayed in Figure 85.

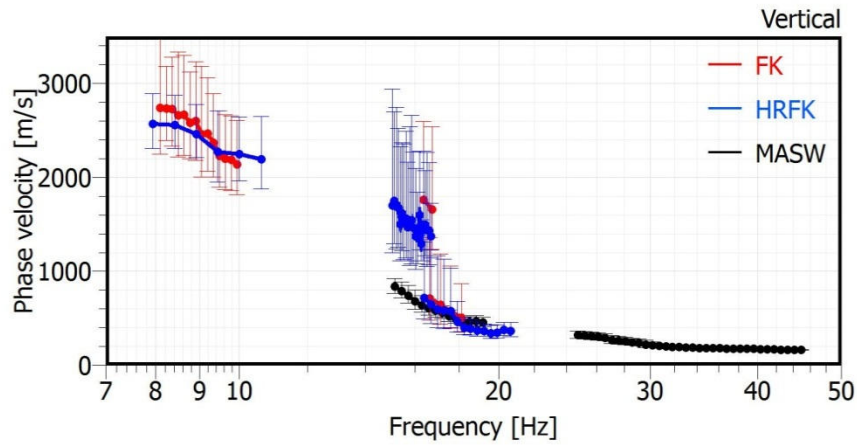


Figure 83: Dispersion curves derived from AVA and MASW analysis at PYBB site.

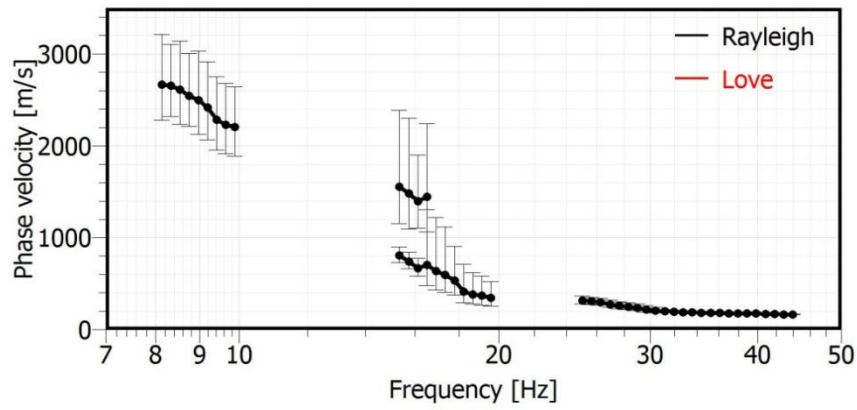


Figure 84: Rayleigh dispersion curves used for the inversion process at PYBB site.

Table 30: Soil parameterization for the 5-layered model of the parameter space at PYBB site.

	Bottom depth (m)		Vs (m/s)	
	Min	Max	Min	Max
Layer 1	0.5	2.6	150	5000
Layer 2	2.6	9.7	150	5000
Layer 3	9.7	33	150	5000
Layer 4	33	110	150	5000
Layer 5	110	169	150	5000
Half-space	> 169		150	5000

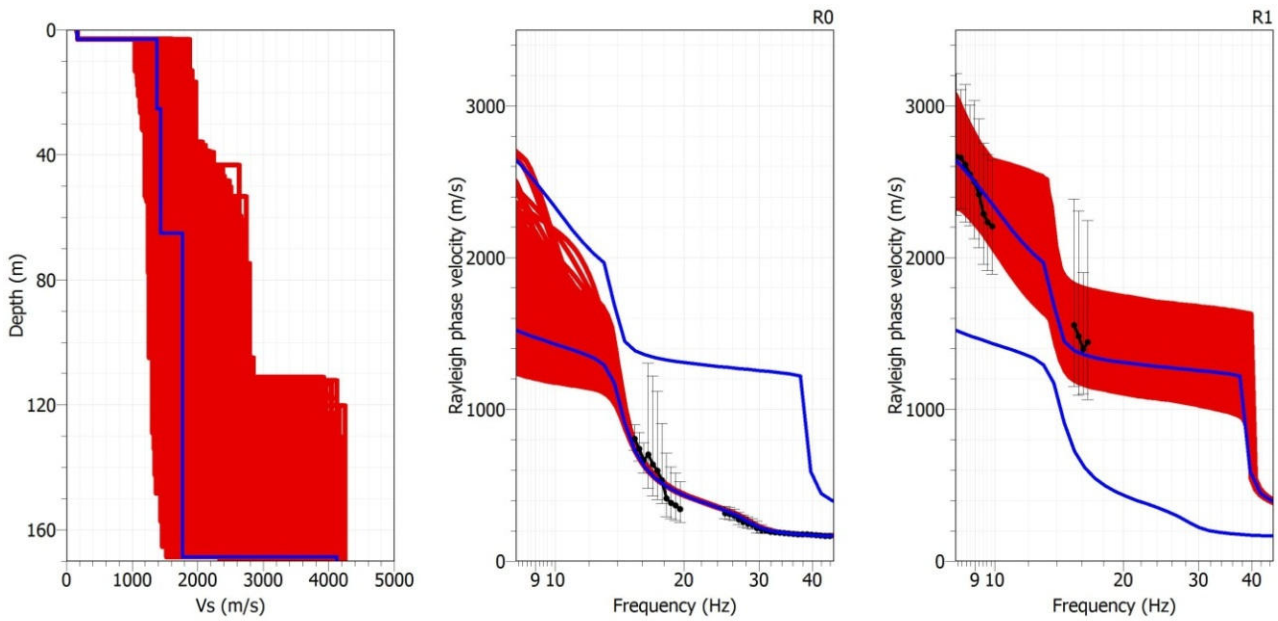


Figure 85: Results for PYBB site: inverted S-wave velocity profile (left) and dispersion curve (right) for the "acceptable models" with misfit equal to one sigma. The Rayleigh and Love waves dispersion curve derived from AVA and MASW analysis are displayed in black dots. Result for the best estimate model (from "classical" inversion) is also shown in blue.

Among the solution shown in Figure 56, one thousand soil profiles having a misfit equal to one sigma were randomly selected in order to compute statistic for Vs30. The associated distribution is displayed in Figure 86. See the section 4.1 for a final estimation of Vs30 and associated uncertainties.

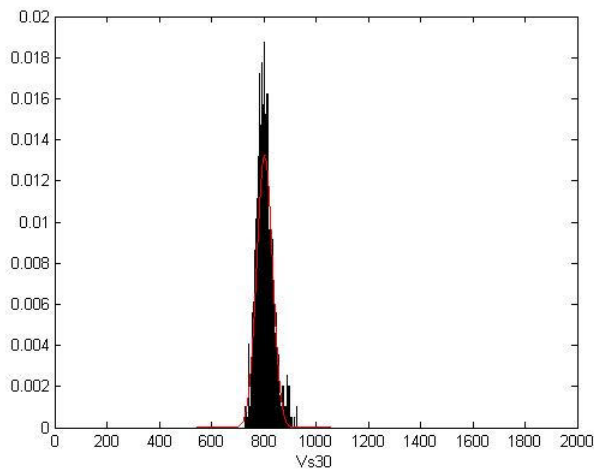


Figure 86: Distribution of Vs30 at PYBB site. The distribution is computed from 1000 soil profiles randomly selected and having a misfit equal to one sigma. The theoretical normal distribution is displayed in red.

3.7 PYLO

3.7.1 Stations information

3.7.1.1 PYLO choice

PYLO station is one of the French Strong Motion Network (RAP) in Lourdes (Hautes-Pyrénées department). PYLO station has been selected because it is used to reference site in Generalized Inversion technic, applied to Pyrenean (Drouet, 2010). Moreover, it is one of stations which records most events. As Bagnères-de-Bigorre, Lourdes city has been studied for site effects.

3.7.1.2 Geographic/Geologic information

Lourdes is located in Hautes-Pyrénées department, in the middle of the mountain chain. Main characteristics of the site are resumed in Table 31.

Table 31: PYLO characteristics

Station	City	Department	X Coord (Long)	Y Coord (Lat)	Network	Site	Slope
PYLO	Lourdes	Hautes-Pyrénées(65)	-0.049408	43.096716	OMP	Pyrenean chain	Steep slope

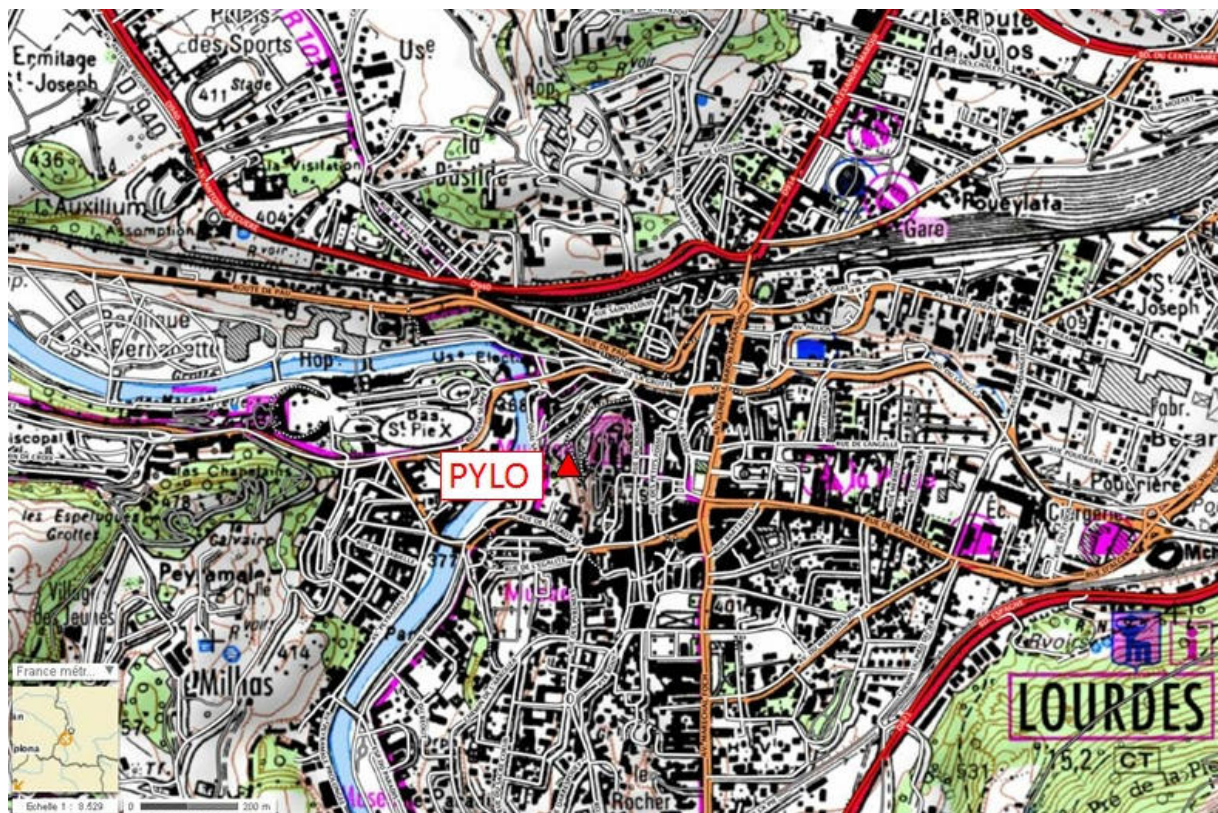


Figure 87 : PYLO location in Lourdes (IGN Geoportail source).

PYLO station is set up on the castle hill, on massifs limestone rocks. Station can be considered as true “rock station” because it is directly fix to limestone, at 5 m depth (Figure 87 to Figure 89).



Figure 88: Picture of PYLO site and limestone bedrock, during the measurement on the 11th September 2012. PYLO station is set up 5m depth into the rock.



Figure 89: Extract of Lourdes geological map.

3.7.2 Measurements

The measurement survey was performed on 11th September 2012. For Ambient Vibration Array method, one configuration with 2 circles of 10, 30m around a central station (close to PYLO station) was performed (8 sensors). Another array (about 70 m aperture) was installed at the top of castle hill, to try study, limestone hill properties. For the second method, MASW, two profiles were recorded (46 m and 24m) just close to PYLO station. It is important to point difficulties to organize geometrical arrays on PYLO site because of complex geomorphology of the site. Parameters of these 3 arrays and MASW investigation are presented in Table 32. Location of investigation is showed at Figure 90.

Table 32: PYLO recording parameters, 11th September 2012

Measurments	Numbers of Sensors	Beginning (TU)	End (TU)	Noise/ environnement	Topography	Weather conditions
Array R = 5m	8	08:10:00	08:35:00	No urban	Flat, (embankment)	good
Array R = 15m	8	11:30:00	12:30:00	No urban	Flat(embankment)	good
Array R = 35m	8	14:20:00	15:20:00	Urban, noise +	Steep slope, top of the hill	good
MASW N0°E 46m, Dx = 2m	24 vertical geophones (V)	11:00:00	12:00:00	No noise	Flat, (embankment)	good
MASW N0°E 24 24m, Dx = 1m	24 geophones (H and V)	11:00:00	12:00:00	No noise	Flat (embankment)	

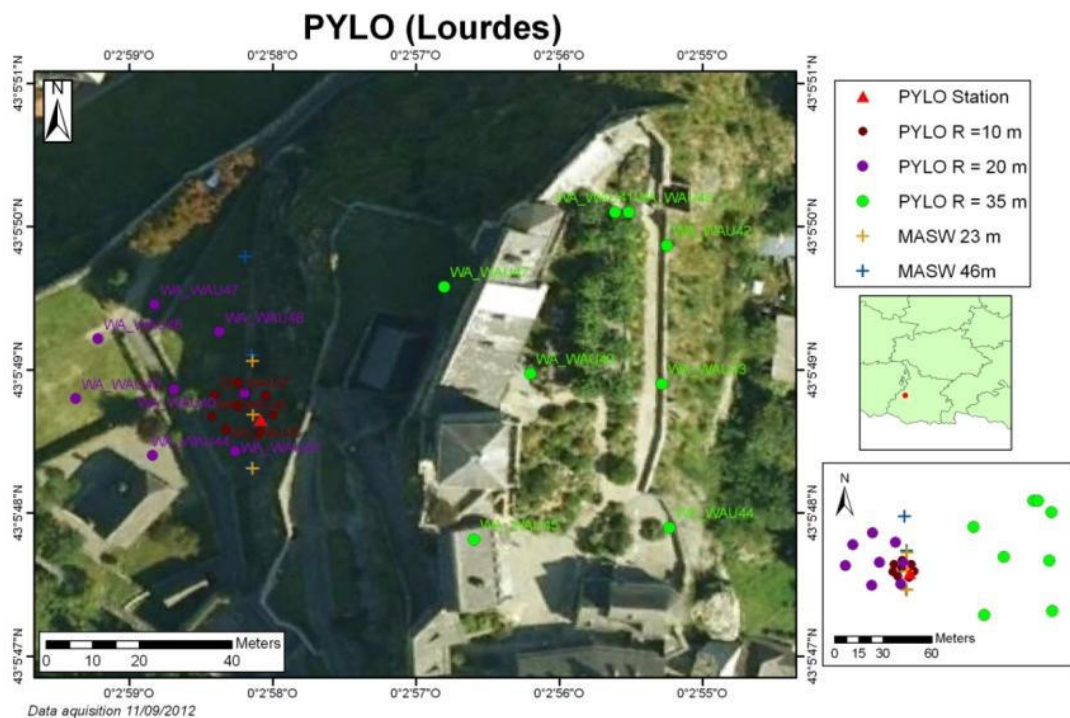


Figure 90: location of the arrays (near the station and at the top of castle site), the MASW shots and PYLO Station.

3.7.3 Processing

3.7.3.1 H/V

The Fourier spectra amplitudes computed on the three component records of ambient vibrations at each PYLO array receiver are shown in Figure 91. The corresponding H/V curves are displayed in Figure 92. Most H/V curves exhibit broad peak with large amplitude below 1 Hz.

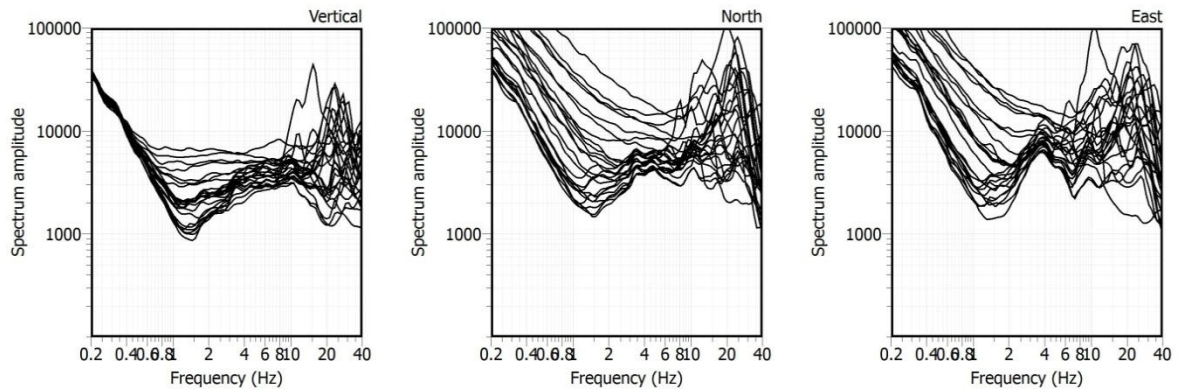


Figure 91: Amplitude of the Fourier spectra computed on 3-C recordings of ambient vibrations at each PYLO array receiver.

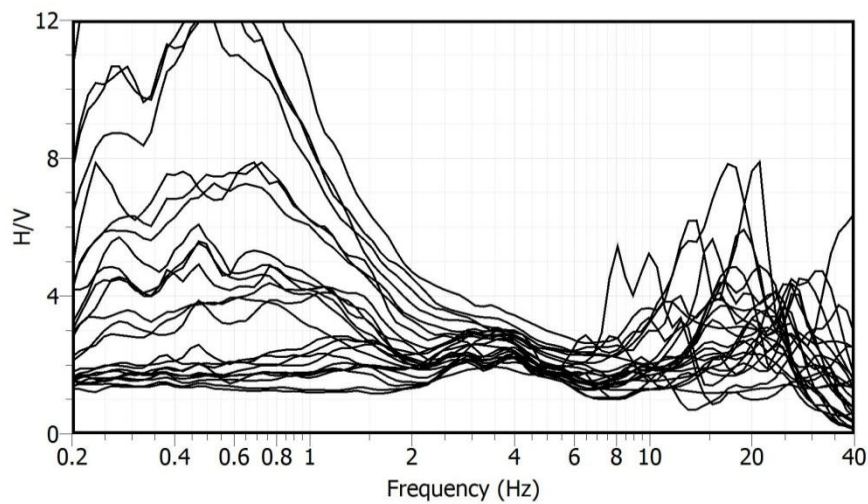


Figure 92: H/V amplitude at each PYLO array receiver.

3.7.3.2 AMV

The parameters used for FK and HRFK analysis at PYLO site are described in Table 33.

Table 33: PYLO FK and HFRK analysis parameters: array radius (Array), windows length according to the centre period of the frequency band T (Windows length), minimum and maximum (central) frequencies (Fmin and Fmax), number of frequency sample (Step), anti-aliasing limits kmin and kmax, fk grid resolution (Grid step), maximum search radius for the fk grid (Grid size), minimum velocity and half-bandwidth for the frequency band (Band width).

Array	Windows length	Fmin Hz	Fmax Hz	Step	Kmin rad/m	Kmax rad/m	Grid step rad/m	Grid size rad/m	Vmin m/s	Band width
FK										
5 m	150 T	26	34	30	0.4565	1.3547	0.1141	2.7100	150	0.1
15 m	150 T	23	36	50	0.1574	0.4517	0.0394	0.9030	150	0.1
35 m	150 T	15	30	50	0.0799	0.1861	0.020	0.3720	150	0.1
HFRK										
5 m	150 T	32	40	40	0.4565	1.3547	0.0228	2.7100	150	0.1
15 m	150 T	20	40	100	0.1574	0.4517	0.0079	0.9030	150	0.03
35 m	200 T	15	30	50	0.0799	0.1861	0.0040	0.3720	300	0.1

FK

The histogram distributions of phase velocities estimation of Rayleigh waves derived from the ensemble of the wave-propagation estimates obtained for each individual time-frequency cell using the FK method are shown in Figure 93 for PYLO arrays.

Rayleigh dispersion curves were determined for the 5 m and 35 m radius arrays. It was not possible to derived dispersion curve from the 15 m radius array.

HFRK

The resulting estimation of Rayleigh waves phase velocities are shown in Figure 94 for PYLO arrays. Rayleigh dispersion curves were determined for the 5 m and 35 m radius arrays. It was not possible to derived dispersion curve from the 15 m radius array.

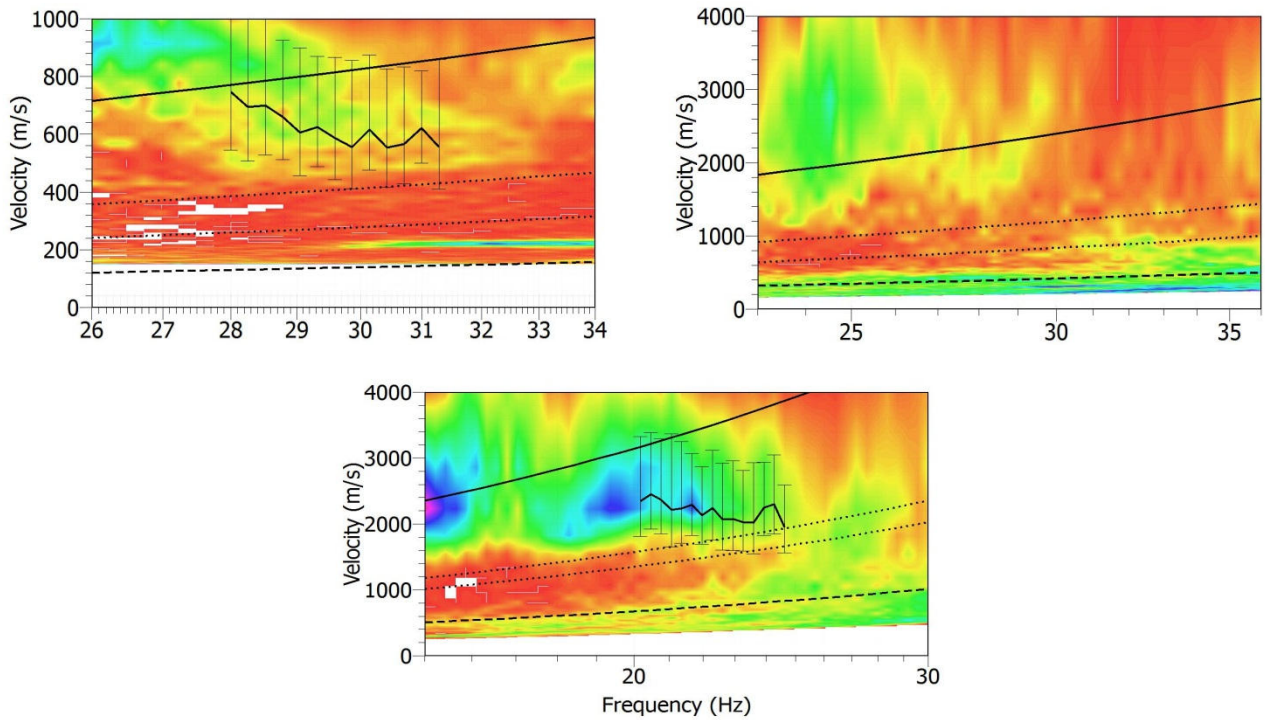


Figure 93: Results for the 5 m (top-left), 15 m (top-right) and 35 m (bottom) radius arrays at PYLO site (vertical component): histogram distributions of phase velocities derived from the ensemble of the wave-propagation estimates obtained for each individual time-frequency cell using the FK method (color scale: red and magenta colors indicate min and max values, respectively). The anti-aliasing limits for each array configuration are also shown: thick line ($k_{min}/2$), dotted lines (k_{min} and $k_{max}/2$) and dashed line (k_{max}).

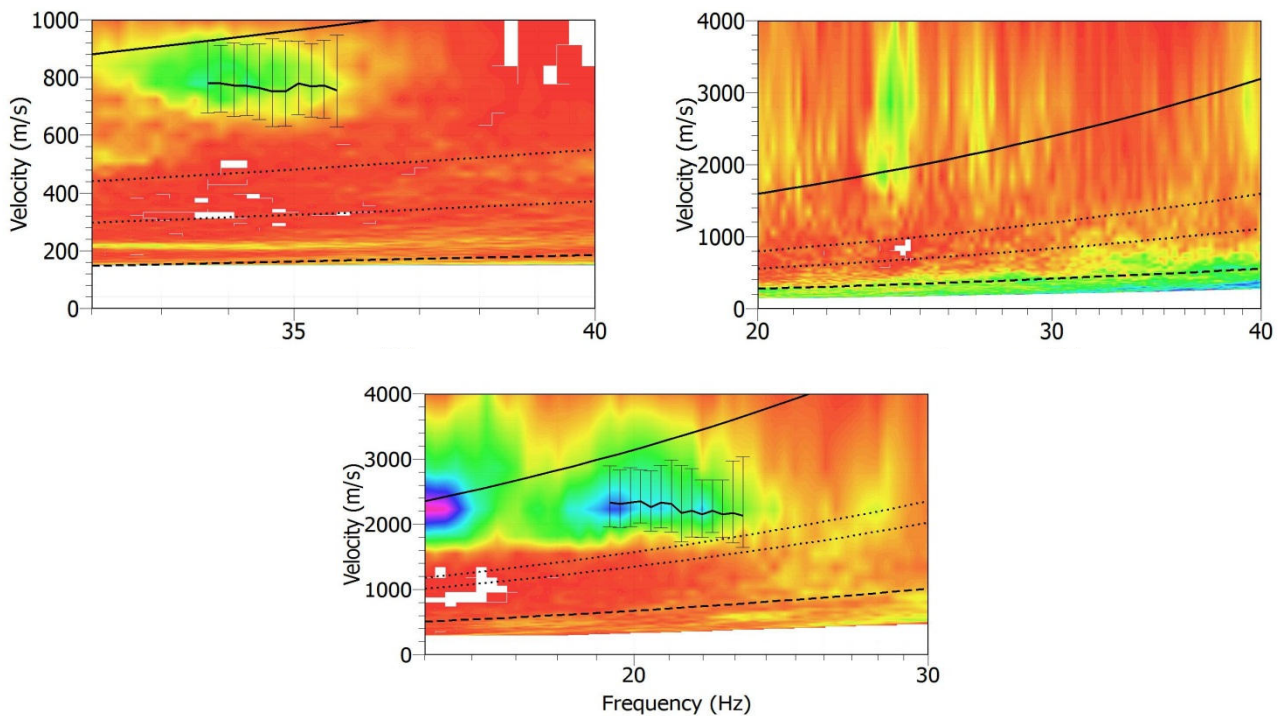


Figure 94: Results for the 5 m (top-left), 15 m (top-right) and 35 m (bottom) radius arrays at PYLO site (vertical component): histogram distributions of phase velocities derived from the ensemble of the wave-propagation estimates obtained for each individual time-frequency cell using the HRFK method (color scale: red and magenta colors indicate min and max values, respectively). The anti-aliasing limits for each array configuration are also shown: thick line ($k_{min}/2$), dotted lines (k_{min} and $k_{max}/2$) and dashed line (k_{max}).

SPAC

The parameters used for the SPAC analysis for the 35 m array at PYLO site are described in Table 34. The computed spatial autocorrelation coefficients are displayed for each ring in the Figure 95. These autocorrelation coefficients don't lead to estimate reliable dispersion curve.

Table 34: PYLO SPAC analysis parameters: array radius (Array), windows length according to the centre period of the frequency band T (Windows length), minimum and maximum (central) frequencies (Fmin and Fmax), number of frequency sample (Step), number of rings, minimum and maximum radius of rings (Rmin and Rmax) and number of pairs of sensors in each ring.

Array	Windows length	Fmin Hz	Fmax Hz	Step	Number of rings	Rmin m	Rmax m	Number of pairs
35 m	70 T	10	40	30	3	12.65	33.99	8
						37.33	48.41	9
						55.17	75.75	9

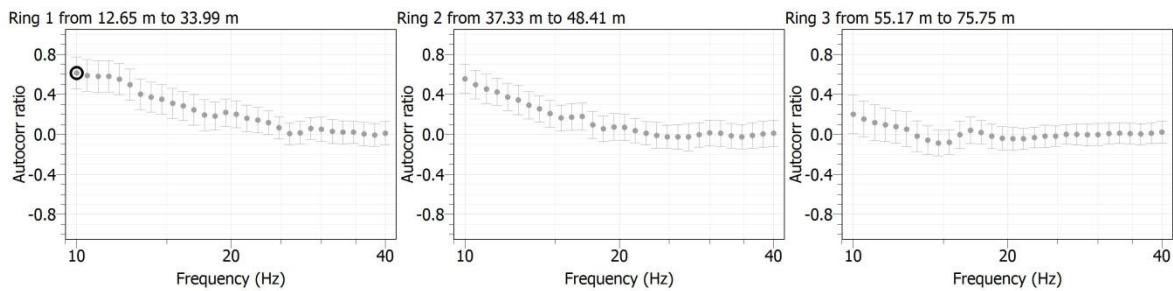


Figure 95: Spatial autocorrelation curves computed for each ring of the 35 m array radius at PYLO site.

3.7.3.3 MASW

The MASW measurements have been done along two profiles. The lengths of the profiles are 46 m (profile 1) and 24 m (profile 2) (see Table 32). For the profile 1, the distance between two geophones is 2 m. The shots were located at both ends (offsets -2 m and 48 m) and in the centre (offset 23 m) of the profile. For the analysis the minimum and maximum distances between source – receiver are 2 m and 48 m respectively. For the profile 2, the length of the profile is 24 m and the distance between two geophones is 1 m. The shots were located at both ends (offsets -2 m and 26 m) and in the centre (offset 11.5 m) of the profile. For the analysis the minimum and maximum distances between source – receiver are 2 m and 12 to 26 m respectively.

The duration of the processing time windows is 1 s. The lowest frequency limit to manually pick the dispersion curve is 20 Hz and the minimum wavelength limits are 23 m for the profile 1 and 12 m for the profile 2. The results are shown in Figure 96. For the PYLO site, ten dispersion curves were manually picked.

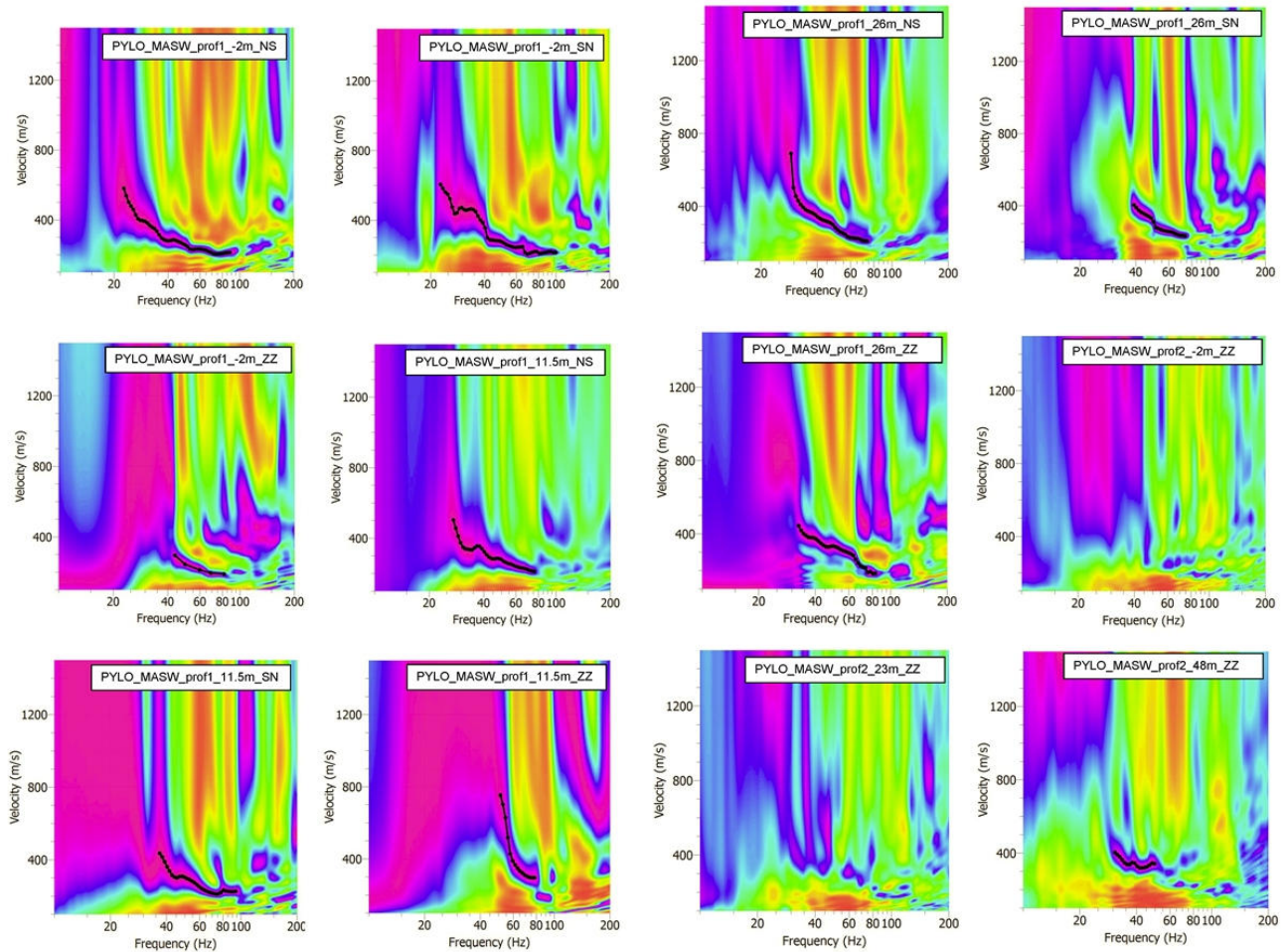


Figure 96: Histogram distributions of phase velocities derived from MASW analysis at PYLO site. The dispersion curves, manually picked, are shown in black dots.

3.7.4 Inversion

Figure 97 shows all dispersion curves derived from AVA and MASW analysis. These curves have been averaged and resampled in order to be inverted (Figure 98). The minimum and maximum wavelengths are 2 m and 120 m respectively. The parameter space for the S-wave velocity profile is defined by the 5-layered soil model described in Table 35. Poisson's ratio ranges between 0.2 and 0.5 for each layer and density is set to 2000 kg/m³. The Vp profile is defined by a gradient soil model (5 layers): Vp velocity ranges between 200 and 5000 m/s, bedrock depth is linked to Vs profile.

The results for the "acceptable models" with misfit equal to two sigma are displayed in Figure 99.

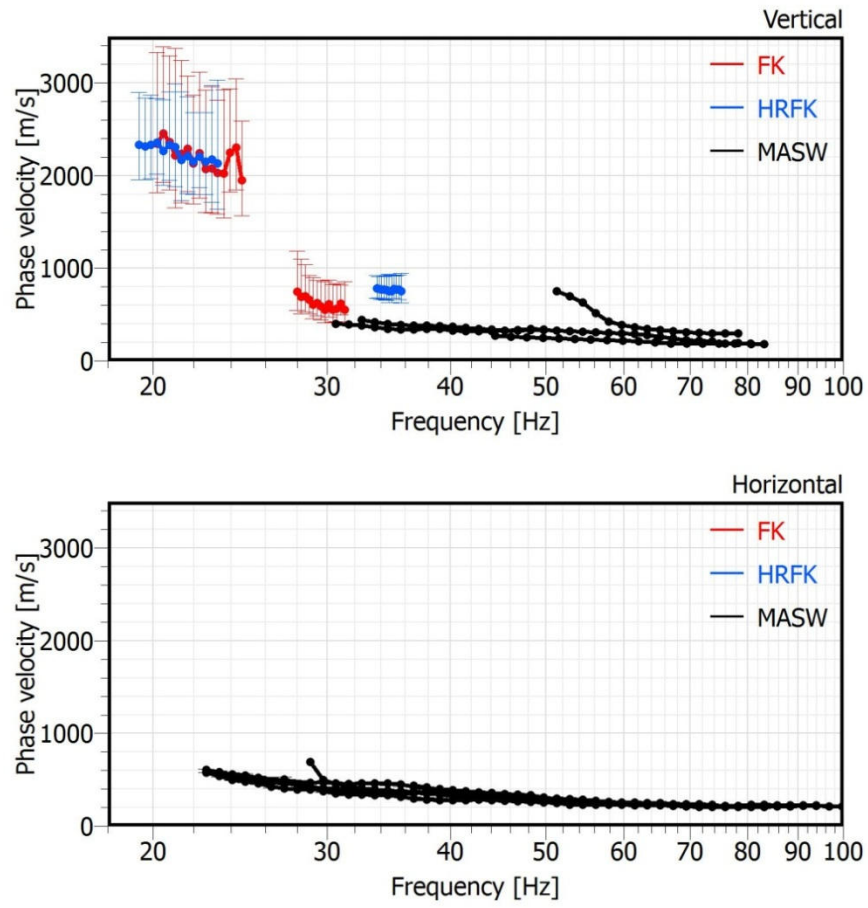


Figure 97: Dispersion curves derived from AVA and MASW analysis at PYLO site.

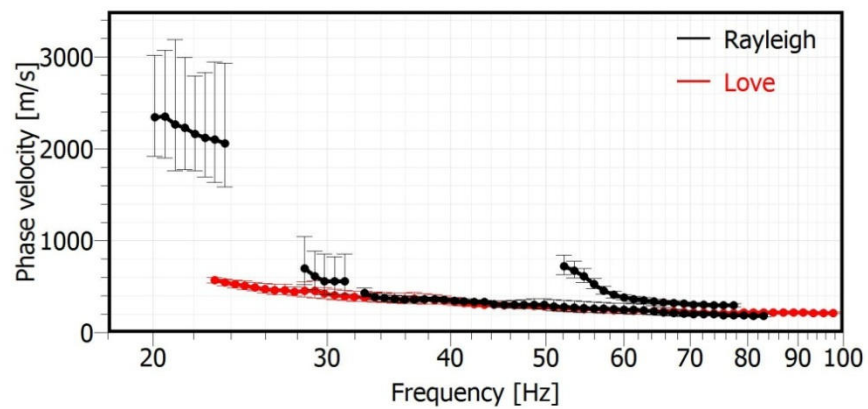


Figure 98: Rayleigh and Love dispersion curves used for the inversion process at PYLO site.

Table 35: Soil parameterization for the 5-layered model of the parameter space at PYLO site.

	Bottom depth (m)		Vs (m/s)	
	Min	Max	Min	Max
Layer 1	0.25	1.25	150	3500
Layer 2	1.25	4.24	150	3500
Layer 3	4.24	13.2	150	3500
Layer 4	13.2	40	150	3500
Layer 5	40	60	150	5000
Half-space	>60		150	5000

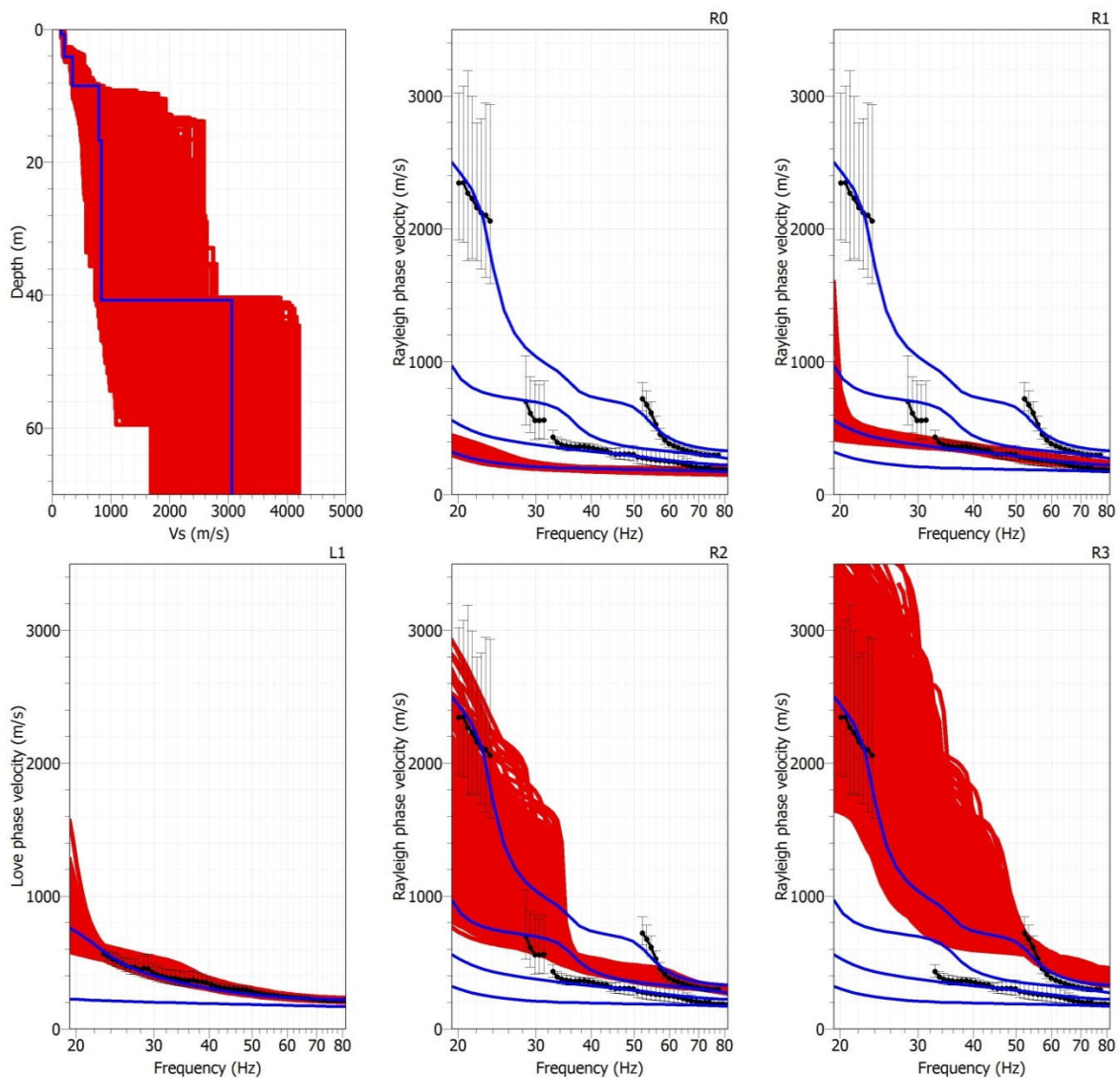


Figure 99: Results for PYLO site: inverted S-wave velocity profile (left) and dispersion curve (right) for the "acceptable models" with misfit equal to two sigma. The Rayleigh and Love waves dispersion curve derived from AVA and MASW analysis are displayed in black dots. Result for the best estimate model (from "classical" inversion) is also shown in blue.

Among the solution shown in Figure 99, one thousand soil profiles having a misfit equal to two sigma were randomly selected in order to compute statistic for Vs30. The associated distribution is displayed in Figure 100. See the section 4.1 for a final estimation of Vs30 and associated uncertainties.

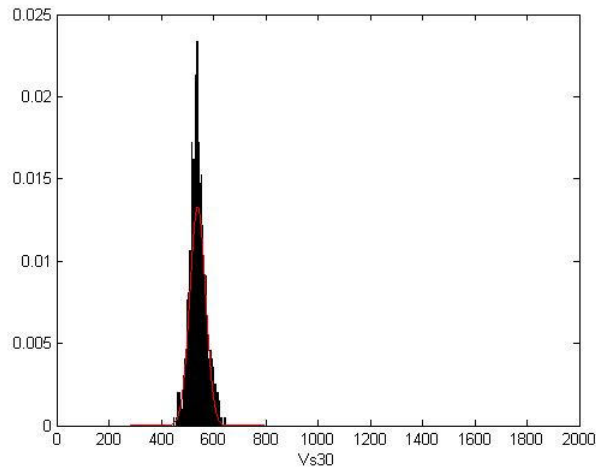


Figure 100: Distribution of Vs30 at PYLO site. The distribution is computed from 1000 soil profiles randomly selected and having a misfit lower equal to two sigma. The theoretical normal distribution is displayed in red.

3.8 EPF

3.8.1 Stations information

3.8.1.1 EPF choice

EPF station is one of the French Strong Motion Network (RAP) in Esparros (Hautes-Pyrénées department). EPF station is has been selected because it is used to reference site in LDG attenuation law, and LDG wanted to better characterise it. It's the accelerometric Pyrenean RAP station which records the most of events.

3.8.1.2 Geographic/Geologic information

Esparros is located in Hautes-Pyrénées department, in the south of Lanmezan. Main characteristics of the site are resumed in Table 36.

Table 36: EPF characteristics

Station	City	Department	X Coord (Long)	Y Coord (Lat)	Network	Site	Slope
EPF	Esparros	Hautes-Pyrénées (65)	0.340559	43.096716	LDG	Col de Coupe	slope

EPF station is set up on rocks, limestone or schist, near Col de Coupe. (Figure 101 to Figure 103).

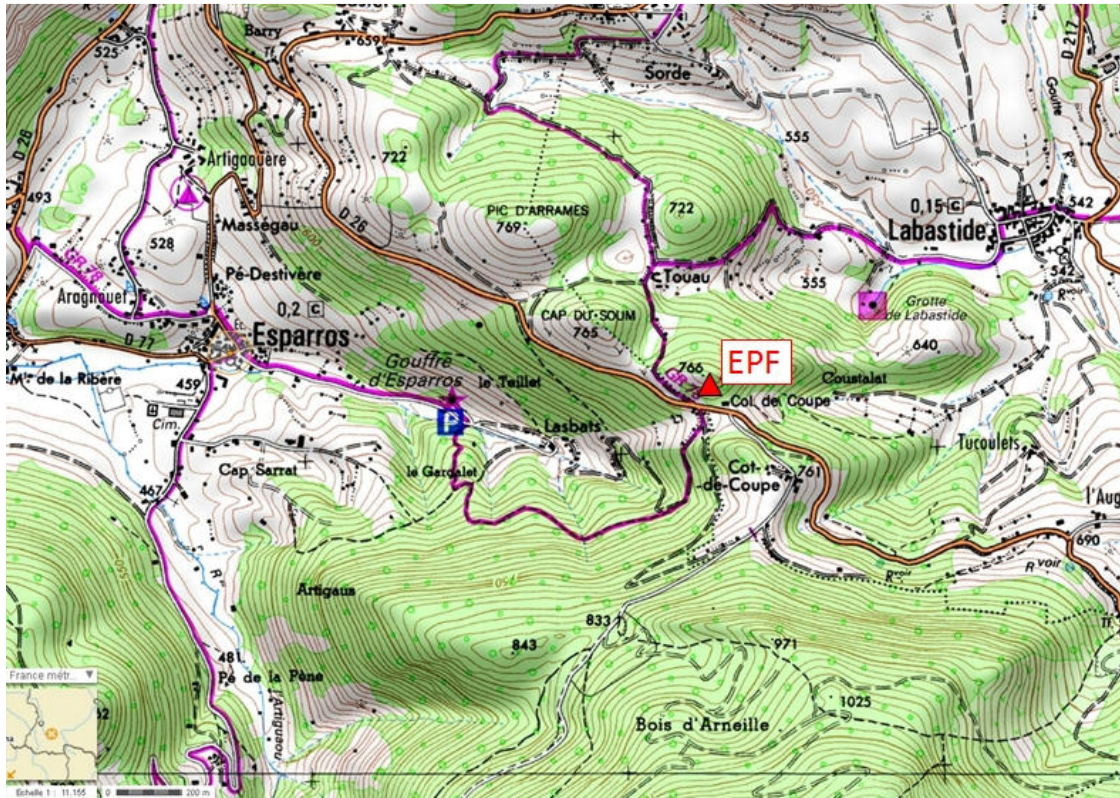


Figure 101 : EPF location near Esparros (IGN Geoportail source)



Figure 102: Picture of EPF site and limestone and schist bedrock, during the measurement on the 12th September 2012.

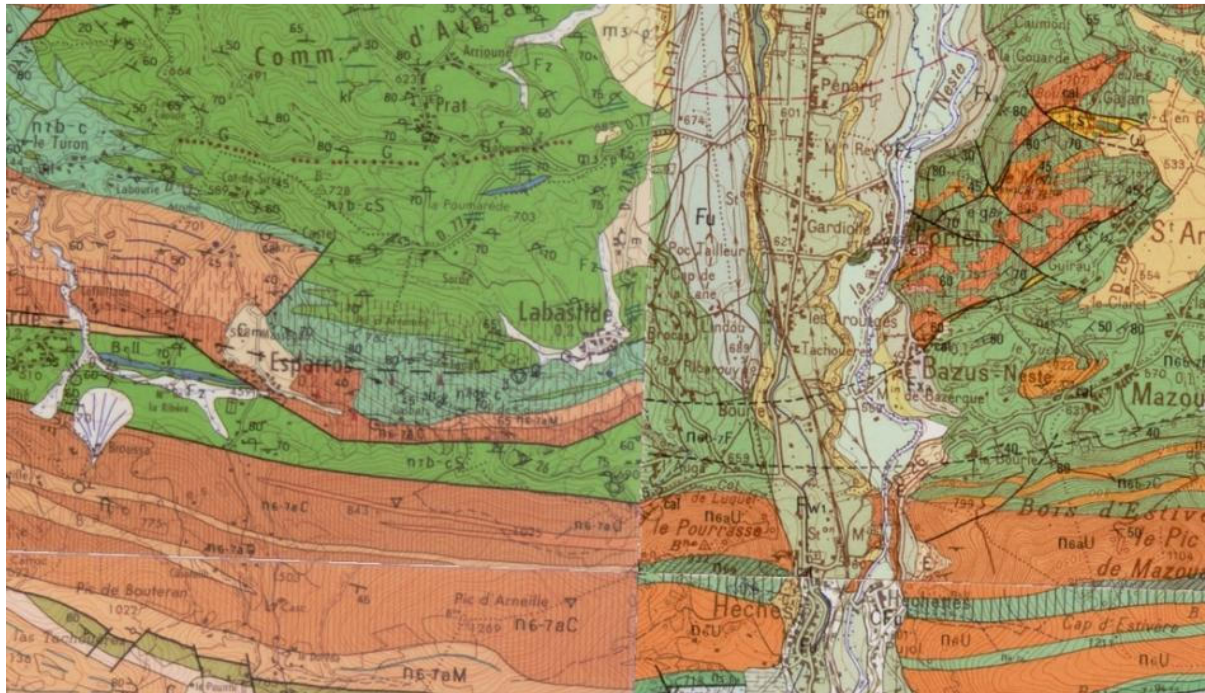


Figure 103: Extract of Esparrros geological map.

3.8.2 Measurements

The measurement survey was performed on 12th September 2012. For Ambient Vibration Array method, one configuration with 2 circles of 10, 30m around a central station (close to EPF station) was performed (8 sensors). For the second method, MASW, one profile was performed (34.5m) just close to EPF station. Weather conditions were very bad during data acquisition, and a lot of technical problems concerning cable sensors occurred. Parameters of these 2 arrays and MASW investigation are presented in Table 37. Location of investigation is showed at Figure 104.

Table 37: EPF recording parameters, 12th September 2012

Measurments	Numbers of Sensors	Beginning (TU)	End (TU)	Noise/ environnement	Topography	Weather conditions
Array R = 10m	8	10:10:00	11:35:00	No urban	Flat,	Rain++
Array R =30m	8	14:50:00	15:45:00	No urban	Flat	Rain++
MASW N70E 34.5m, Dx = 1.5m	24 geophones (H and V)	12:00:00	13:00:00	No noise	Flat, (embankment)	good

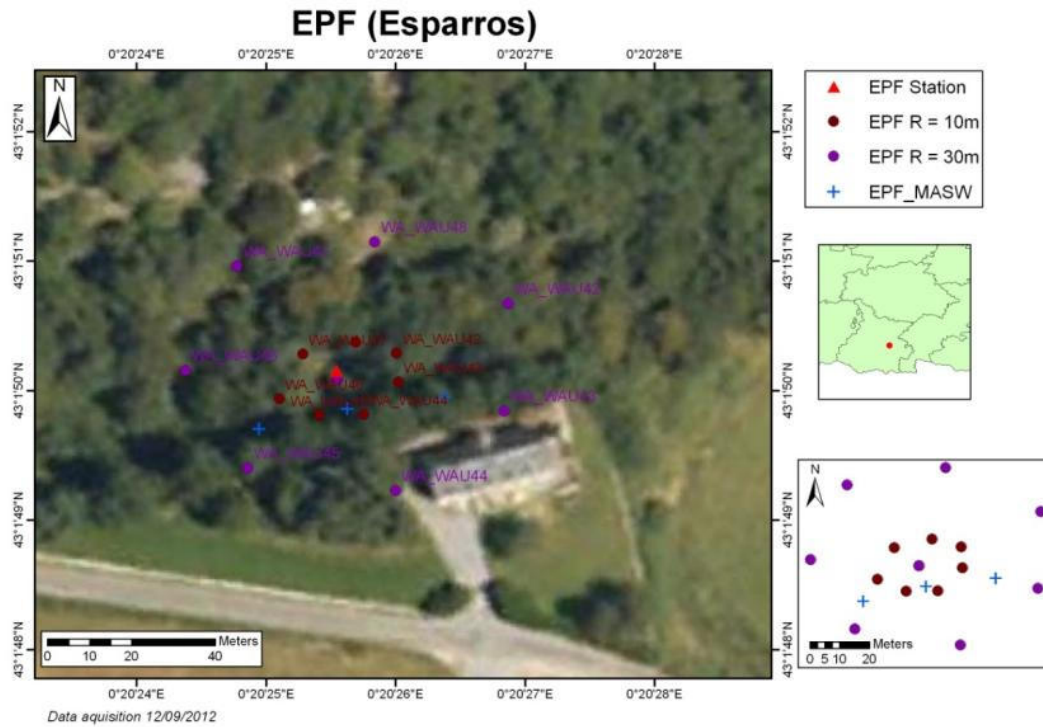


Figure 104: location of the arrays, the MASW shots and EPF Station.

3.8.3 Processing

3.8.3.1 H/V

The Fourier spectra amplitudes computed on the three component records of ambient vibrations at each EPF array receiver are shown in Figure 105. The corresponding H/V curves are displayed in Figure 106. Most H/V curves are almost flat below 20 Hz. Some H/V curves have large amplitude over a broad frequency range.

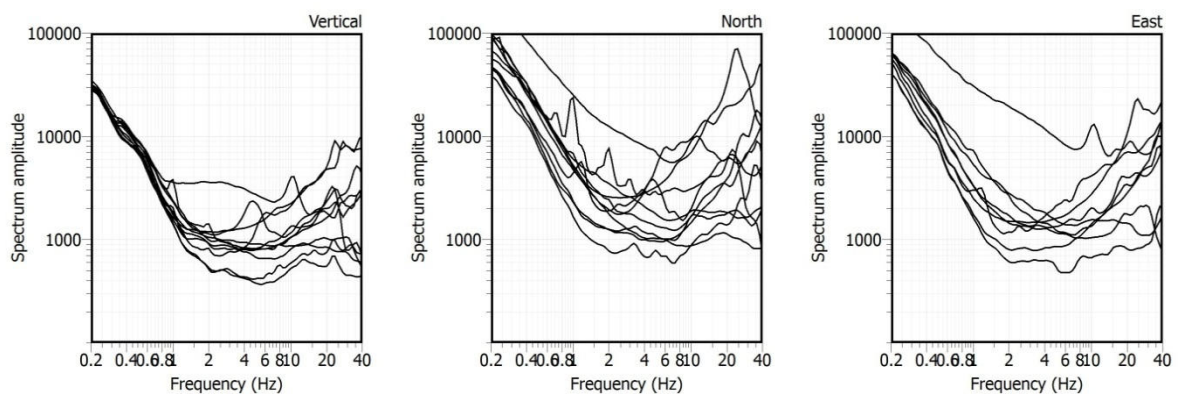


Figure 105: Amplitude of the Fourier spectra computed on 3-C recordings of ambient vibrations at each EPF array receiver.

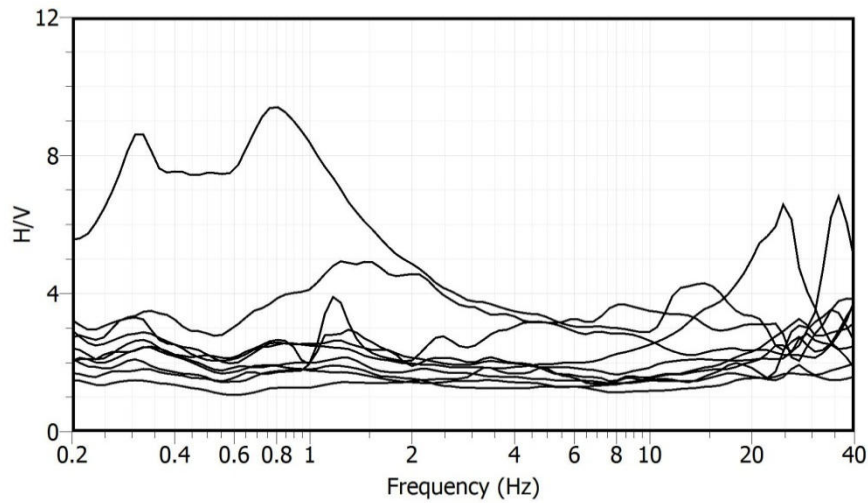


Figure 106: H/V amplitude at each EPF array receiver.

3.8.3.2 AMV

The parameters used for FK and HRFK analysis at EPF site are described in Table 38.

Table 38: EPF FK and HRFK analysis parameters: array radius (Array), windows length according to the centre period of the frequency band T (Windows length), minimum and maximum (central) frequencies (Fmin and Fmax), number of frequency sample (Step), anti-aliasing limits kmin and kmax, fk grid resolution (Grid step), maximum search radius for the fk grid (Grid size), minimum velocity and half-bandwidth for the frequency band (Band width).

Array	Windows length	Fmin Hz	Fmax Hz	Step	Kmin rad/m	Kmax rad/m	Grid step rad/m	Grid size rad/m	Vmin m/s	Band width
FK										
10 m	70 T	10	40	30	0.2715	0.5646	0.0678	1.129	150	0.1
30 m	150 T	2	40	30	0.0797	0.2296	0.0254	0.480	150	0.1
HRFK										
10 m	70 T	10	40	20	0.2715	0.5646	0.0136	1.129	150	0.1
30 m	200 T	12	20	50	0.0797	0.2296	0.0051	0.480	400	0.02

FK

The histogram distributions of phase velocities estimation of Rayleigh waves derived from the ensemble of the wave-propagation estimates obtained for each individual time-frequency cell using the FK method are shown in Figure 107 for EPF arrays. It was not possible to derive Rayleigh dispersion curve from the FK analysis.

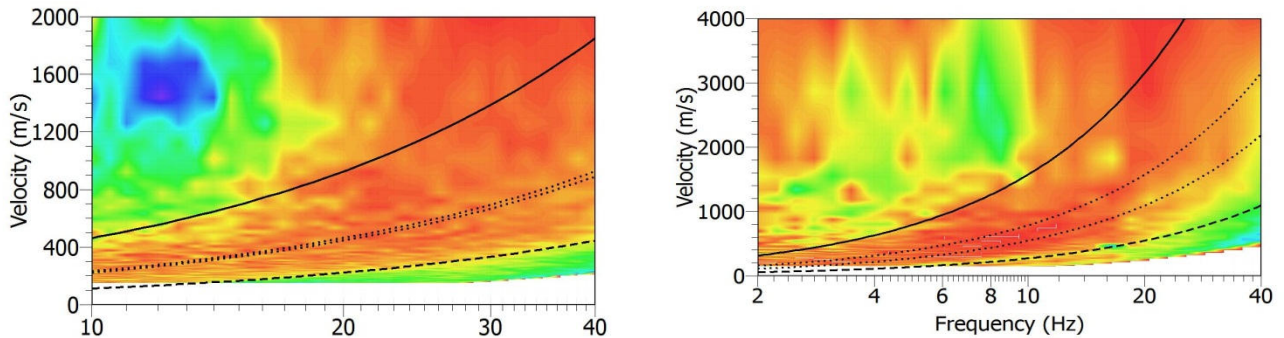


Figure 107: Results for the 10 m (left) and 30 m (right) radius arrays at EPF site (vertical component): histogram distributions of phase velocities derived from the ensemble of the wave-propagation estimates obtained for each individual time-frequency cell using the FK method (color scale: red and magenta colors indicate min and max values, respectively). The anti-aliasing limits for each array configuration are also shown: thick line ($k_{min}/2$), dotted lines (k_{min} and $k_{max}/2$) and dashed line (k_{max}).

HRFK

The resulting estimation of Rayleigh waves phase velocities are shown in Figure 108 for EPF arrays. It was not possible to derive Rayleigh dispersion curve from the HRFK analysis.

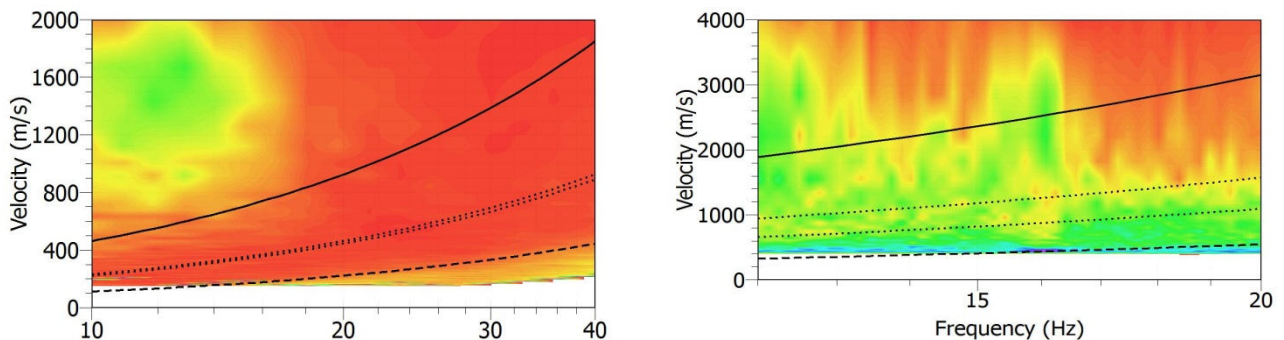


Figure 108: Results for the 10 m (left) and 30 m (right) radius arrays at EPF site (vertical component): histogram distributions of phase velocities derived from the ensemble of the wave-propagation estimates obtained for each individual time-frequency cell using the HRFK method (color scale: red and magenta colors indicate min and max values, respectively). The anti-aliasing limits for each array configuration are also shown: thick line ($k_{min}/2$), dotted lines (k_{min} and $k_{max}/2$) and dashed line (k_{max}).

SPAC

The parameters used for the SPAC analysis for the 30 m array at EPF site are described in Table 39. The computed spatial autocorrelation coefficients are displayed for each ring in the Figure 109. These autocorrelation coefficients don't lead to estimate reliable dispersion curve.

Table 39: EPFSPAC analysis parameters: array radius (Array), windows length according to the centre period of the frequency band T (Windows length), minimum and maximum (central) frequencies (Fmin and Fmax), number of frequency sample (Step), number of rings, minimum and maximum radius of rings (Rmin and Rmax) and number of pairs of sensors in each ring.

Array	Windows length	Fmin Hz	Fmax Hz	Step	Nimber of rings	Rmin m	Rmax m	Number of pairs
30 m	150 T	2	30	50	2	26.96 47.98	34.95 73.45	8 6

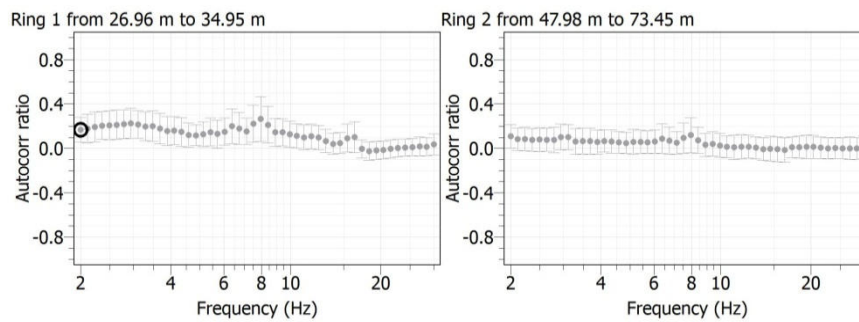


Figure 109: Spatial autocorrelation curves computed for each ring of the 30 m array radius at EPF site.

3.8.3.3 MASW

The MASW measurements have been done along one profile. The length of the profile is 34.5 m and the distance between two geophones is 1.5 m (see Table 37). The shots were located at both ends (offsets -2 m and 36.5 m) and in the centre (offset 17.25 m) of the profile. For the analysis the minimum and maximum distances between source – receiver are 2 m and 37 m respectively. The duration of the processing time windows is 1 s. The lowest frequency limit to manually pick the dispersion curve is set to 15 Hz and the minimum wavelength limit is 17 m. The results are shown in Figure 110. For the EPF site, eight dispersion curves were manually picked.

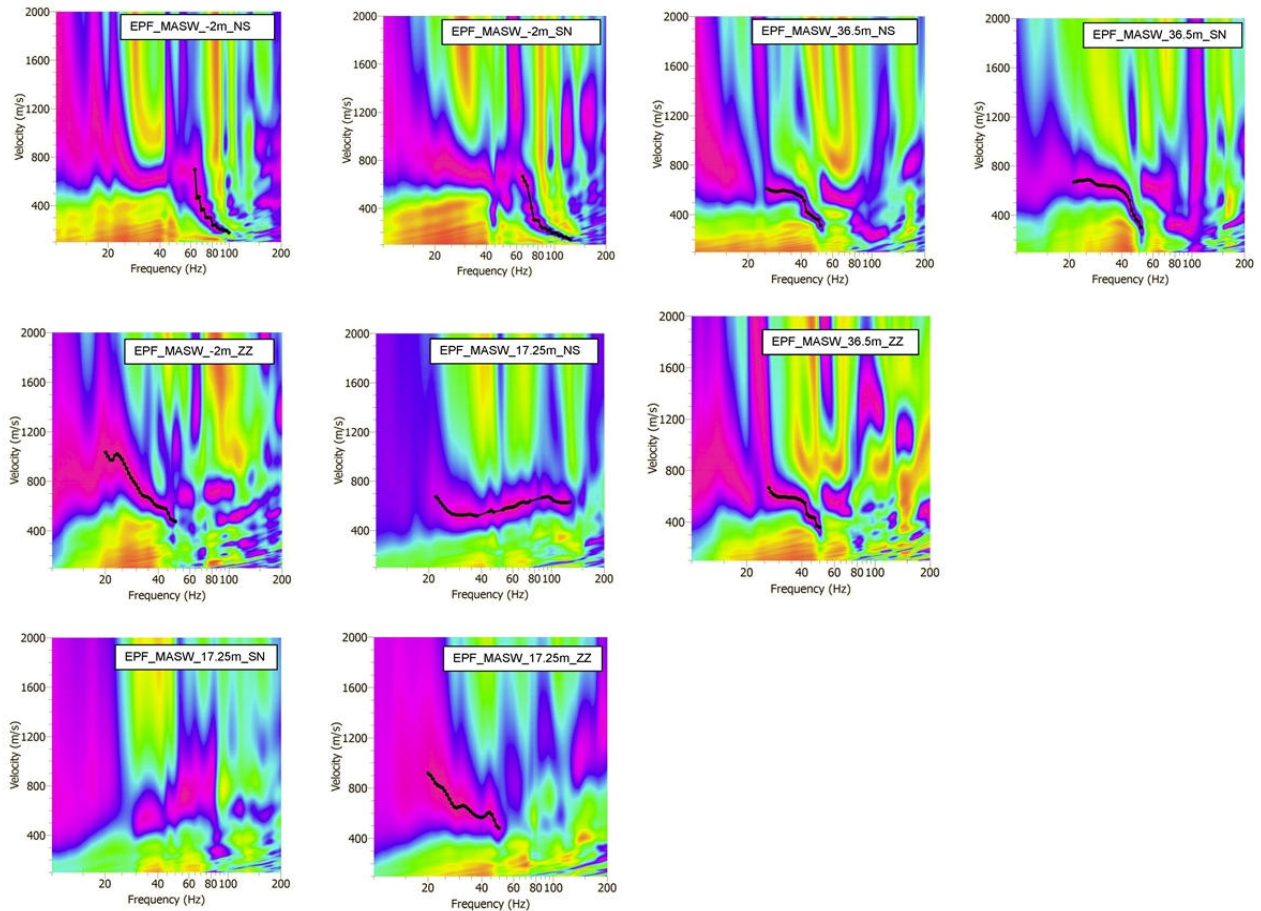


Figure 110: Histogram distributions of phase velocities derived from MASW analysis at EPF site. The dispersion curves, manually picked, are shown in black dots.

3.8.4 Inversion

Figure 111 shows all dispersion curves derived from MASW analysis. These curves have been averaged and resampled in order to be inverted (Figure 112). The minimum and maximum wavelengths are 7 m and 50 m respectively. The parameter space for the S-wave velocity profile is defined by the 5-layered soil model described in

Table 40. Poisson's ratio ranges between 0.2 and 0.5 for each layer and density is set to 2000 kg/m³. The Vp profile is defined by a gradient soil model (5 layers): Vp velocity ranges between 200 and 5000 m/s, bedrock depth is linked to Vs profile.

The results for the "acceptable models" with misfit equal to two sigma are displayed in Figure 113. The investigation depth is shallow (25 m) because Rayleigh and Love wave dispersion curves are based only on MASW analysis. The Vs profile is thus truncated at 25 m deep.

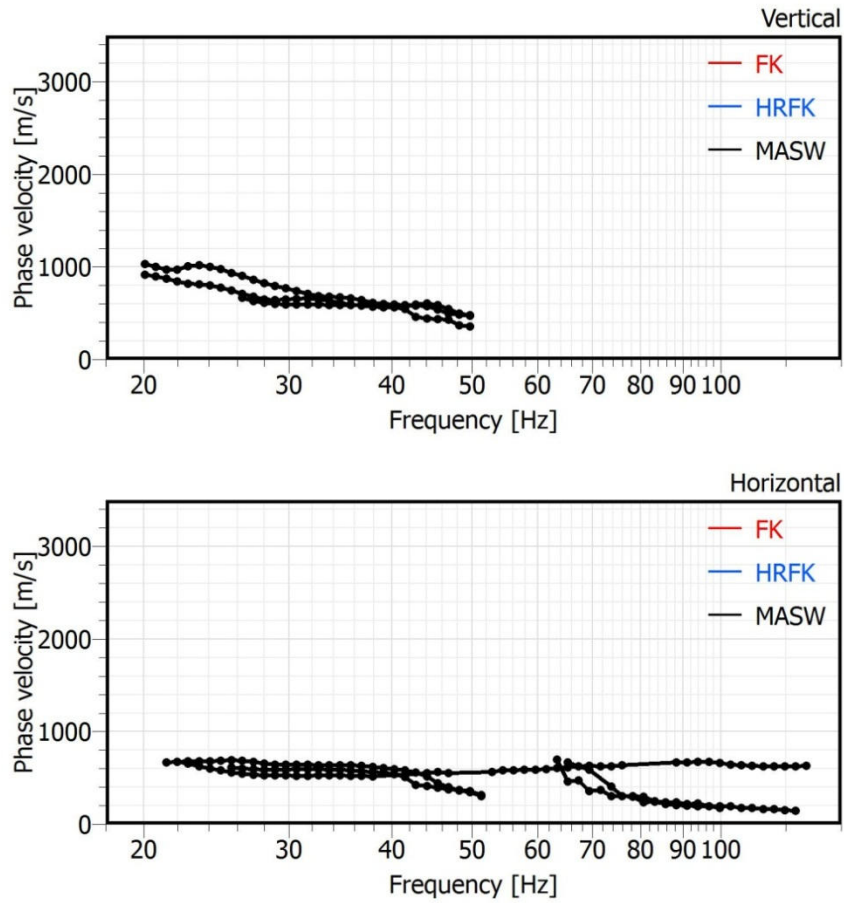


Figure 111: Dispersion curves derived from MASW analysis at EPF site.

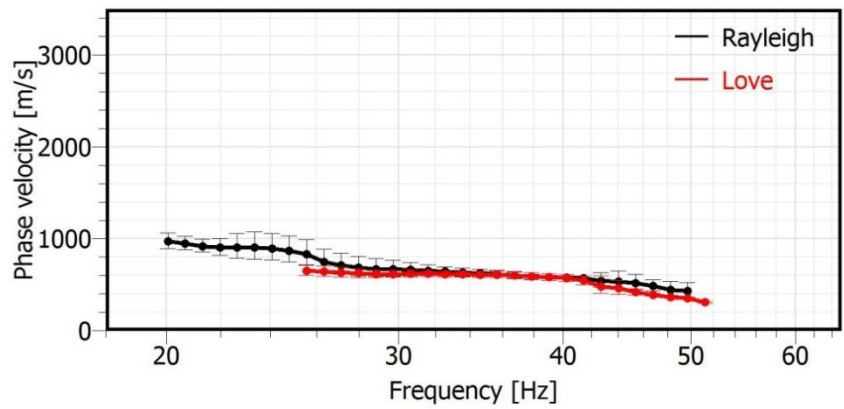


Figure 112: Rayleigh and Love dispersion curves used for the inversion process at EPF site.

Table 40: Soil parameterization for the 5-layered model of the parameter space at EPF site.

	Bottom depth (m)		Vs (m/s)	
	Min	Max	Min	Max
Layer 1	0.875	3.10	150	3500
Layer 2	3.10	6.54	150	3500
Layer 3	6.54	11.84	150	3500
Layer 4	11.84	20.03	150	3500
Layer 5	20.03	25	150	3500
Half-space	> 25		150	3500

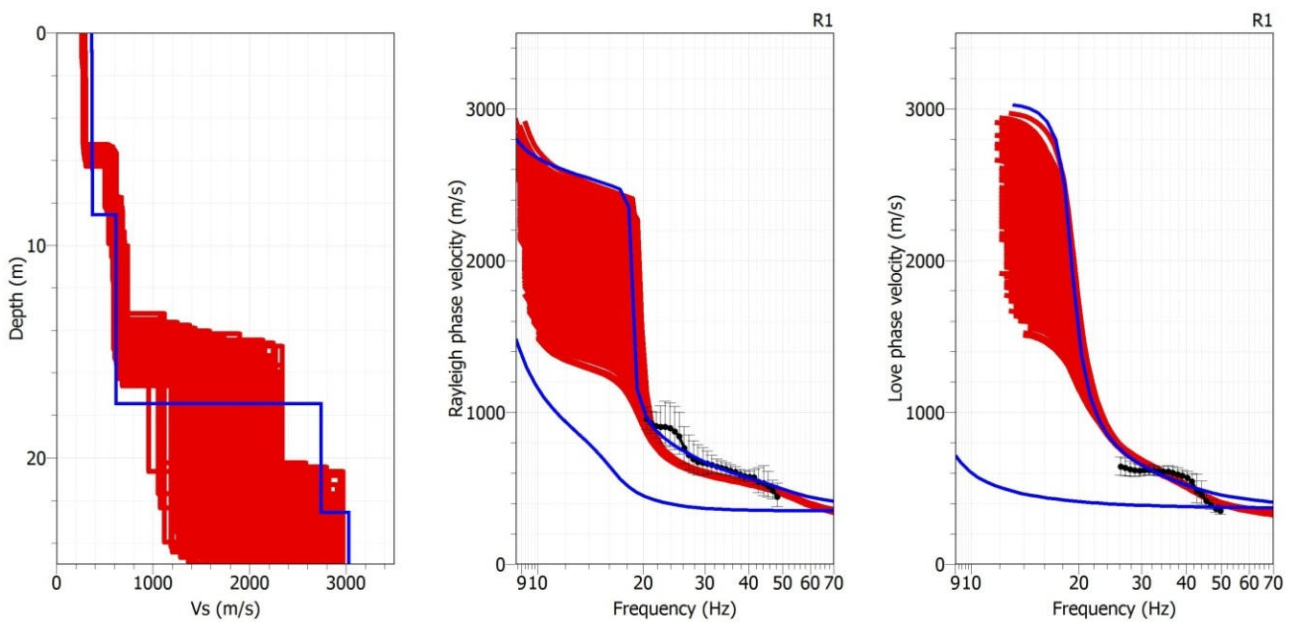


Figure 113: Results for EPF site: inverted S-wave velocity profile (left) and dispersion curve (right) for the "acceptable models" with misfit equal to two sigma. The Rayleigh and Love waves dispersion curve derived from MASW analysis are displayed in black dots. Result for the best estimate model (from "classical" inversion) is also shown in blue.

For EPF site the investigation depth is too shallow (25 m) to be able to calculate accurate Vs30. See the section 4.1 for a final estimation of Vs30 and associated uncertainties.

3.9 PYAT

3.9.1 Stations information

3.9.1.1 PYAT choice

PYAT station is of the French Strong Motion Network (RAP) in Arrette (Atlantic Pyrenean). It had be retained in this project because of his position in the line of Nord-Pyrenean fault, in the boundary front between North part and south part of Pyrenean chain (Figure 2). It records a lot of events, with high PGA.

3.9.1.2 PYAT topography and geology

Arette is located in Pyrenean Atlantic department, at the south of Pau. Main characteristic of the site is resumed in Table 41.

Table 41: main characteristic of PYAT station location

Station	Town	Department	X Coord (Long)	Y Coord (Lat)	Network	Site	Slope
PYAT	Arette	Pyrénées-Atlantiques (64)	-0.713055	43.094172	OMP - RAP	Pyrenean valley	At the bottom of pronounced bank

It is located at the bottom of shisto-marls of Albién formation, above the sedimentary valley (Fig X). Topography is quite important in Arette, and on the investigation scale too (about 40 m in Z). PYAT station is set up in free field, in a little wood shelter (Figure 114 to Figure 117).

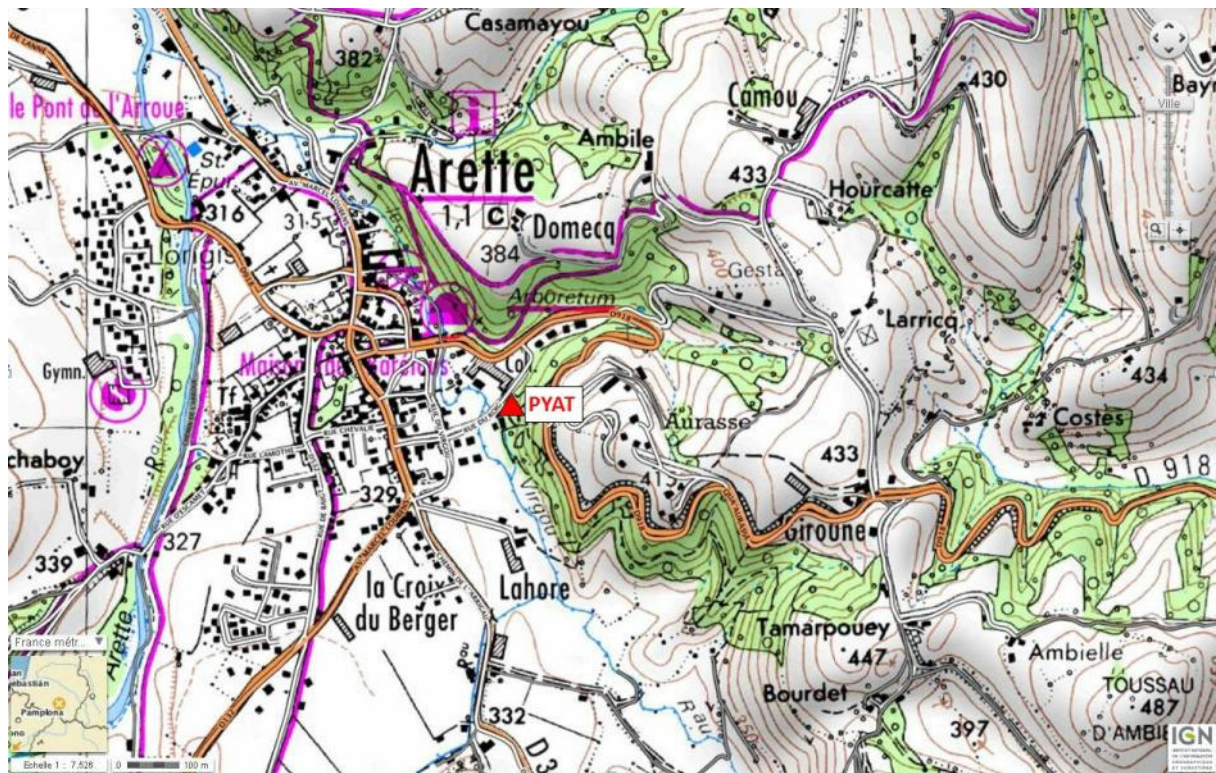


Figure 114: PYAT location in Arette (IGN Geoportail source).



Figure 115: Picture of the site PYAT, during the measurement on the 12th September 2012.

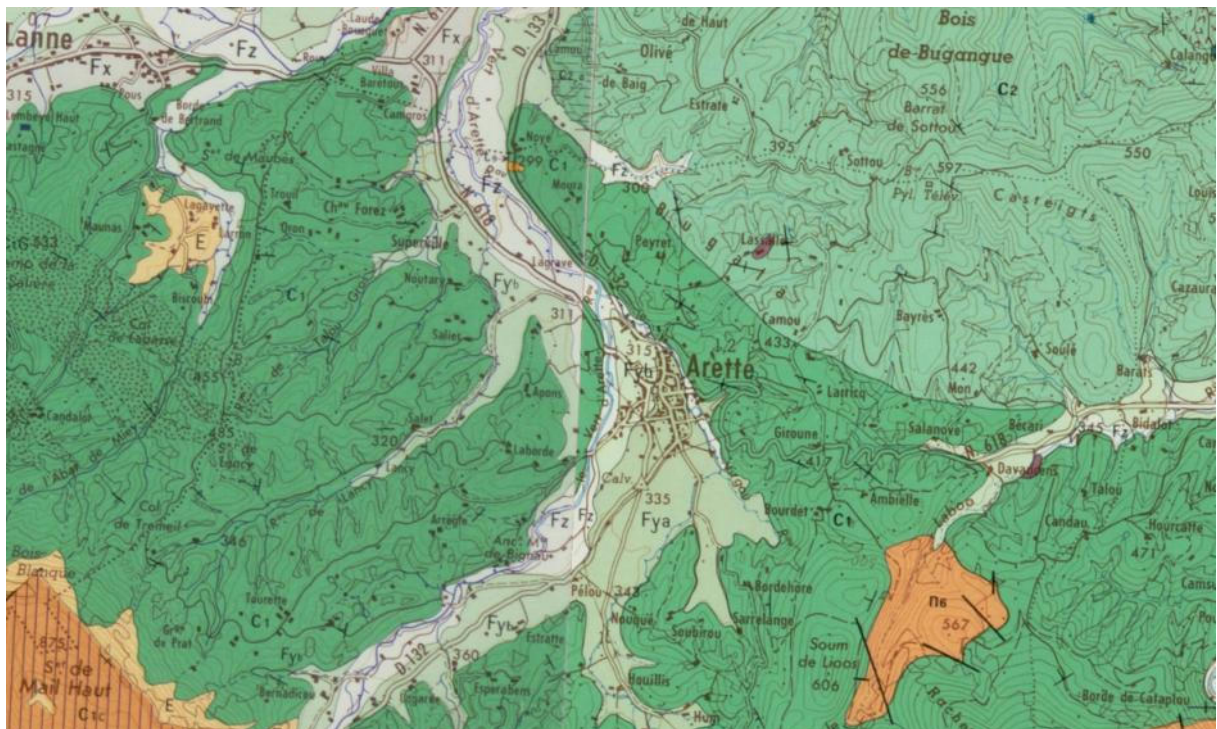


Figure 116: Extract of Arette geologic map (dark green : Albian spicules "schisto-marls à spicules").



Figure 117: zoom on Albian Formation

3.9.2 Measurements

The measurement survey was performed on 12th September 2012. For the first method, Ambient Vibration Arrays, one configuration with 3 circles of 10, 40 and 100m around a central station (near real PYAT station) was performed (8 sensors). For the second method, MASW, one 34.5 m profile was done, with Rayleigh and Love waves recording. Parameters of these 3 arrays and MASW investigation are presented in Table 42.

Table 42: PYAT recording parameters, 12th September 2012.

Measurments	Numbers of Sensors	Beginning (TU)	End (TU)	Noise/ environnement	Topography	Weather conditions
Array R = 10m	8	09:50:00	10:28:00	Mid-urban	slope	Rain, wind
Array R = 40m	8	11:53:00	13:05:00	Mid-urban	slope	Rain, wind
Array R = 100m	8	15:39:00	16:43:00	Mid-urban	slope	sun
MASW N44°E 34.5m, Dx = 1.5m	24 géophones (H and V)	11:10:00	11:50:00	Quiet	slope	Rain, wind

Even if PYAT morphology is complex, sensors were implemented as soon as possible next to the accelerometric station. So, the slope of site measurement was relatively important and vegetation was heavy. Location of investigation is showed a Figure 118. All coordinates are available in Appendix.

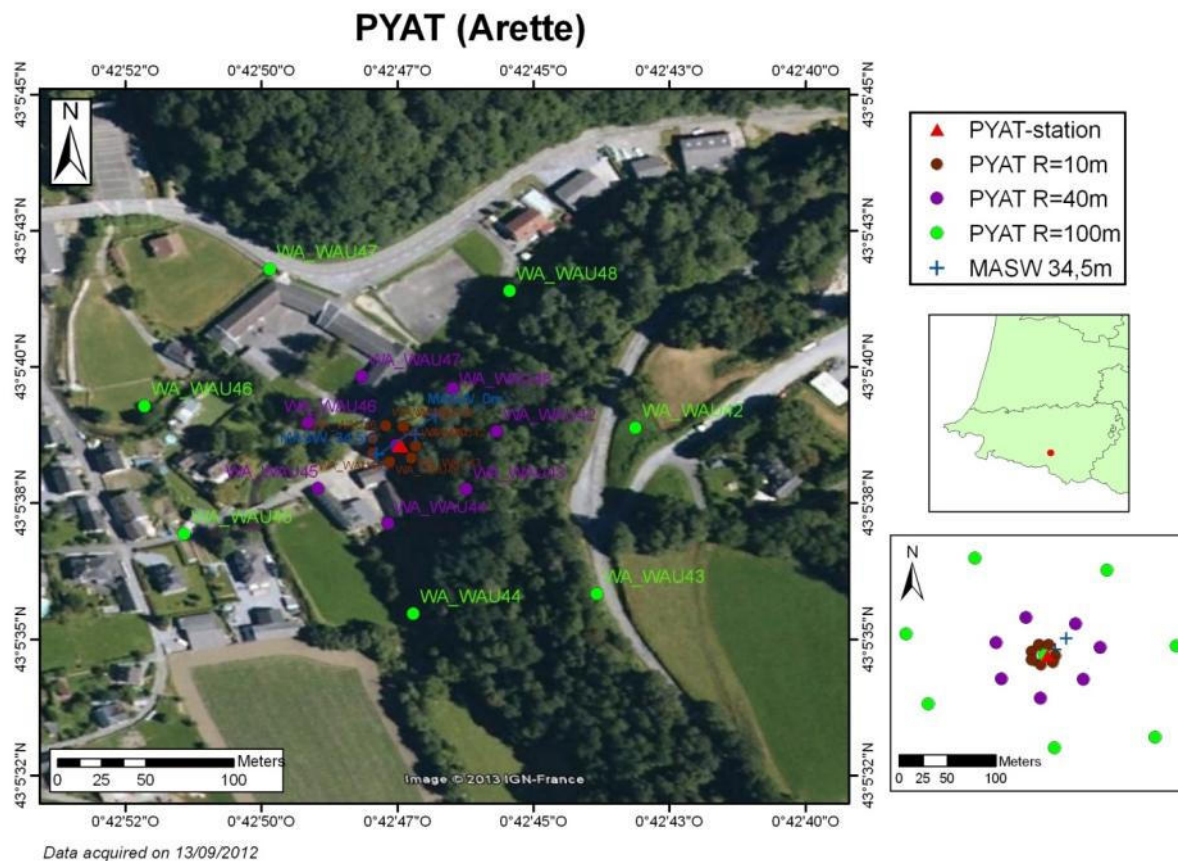


Figure 118: location of the arrays, the MASW shots and the PYAT Station

3.9.3 Processing

3.9.3.1 H/V

The Fourier spectra amplitudes computed on the three component records of ambient vibrations at each PYAT array receiver are shown in Figure 119. The corresponding H/V curves are displayed in Figure 120. H/V curves exhibit peaks but their frequencies vary a lot from one sensor to the other.

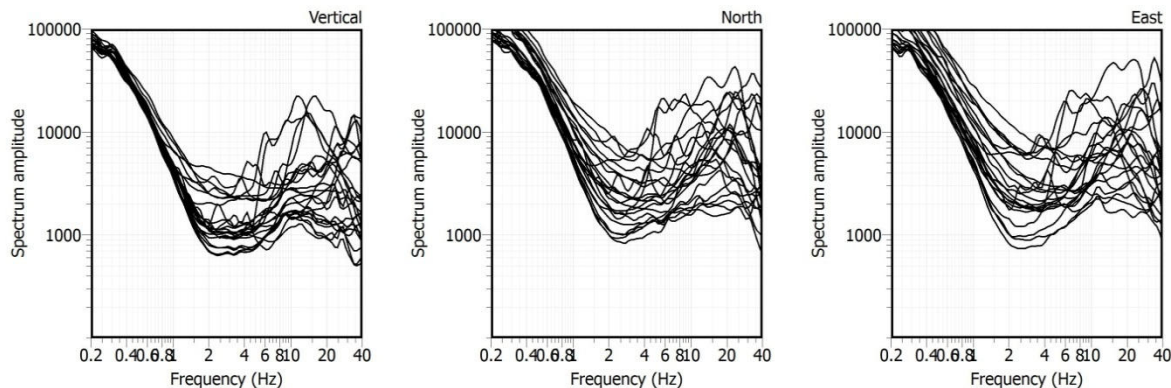


Figure 119: Amplitude of the Fourier spectra computed on 3-C recordings of ambient vibrations at each PYAT array receiver

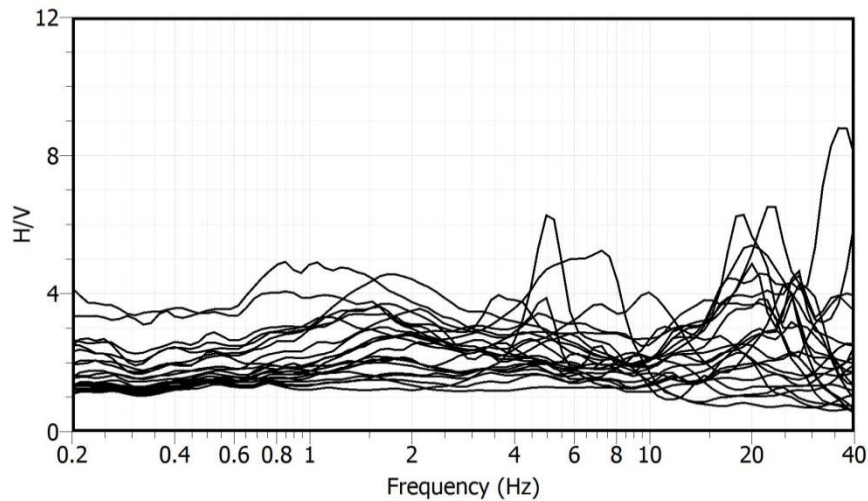


Figure 120: H/V amplitude at each PYAT array receiver

3.9.3.2 AMV

The parameters used for FK and HRFK analysis at PYAT site are described in Table 43.

Table 43: PYAT FK and HRFK analysis parameters: array radius (Array), windows length according to the centre period of the frequency band T (Windows length), minimum and maximum (central) frequencies (Fmin and Fmax), number of frequency sample (Step), anti-aliasing limits kmin and kmax, fk grid resolution (Grid step), maximum search radius for the fk grid (Grid size), minimum velocity and half-bandwidth for the frequency band (Band width).

Array	Window s length	Fmin Hz	Fmax Hz	Step	Kmin rad/m	Kmax rad/m	Grid step rad/m	Grid size rad/m	Vmin m/s	Band width
FK										
10 m	70 T	20	40	50	0.2290	0.5393	0.0573	1.079	150	0.1
40 m	70 T	10	20	50	0.0594	0.1540	0.0149	0.308	150	0.1
100 m	200 T	5	8	50	0.0242	0.0678	0.0061	0.136	150	0.1
HRFK										
10 m	50 T	20	40	30	0.2290	0.5393	0.0115	1.079	150	0.1
40 m	200 T	15	20	50	0.0594	0.1540	0.0030	0.308	150	0.02
100 m	200 T	5	12	100	0.0242	0.0678	0.0012	0.136	150	0.1

FK

The histogram distributions of phase velocities estimation of Rayleigh waves derived from the ensemble of the wave-propagation estimates obtained for each individual time-frequency cell using the FK method are shown in Figure 121 for PYAT arrays. Rayleigh dispersion curves were determined for the 10 m and 100 m radius arrays. It was not possible to derived dispersion curve from the 40 m radius array.

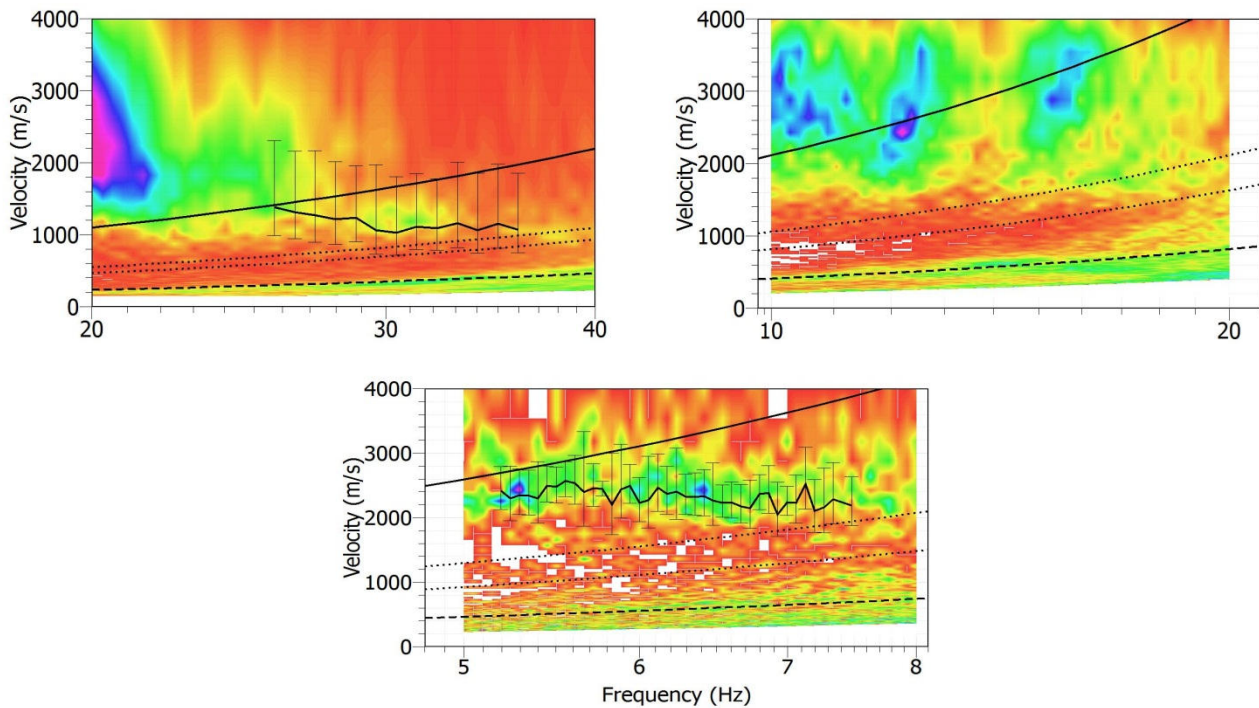


Figure 121: Results for the 10 m (top-left), 40 m (top-right) and 100 m (bottom) radius arrays at PYAT site (vertical component): histogram distributions of phase velocities derived from the ensemble of the wave-propagation estimates obtained for each individual time-frequency cell using the FK method (color scale: red and magenta colors indicate min and max values, respectively). The anti-aliasing limits for each array configuration are also shown: thick line ($k_{min}/2$), dotted lines (k_{min} and $k_{max}/2$) and dashed line (k_{max}).

HRFK

The resulting estimation of Rayleigh waves phase velocities are shown in Figure 122 for PYAT arrays. Rayleigh dispersion curves were determined only for the 100 m radius array. It was not possible to derived dispersion curve from the other radius arrays.

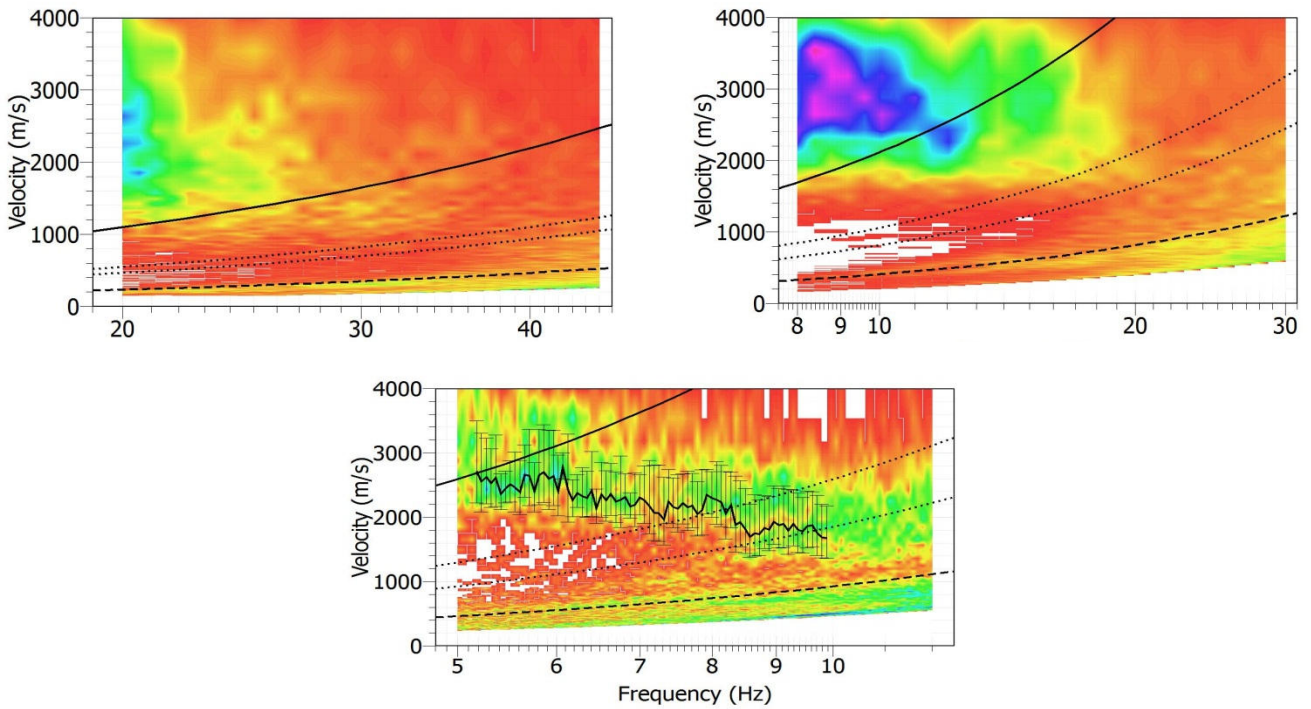


Figure 122: Results for the 10 m (top-left), 40 m (top-right) and 100 m (bottom) radius arrays at PYAT site (vertical component): histogram distributions of phase velocities derived from the ensemble of the wave-propagation estimates obtained for each individual time-frequency cell using the HRFK method (color scale: red and magenta colors indicate min and max values, respectively). The anti-aliasing limits for each array configuration are also shown: thick line ($k_{min}/2$), dotted lines (k_{min} and $k_{max}/2$) and dashed line (k_{max}).

SPAC

The parameters used for the SPAC analysis for the 100 m array at PYAT site are described in Table 44. The computed spatial autocorrelation coefficients are displayed for each ring in the Figure 123. These autocorrelation coefficients don't lead to estimate reliable dispersion curve.

Table 44: PYATSPAC analysis parameters: array radius (Array), windows length according to the centre period of the frequency band T (Windows length), minimum and maximum (central) frequencies (F_{min} and F_{max}), number of frequency sample (Step), number of rings, minimum and maximum radius of rings (R_{min} and R_{max}) and number of pairs of sensors in each ring.

Array	Windows length	Fmin Hz	Fmax Hz	Step	Number of rings	Rmin m	Rmax m	Number of pairs
100 m	200 T	4	20	30	2	75.01 156.13	135.25 261.60	14 14

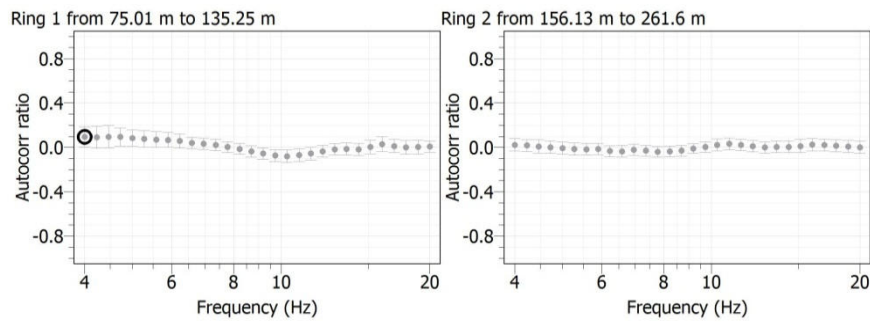


Figure 123: Spatial autocorrelation curves computed for each ring of the 30 m array radius at PYAT site.

3.9.3.3 MASW

The MASW measurements have been done along one profile. The length of the profile is 34.5 m and the distance between two geophones is 1.5 m (see Table 42). The shots were located at both ends (offsets -2 m and 36.5 m) and in the centre (offset 17.25 m) of the profile. For the analysis the minimum and maximum distances between source – receiver are 2 m and 37 m respectively. The duration of the processing time windows is 1 s. The lowest frequency limit to manually pick the dispersion curve is set to 50 Hz and the minimum wavelength limit is 18 m. The results are shown in Figure 124. For the PYAT site, only four dispersion curves were manually picked.

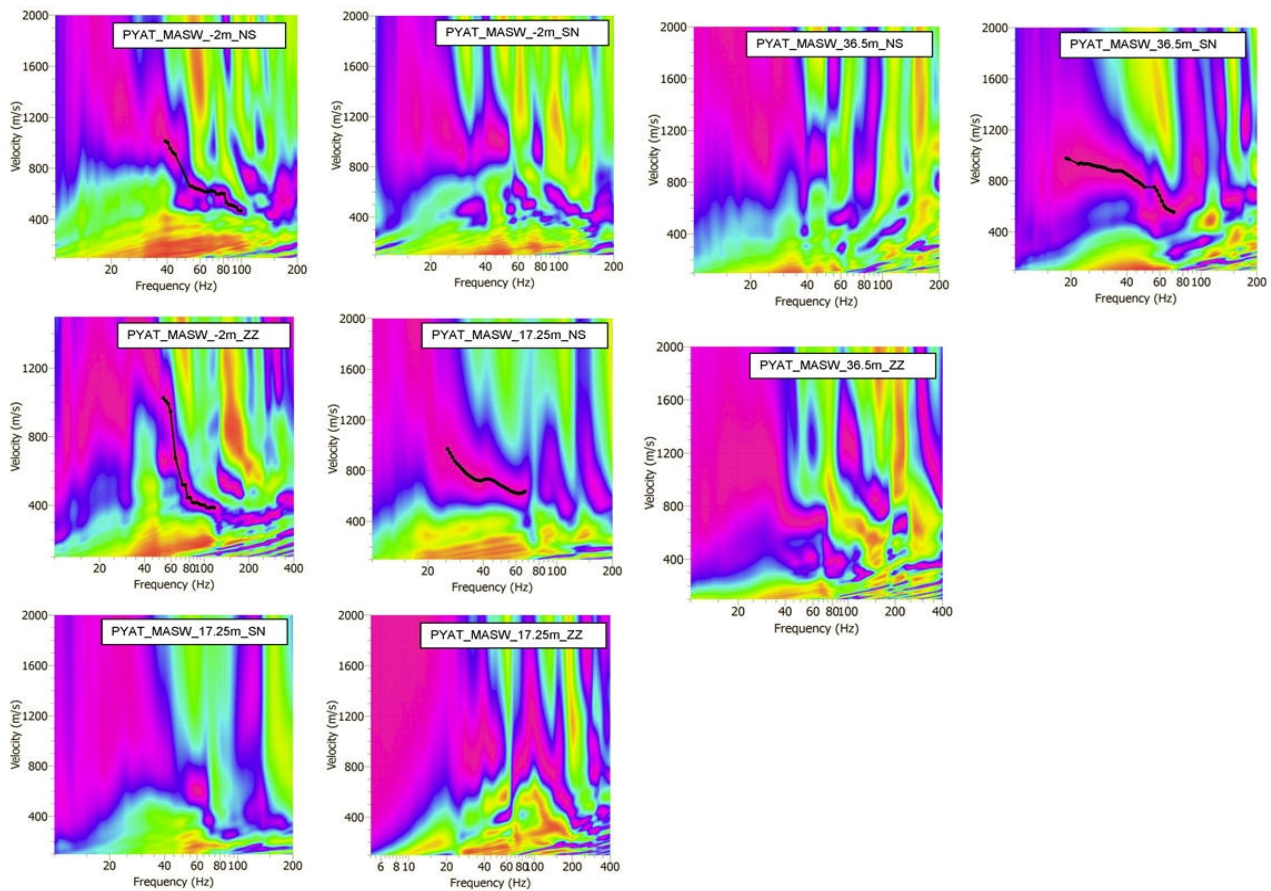


Figure 124: Histogram distributions of phase velocities derived from MASW analysis at PYAT site. The dispersion curves, manually picked, are shown in black dots.

3.9.4 Inversion

Figure 125 shows all dispersion curves derived from AVA and MASW analysis. These curves have been averaged and resampled in order to be inverted (Figure 126). The minimum and maximum wavelengths are 3 m and 525 m respectively. The parameter space for the S-wave velocity profile is defined by the 5-layered soil model described in Table 45. Poisson's ratio ranges between 0.2 and 0.5 for each layer and density is set to 2000 kg/m³. The Vp profile is defined by a gradient soil model (5 layers): Vp velocity ranges between 200 and 5000 m/s, bedrock depth is linked to Vs profile.

The results for the "acceptable models" with misfit equal to one sigma are displayed in Figure 127.

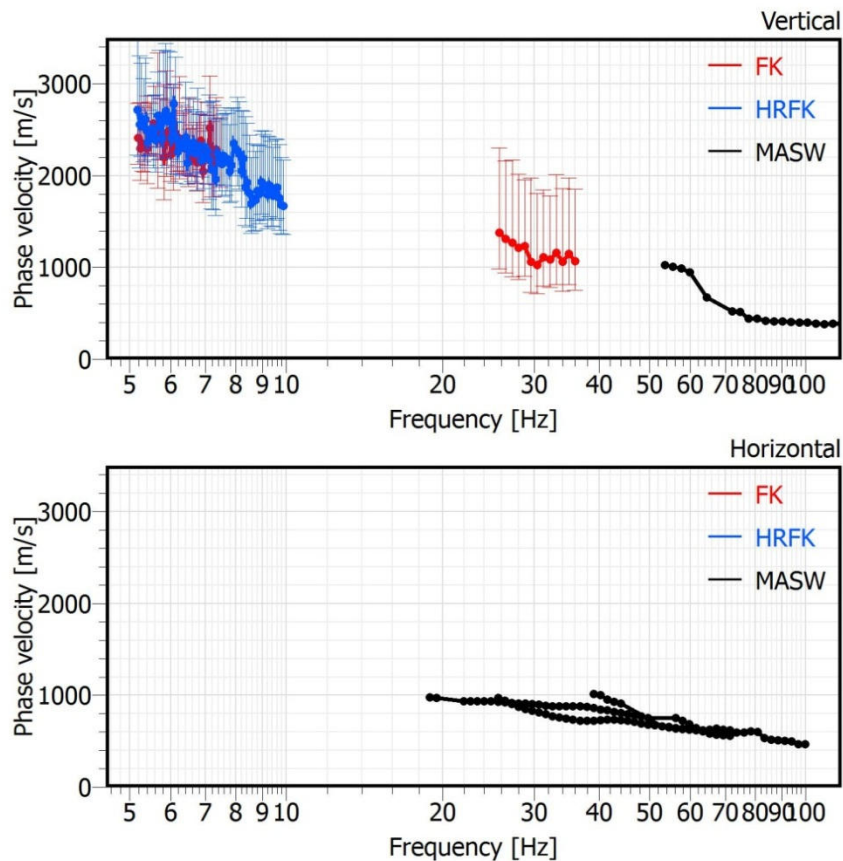


Figure 125: Dispersion curves derived from AVA and MASW analysis at PYAT site.

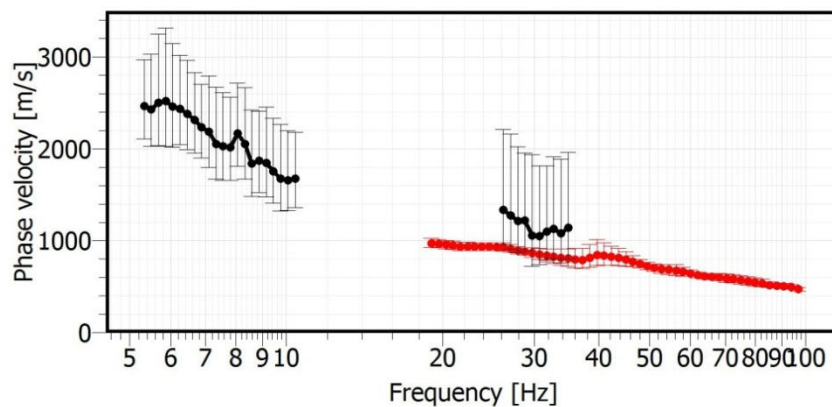


Figure 126: Rayleigh and Love dispersion curves used for the inversion process at PYAT site.

Table 45: Soil parameterization for the 5-layered model of the parameter space at PYAT site.

	Bottom depth (m)		Vs (m/s)	
	Min	Max	Min	Max
Layer 1	0.375	2.3	150	3500
Layer 2	2.3	9.9	150	3500
Layer 3	9.9	40	150	3500
Layer 4	40	164	150	3500
Layer 5	164	262	150	5000
Half-space	>262		150	5000

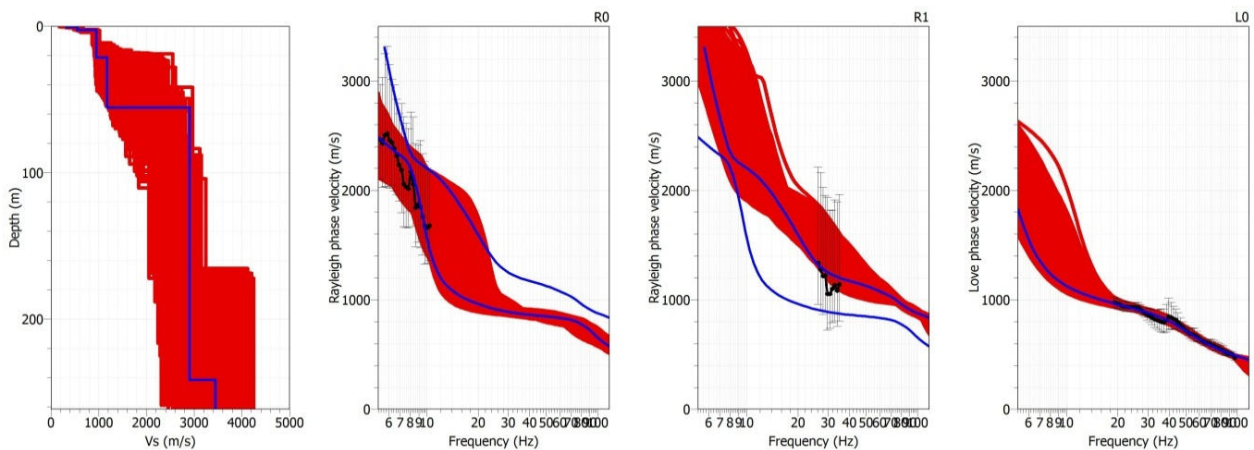


Figure 127: Results for PYAT site: inverted S-wave velocity profile (left) and dispersion curve (right) for the "acceptable models" with misfit equal to one sigma. The Rayleigh and Love waves dispersion curve derived from AVA and MASW analysis are displayed in black dots. Result for the best estimate model (from "classical" inversion) is also shown in blue.

Among the solution shown in Figure 127, one thousand soil profiles having a misfit equal to one sigma were randomly selected in order to compute statistic for Vs30. The associated distribution is displayed in Figure 128. See the section 4.1 for a final estimation of Vs30 and associated uncertainties.

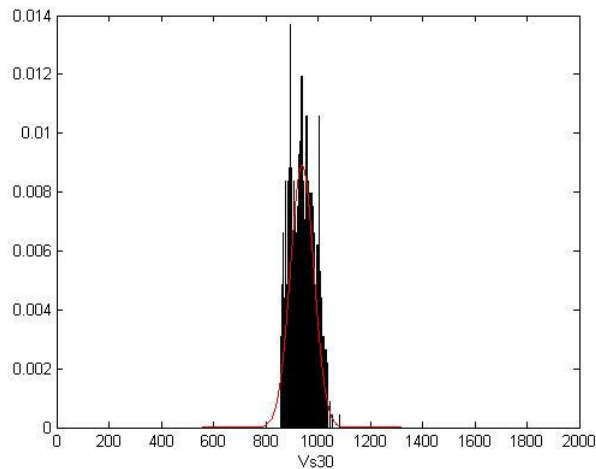


Figure 128: Distribution of Vs30 at PYAT site. The distribution is computed from 1000 soil profiles randomly selected and having a misfit equal to one sigma. The theoretical normal distribution is displayed in red.

4 DISCUSSIONS

4.1 RESULTS SYNTHESIS AND UNCERTAINTY ESTIMATION ATTEMPT

The results from this work can be expressed in different parameters:

- Dispersion curves themselves,
- Velocity profiles,
- Vs30,
- Soil class,
- 1D transfer function deriving from velocity profiles.

The Table 46 synthesizes the obtained results for velocity profiles, Vs30 and soil classes.

One difficulty is to assess the uncertainties associated to these different parameters. The uncertainties associated to dispersion curves are quite easily estimated when data are processed. The one affecting velocity profiles after inversion is more difficult. In this report, we used the “acceptable misfit” approach that aims to generate a set of profiles (here, one thousand per site) that produce the same misfit (eg. one sigma) between the corresponding forward-calculated dispersion curves and the observed dispersion curve. But it is worth to note that profiles that produced lower misfit than the target misfit are not included within this set of profiles (eg: the “best estimate” one). So, the other parameters one can derive from these sets of profiles, and especially the corresponding standard deviation, do not still correspond to a true standard deviation. Being able to estimate better quantified uncertainties from surface waves methods is one of the objectives of the ongoing InterPacific sub-project.

In this report, for velocity profiles, we show the sets of one thousand profiles per site + the best estimate profile per site. For Vs30, we propose quite qualitative uncertainty values, usually larger than to one that derived from Vs30 values calculated from the whole profile sets. These uncertainty values take also into account the quality of the acquisition itself and a part of author judgment.

We draw on all figures the velocity profiles to the depth that corresponds to the half of the maximum wavelength usable on DC curves. This leads to very variable results, from 10 m for PYLL to 350 m for PYLU.

The soil class attribution derives directly from Vs30 estimation. Note that when there is an interrogation between two classes (eg. A or B), this is usually due to a Vs30 value close to 800 m/s, not from high uncertainty on Vs30 itself.

The uncertainties affecting 1D transfer function, recalculated from velocity profiles, are quite low in comparison with the profiles themselves as we will see later.

Table 46: Results summary for all sites. We present the velocity profiles (best estimated in blue, set of 1000 profiles from the “acceptable misfit” approach in red); the Vs30 estimation with evaluated uncertainties; soil class attribution. We also formulate some remarks. The background colours indicate the author appreciation of the overall results quality. Green: good and reliable results, yellow: some cautions, red: quite bad results.

Site	Profiles	Vs30	Soil class (EC8)	Remarks
PYLL		800 ± 300 m/s	A or B	High estimated uncertainty on Vs30 due to a very limited investigated depth. Vs30 was estimated extrapolated deepest values. This is taken into account in the Vs30 uncertainty.
PYOR		300 ± 30 m/s	E (most likely) or C	The results are here highly sensitive to the identification of observed higher surface wave modes. The uncertainty associated to possible errors in mode identification is not taken into account here for Vs30 estimation.

Table 46: (continuation).

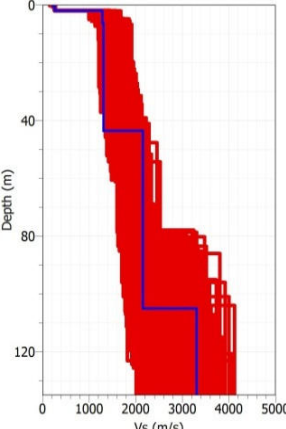
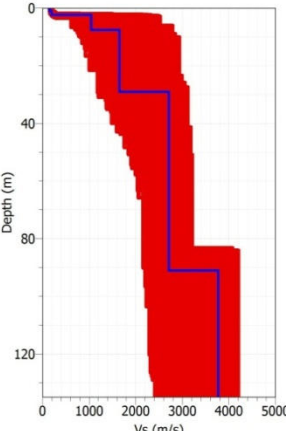
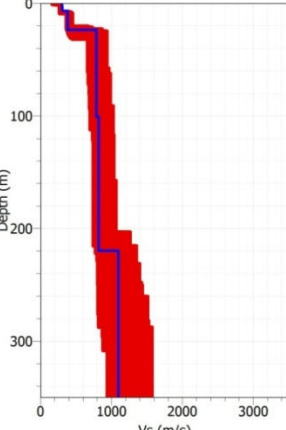
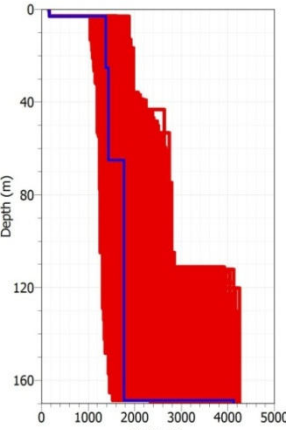
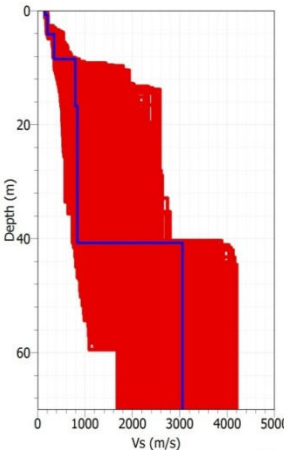
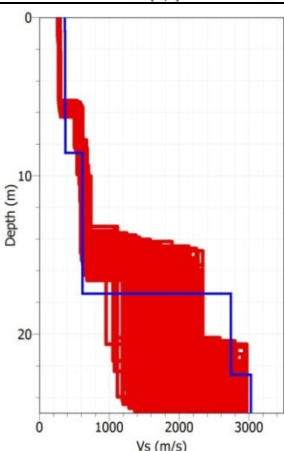
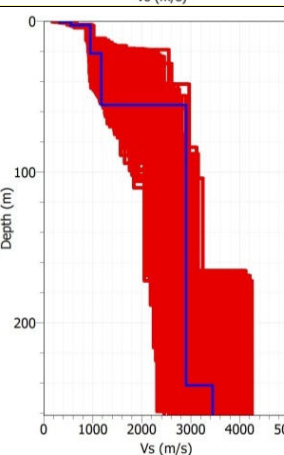
<p>PYLI</p>		<p>1150 ± 150 m/s</p>	<p>A</p>	<p>Overall very good and reliable results</p>
<p>PYAS</p>		<p>1000 ± 150 m/s</p>	<p>A</p>	<p>Overall very good and reliable results</p>
<p>PYLU</p>		<p>390 ± 40 m/s</p>	<p>B (most likely) or C</p>	<p>Overall very good and reliable results</p>
<p>PYBB</p>		<p>800 ± 100 m/s</p>	<p>A or B</p>	<p>Overall very good and reliable results</p>

Table 46: (continuation).

<p>PYLO</p>		<p>540 ± 50 m/s</p>	<p>B</p>	<p>Same remarks as PYOR about mode identification.</p>
<p>EPF</p>		<p>650 ± 150 m/s</p>	<p>B (most likely) or A</p>	<p>Investigation depth quite limited (25 m). Vs30 was estimated extrapolated deepest values. This is taken into account in the Vs30 uncertainty.</p>
<p>PYAT</p>		<p>900 ± 100 m/s</p>	<p>A (most likely) or B</p>	<p>Overall very good and reliable results</p>

4.2 METHODOLOGICAL LEARNINGS

The major methodological learning is that surface-wave methods can be applied for such application! We remind that we cumulated complications within the framework on this study: strong topography, difficult access to sites, time constraints, a priori “rock stations” for which the amount of surface wave within the ambient vibration wave field is relatively low in comparison with soft sites... Lot of persons was quite pessimistic at the beginning of the survey... But this was definitively one of the objectives of this work to push the method into their limits, at this was also mandatory in complement with InterPacific subproject.

The Table 47 summarized the performed acquisition and associated processing in order to highlight the processing and/or geometries that produced information (part of DC curves) or not.

The first observation is that SPAC processing failed in almost all cases. One possible explanation is the following. The SPAC method needs that the ambient vibration sources are homogeneously distributed in azimuth. This is a met condition in cities or in “noisy” context, but this definitely not the case in very quiet area, far from large cities, as for the Pyrenean RAP stations.

Fortunately, the FK (or HRFK) processing (that can be used even with noise sources that are not well distributed in azimuth) produced results in a lot of cases. For four sites (PYAS, PYBB, PYLO, PYAT), the intermediate radius circle array did not produce DC curve. This is possibly due to the fact that these geometries corresponded to wavelength where the velocity gradient was very high. Then the resolving capabilities may not be sufficient enough to sample these gradients. Fortunately, this did not affect the inversion since the other acquisitions were able to produce DC curves at high and low frequencies. For further survey, the use of a higher number of stations per acquisition array may produce better results.

The MASW produced information in all cases, and it is worth to note that the Love dispersion curves could be used in inversion in most cases and were useful in the work of mode identification. The use on both polarizations (horizontal and vertical that leads to Love and Rayleigh wave dispersion curves) must be preserve for further acquisition.

For EPF and PYLL, no passive measurements produced valuable results. These two RAP sites correspond likely to the two most isolated sites of this work, and ambient vibrations were probably not large enough to be interpreted.

Finally, we can point out that the WARAN acquisition system, even if its features could be very interesting and useful, was not rugged enough for this survey (lack of waterproofness, issues in memory card connection ruggedness and cable welding quality). This leads to a progressive decrease of the “productivity” along the survey and time wasting. We suggest that further developments on WARAN system allow increasing its robustness.

4.3 IS THERE ANY REFERENCE STATIONS?

Four sites out of the nine investigated sites (PYAS, PYLI, PYLL and PYLO) were previously considered by Drouet et al. (2010) as reference stations within a generalized inversion work. Within this work, these stations were assumed to have a Vs30 value of 2000 m/s. All Vs30 values determined within the framework of the present work are much lower: PYAS = 1000 m/s, PYLI= 1150 m/s, PYLL=800 m/s and PYLO=540 m/s. PYAS and PYLI Vs30 values are accurate. Even if the exact values might be commented for PYLL or PYLO, the data recorded in the present work demonstrate that Vs30 on these stations cannot reach 2000 m/s.

Beyond the discussion about the Vs30 values, an important issue is the notion of “reference station”. If we focused on PYAS and PYLI, even if these two sites belong clearly to the EC8 “A” soil class, they both show a thin layer of low-velocity material with a thickness of few meters (due to a weather zone or thin quaternary colluvium deposits). This leads to a very high frequency site effect. The Figure 129 illustrates this feature showing the 1D transfer functions computed with “best estimated” and the one thousand profile sets for both PYAS and PYLI sites.

Table 47: Summary of acquisition geometries (AVA and MASW) and corresponding processing. Lot of acquisition/processing did not lead to usable dispersion curve (almost all SPAC processing whatever the geometry, lot of intermediate radius geometry for FK processing: see comments in text).

		AVA			MASW		
		Array 1 radius [m]	Array 2 radius [m]	Array 3 radius [m]	Rayl.	Love	
PYLL	Acquisition	10 m	30 m	-	Yes	Yes	
	Obtained dispersion curve?	FK and/or HRFK	No	No	-	-	-
		SPAC	No	No	-	-	-
	Linear FK (MASW)	-	-	-	Yes	Yes	
PYOR	Acquisition	10 m	40 m	-	Yes	Yes	
	Obtained dispersion curve?	FK and/or HRFK	Yes	Yes	-	-	-
		SPAC	No	No	-	-	-
	Linear FK (MASW)	-	-	-	Yes	Yes	
PYLI	Acquisition	3 m	20 m	60 m	Yes	Yes	
	Obtained dispersion curve?	FK and/or HRFK	No	Yes	Yes	-	-
		SPAC	No	No	No	-	-
	Linear FK (MASW)	-	-	-	Yes	Yes	
PYAS	Acquisition	5 m	30 m	50 m	Yes	Yes	
	Obtained dispersion curve?	FK and/or HRFK	Yes	No	Yes	-	-
		SPAC	No	No	No	-	-
	Linear FK (MASW)	-	-	-	Yes	Yes	
PYLU	Acquisition	10 m	30 m	80 m	Yes	Yes	
	Obtained dispersion curve?	FK and/or HRFK	Yes	Yes	Yes	-	-
		SPAC	No	No	Yes	-	-
	Linear FK (MASW)	-	-	-	Yes	Yes	
PYBB	Acquisition	25 m	50 m	80 m	Yes	-	
	Obtained dispersion curve?	FK and/or HRFK	Yes	No	Yes	-	-
		SPAC	No	No	No	-	-
	Linear FK (MASW)	-	-	-	Yes	-	
PYLO	Acquisition	5 m	15 m	35 m	Yes	Yes	
	Obtained dispersion curve?	FK and/or HRFK	Yes	No	Yes	-	-
		SPAC	No	No	No	-	-
	Linear FK (MASW)	-	-	-	Yes	Yes	
EPF	Acquisition	10 m	30 m	-	Yes	Yes	
	Obtained dispersion curve?	FK and/or HRFK	No	No	-	-	-
		SPAC	No	No	-	-	-
	Linear FK (MASW)	-	-	-	Yes	No	
PYAT	Acquisition	10 m	40 m	100m	Yes	Yes	
	Obtained dispersion curve?	FK and/or HRFK	Yes	No	Yes	-	-
		SPAC	No	No	No	Yes	Yes
	Linear FK (MASW)	-	-	-	Yes	Yes	

Beyond the discussion about the V_{s30} values, an important issue is the notion of “reference station”. If we focused on PYAS and PYLI, even if these two sites belong clearly to the EC8 “A” soil class, they both show a thin layer of low-velocity material with a thickness of few meters (due to a weather zone or thin quaternary colluvium deposits). This leads to a very high frequency site effect. The Figure 129 illustrates this feature showing the 1D transfer functions computed with “best estimated” and the one thousand profile sets for both PYAS and PYLI sites.

As demonstrated by other previous works, especially in Italy (Pileggi et al. 2011), the reference stations are rare in accelerometric network. The “A class” information is definitely not sufficient to characterize accelerometric site and we may add a new class (for example “AA”?) that could describe true reference site where proofs were produced that no local high frequency amplification can bias records. In our survey of 9 RAP stations in Pyrenees, we did not find any “AA” sites...

Note also on Figure 129 that even if velocity profiles produced by the inversion on a given site can be very different, the deriving 1D transfer functions are very similar.

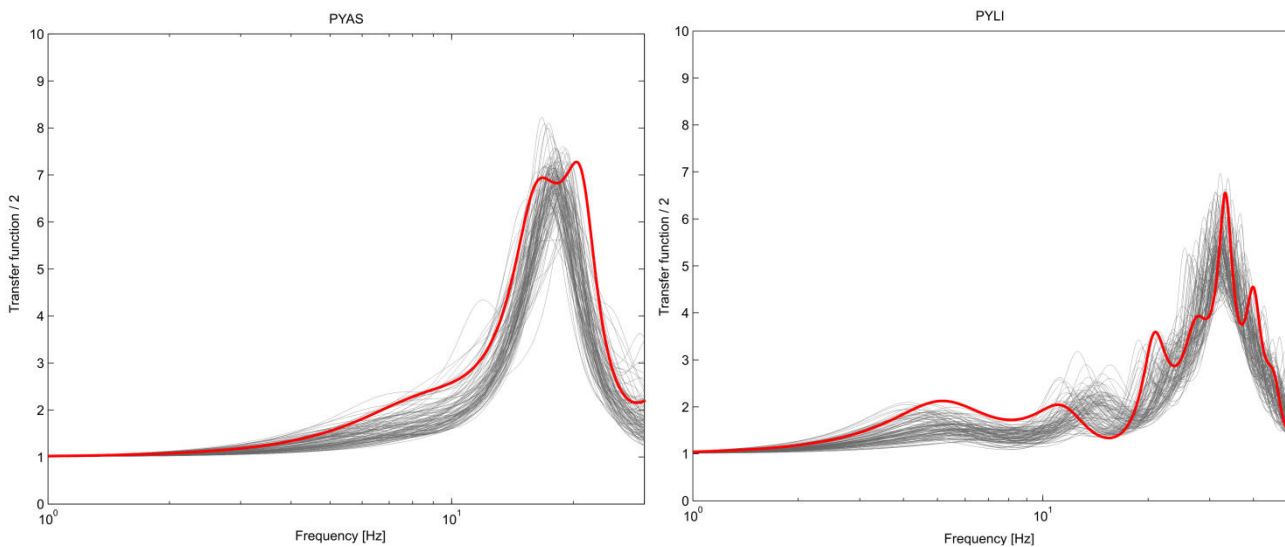


Figure 129: 1D transfer functions computed with “best estimated” V_{s30} profile (red) and the one thousand profile sets deriving from the “acceptable misfit” approach (gray) for both PYAS and PYLI sites.

4.4 WHAT ABOUT THE IMPACT ON KAPPA ESTIMATION?

The kappa parameter is now widely used and discussed. Its impact on seismic hazard assessment can be huge. Kappa is usually measured on earthquake records at high frequency (typically above 10 Hz) and aims to characterize the attenuation at high frequency. The common interpretation considers usually that when kappa is low, this means that high frequencies are weakly damped at a scale of few hundred meters to few kilometers beneath the studied site. If kappa is high, this is usually explained as a high damping of high frequencies at the same scale.

From a statistical point of view, “rock station” usually shows low kappa values and this means, at the first order, that the high frequency content of EQ records is high. But is this feature only due to a lack of attenuation at a hecto- to kilometric scale or this could also be due to high frequency site effect?

The Figure 130 shows the site response of PYAS and PYLI obtained by GIM performed by Drouet et al. (2010) and corresponding kappa estimation. On PYAS, one can guess the high frequency site effect (bump between 10 and 20 Hz). This clearly affects the kappa estimation. On PYLI, one does not see this effect but here, the possible local site effect (> 25 Hz) is at an even higher frequency and it is more difficult to conclude at a bias on kappa (here determined between 10 and 25 Hz).

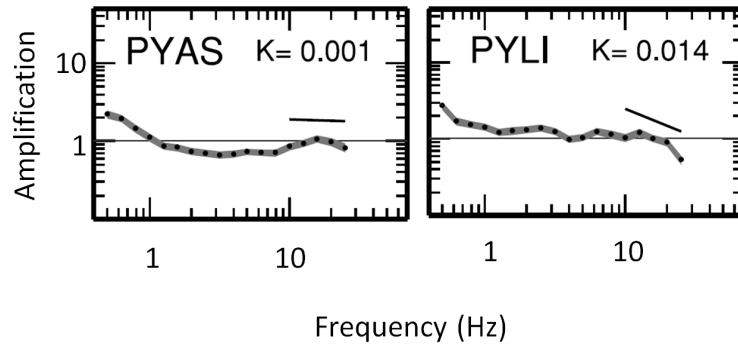


Figure 130: Site transfer functions \pm one standard deviation for the horizontal component (black line and dark grey shaded area) for PYAS and PYLI from generalized inversion of Drouet et al. (2010). Solid lines indicate the regression of the high frequency part of the transfer functions, which leads to the κ -values indicated on top of each frame.

5 CONCLUSIONS AND PERSPECTIVES

In this study, we aimed to produce metadata for a set of RAP stations in Pyrenees and to test non-invasive approaches in complex conditions. The survey was performed on 9 stations. We obtained reliable results (V_s profile, V_{s30} , class soil...) on at least 5 of them (PYLI, PYAS, PYLU, PYBB and PYAT) up to 130 to 350 m depth (depending on the site). On two other stations (PYLL and EPF) the investigation ranges were more limited but still allow giving V_{s30} bounds. On the two last station (PYOR and PYLO), the surface wave upper mode identification was more complex and the results may strongly depend on this identification. The final results given in this report for those both stations are likely exact, but it is reasonable to keep in mind this mode identification issue. Further processing and/or acquisitions on these sites may improve the robustness of the results.

From a methodological point of view, the major learning is that surface-wave methods can be applied for site characterization of accelerometric network stations, that is to say, even when survey and processing complications are cumulated (strong topography, difficult access to sites, time constraints, a priori “rock stations” for which the amount of surface wave within the ambient vibration wave field is low). Of course, some acquisition and/or processing did not produce results (eg. SPAC processing), but on each site, we could produce information that enhance the site condition knowledge.

On 9 stations, we did not identify any true “reference station” since all station are characterized by amplification. For the most “rigid” sites (PYLI, $V_{s30}=1150$ m/s; PYAS, $V_{s30}=1000$ m/s; PYAT, $V_{s30}=900$ m/s), we systematically found a quite soft layer underling the “true rock” that induces an high frequency site effect, even if these site are classified in the EC8 “A class”. We also illustrated that this high frequency site effect could be different between stations (here PYLI and PYAS) even for quite similar V_{s30} values. The V_{s30} cannot characterize alone such amplification effects.

Even if we did not identify reference station in our work, it seems important to add a clear identification “flag” within in accelerometric database metadata for stations that are really reference stations. The characterization of the possible high-frequency site effect for “rock” station (that cannot be considered as “reference station”) has also an influence on the kappa parameter determination.

It appears important to continue the work of accelerometric station characterization.

6 REFERENCES

- Aki, K., **1957**, *Space and time spectra of stationary stochastic waves, with special reference to microtremors*, Bull. Earth. Res. Inst. Tokyo Univ. 25, 415-457.
- Capon, J., **1969**, *High-resolution frequency–wavenumber spectrum analysis*, Proc. IEEE 57:8, 1408–1418.
- Drouet S., Cotton F. and Gueguen Ph., **2010**, *V_{s30}, κ , regional attenuation and Mw from accelerograms: application to magnitude 3–5 French earthquakes*, Geophysical journal international, doi: 10.1111/j.1365-246X.2010.04626.x.
- Hollender F., Cornou C., Bard P.-Y., Guyonnet-Benaize C., **2012**, *Site characterization (soil classes, V_{s30}, V_s profile...): Review of existing methods and state-of-the-art of noninvasive approaches - presentation of upcoming work*. Sigma program deliverable SIGMA-2012-D3-37.
- Pileggi D., Rossi D., Lunedei E. and Albarello D., **2011**, *Seismic characterization of rigid sites in the ITACA database by ambient vibration monitoring and geological surveys*, Bull Earthquake Eng (2011) 9:1839–1854.
- Wathelet, M., **2008**, *An improved neighborhood algorithm: parameter conditions and dynamic scaling*, Geophysical Research Letters, 35.

Review of the deliverable SIGMA-2014-D3-115 “Characterizing site metadata of accelerometric network stations: results and methodological feedback from a RAP station survey” by Aline DECHAMP, Sylvette THOMASSIN, Fabrice HOLLENDER and Cécile CORNOU. [Reviewer: F. Pacor]

The report describes the application of different surface-wave methods to selected accelerometric stations belonging to the RAP network. The aims of this works are

- 1) to improve the site-information of these accelerometric stations;
- 2) to test the applicability of non-invasive approaches in contexts where they are not usually applied, such as rock sites and non-flat topographies;
- 3) to compare the results with those from the Generalize Inverted Method (Drouet et al., 2010).

My impression is that the report is in a preliminary form: the English should be improved and several typographical errors be corrected; repetitions should be avoided and some figures improved (see specific comments in the following).

The bulk of the deliverable is represented by chapter 3 and consists in the presentation of the results achieved for the 9 investigated stations in terms of details about surveys, processing schemes and inversion procedures (about 100 pages). Each paragraph corresponds to one station and has the same structure of the others. I think that this chapter can be moved in an appendix. Indeed, the deliverable should be focused on methods, summary of results, discussion and conclusion.

Chapter 2

This chapter is devoted to describe acquisition/processing/inversion of the measurements. It is very short and I suppose that description on methods is reported in some previous deliverable/document. Otherwise, I suggest to expand this part, highlighting advantages and limits about the non-invasive techniques used in this study.

2.2.2 Ambient vibration arrays. The authors state that, before processing passive measurements, a data quality analysis on Fourier spectra has been performed. No explanation is given about this analysis, then I suggest to add more details on this point (e.g. time window duration, treatment of transients, eventual smoothing, criteria of exclusion of some portion of signal, etc.)

2.3 Inversion.

In my opinion the concept of “acceptable misfit” to take into account the uncertainties related to an inversion problem, it is not clear. This point should be expanded.

Chapter 3

In the following, I discuss some points on the base of the results on a specific station (PYOR), but they are valid also for the other investigated sites.

Geological/geographic information

I suggest to plot the location of the station on the geological map and explicit its scale.

Measurements

I observe that the acquisition of the passive measurement lasts about 1 hour. How do the authors select this duration? Have they performed some tests on the effect of using longer duration? My impression is that it could be a little bit short, especially in case of distortions or spikes in the signal (i.e. when Lennartz 5s is used for passive measurements, this sensor usually exhibits about 5-10 min of large transients just after starting the acquisition).

H/V

The authors present Fourier spectra for passive recordings computed on the three components for each station of the arrays. Do you adopt some exclusion criteria? For instance, I note that one spectrum is flat in figure 21 for the north component. How do the authors treat this record?

Then, in Figure 22 the H/V curves are plotted all together. I suggest to plot them on a map. The overview of the spatial distribution of the H/V spectral ratio allow to

check about the homogeneity in the site response within the array, as a validation of the hypothesis of 1D model which is at the base of FK, HRFK and SPAC methods.

Inversion

The results of the inversion provide the ensemble of acceptable models having misfit equal to two sigma. Figure 29 present the results plotting a) the *inverted S-wave velocity profile* and b) the *dispersion curves for the "acceptable models" with misfit equal to two sigma, together the curves relative to the best model ("classical inversion")*.

For me, this point is not clear and I think that more methodological details should be added at the beginning of the deliverable to better explain how the sigma is computed and what is the "classical inversion". In some case (PYLL, EPF) I note that the blue curve is not within the red curves. What does it mean? Why the best model is not in the range of the acceptable models?

If I have well understood, the sigma on Vs30 is computed from the selected set of acceptable models. If the models do not arrive to 30 m, how the authors extrapolate the S-wave profile (e.g. at PYLL station)?

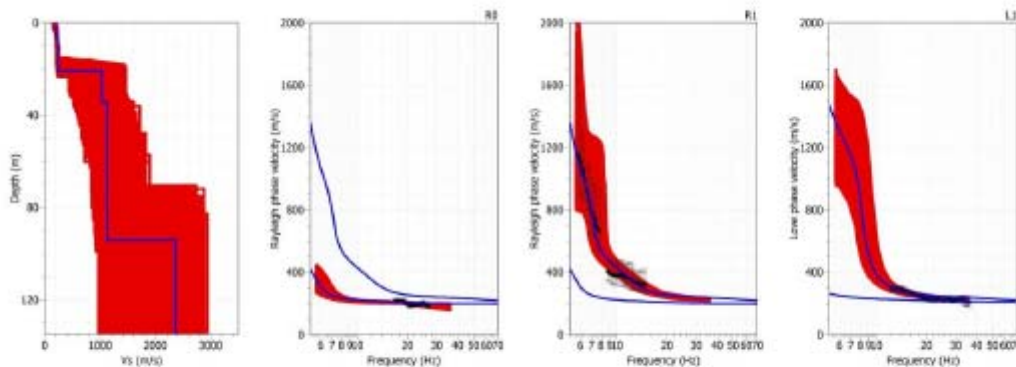


Figure 29: Results for PYOR site: inverted S-wave velocity profile (left) and dispersion curve (right) for the "acceptable models" with misfit equal to two sigma. The Rayleigh and Love waves dispersion curve derived from AVA and MASW analysis are displayed in black dots. Result for the best estimate model (from "classical inversion) is also shown in blue.

Do the authors consider the possibility of velocity inversion in their models? How is this problem handled?

Discussions

I suggest to add a table which reports, for each station, some information such as: coordinates, number of records, minimum and maximum PGA recorded, previous site classification and the metadata obtained as results of this study: depth reached by the survey and, if any, others parameters, such as, the new site classification, the site fundamental frequency, V_{s30} with its sigma, bedrock-depth (e.g. considering “the bedrock” as $V_{s30} > 800$ m/s), etc.

Concerning the maximum depth for which the Vs profile can be considered reliable, I think that it has to be very clear. For instance, at PYLL station, is the profile reliable down to 10m or less?

4.2 Methodological learning

The authors state that *“surface-wave methods can be applied for such application!”*

I agree with them, but I think that this point should be discussed. Have the authors validated the results with independent measurements? Have the authors compared the 1D response site with the empirical ones obtained by the Generalized inversion method? If yes, I suggest to add some figure with these comparisons.

Report on the deliverable SIGMA-2014-D3-115 entitled “Characterizing site metadata of accelerometric network stations: results and methodological feedback from a RAP station survey” by Aline DECHAMP, Sylvette THOMASSIN, Fabrice HOLLENDER and Cécile CORNOU. [Reviewer: M. Granet].

This work is a contribution to Work Package 3 (“Site effects”) and in particular represents an application and a continuation of a previous work done by F. Hollender, C. Cornou, P.-Y. Bard and C. Guyonnet-Benaize which was presented during the SIGMA CS meeting N° 3 held in Roma in June 2012 (deliverable SIGMA-2012-D3-37: “Site characterization [soil classes, Vs30, Vs profile...]: review of existing methods and state-of-the-art of non-invasive approaches, presentation of upcoming work”).

A short abstract about this former work (content and review)

The goal of this former study was to give a review of the most common techniques for seismic site characterization, both non-invasive techniques based on inversion of surface wave dispersion curves (i.e. phase velocity of surface waves as a function of frequency), and invasive techniques, like cross-hole or down-hole testing.

Among different comments (especially the ones concerning the inversion process: non uniqueness and a soil profile layered horizontally), the reviewers stated:

- i) would have liked to see more advice and guidance as to the usefulness of each technique, with some general recommendations of where and when to use them;*
- ii) point out the necessity to complete the task with a determination of which are, at the minimum, the parameters that should be estimated to exercise the various existing non-linear codes.*

I- The objectives of this present study

This study is essential because it is necessary to associate a given accelerogram to a given type of site conditions when defining the seismic hazard level. The site conditions are “modeled” by the Vs30¹ parameter, which knowledge is based on the whole Vs distribution (2D or 3D) down to the bedrock; shear wave velocity is a “rock property” that controls the ground motion amplification.

Besides the fact that such studies are the basis to better characterize the site effects, essential for seismic hazard assessment and for Ground Motion Prediction Equations (GMPEs) derivation, the two main objectives of this study are:

- production of metadata for a first set of 9 RAP stations (the knowledge of the parameters characterizing each accelerometric recording site should be improved in France);
- A methodological effort (which complements the InterPacific² subproject) that aims to test non-invasive approaches on accelerometric sites (with measurements performed within a day for each site) which are not well adapted to surface-wave approaches (for example, due to topography), and then to compare the results from surface wave methods to those based on the use of accelerometric data themselves, for example the Generalized Inversion Method (GIM) used by Drouet et al. (2010) which is a third way to investigate site effects. As one advantage, non-invasive approaches average the rock properties on a large volume.

Another output of this study will be the validation - or not - of the soil class (from Vs30 values) formerly identified at each of these 9 RAP stations and hence to detect possibly a “true reference station”.

II- Short presentation of the methods used and of their characteristics

¹ Vs30: harmonic mean for shear wave velocity within the first 30 meters.

² InterPacific: **Inter**-comparison of methods for site **parameter** and **velocity profile** characterization (A benchmark to better understand differences and complementarities between invasive and non-invasive methods).

As already indicated, the study is based on surface waves methods for geotechnical site characterization, which implies the full wave field recording. The recorded data are analyzed with different techniques to estimate the experimental dispersion curves. At the end, the dispersion curves are inverted to estimate the variations of the elastic properties with depth (i.e. the Vs profiles).

The implementation of the state-of-the-art of a non-invasive survey needs a procedure in three steps: acquisition, data processing and inversion.

Two methods were retained and systematically used for these 9 non-invasive surveys: an active method, the MASW (Multi Analysis Surface Waves), and a passive one based on Ambient Vibrations Array (AVA).

II.A- The Multichannel Analysis of Surface Waves - MASW - method (active method)

MASW is an active and non-invasive method, which is shortly described in deliverable SIGMA-2012-D3-37 (Hollender et al., 2012). This method is based on the study of Rayleigh (and Love) surface waves and their dispersive properties (the phase velocity depends on the frequency). The study of the fundamental mode and other modes allows characterizing the soil. From the obtained dispersion curves (the relationship between phase velocity and frequency), and after inversion, it is possible to determine a 1D vertical Vs profile. Practically, seismic waves are artificially generated using active sources like a hammer source, and are recorded by vertical and/or horizontal geophones, placed along a line.

One should note that Rayleigh waves do not propagate into the voids.

To summarize MASW: a profile with vertical and horizontal geophones, 1 active source and recordings of the full wave field.

II.B- Ambient vibrations array - AVA - method

AVA is a passive and non-invasive method, which is shortly described in deliverable SIGMA-2012-D3-37 (Hollender et al., 2012).

From D3-37:

“The acquisition consists to deploy temporary, small aperture (from a few meters up to kilometric scale), 3-component, and high sensitivity seismological 2D arrays, to record the ambient vibrations. The geometry adopted for building these arrays is important and depends on the available number of sensors and on the site configuration”.

In this study, Dechamp and co-workers use circle geometries (3 different circles, when possible) for 2D arrays with one sensor in the middle and 7 or 9 sensors on a circle. The ambient vibrations are measured consecutively for each circle, by increasing the diameter in order to get a dispersion curve and a wide frequency range.

The data are then processed in order to get dispersion curves or spatial autocorrelation curves. Dispersion curves are obtained following the Finite-Wavenumber FK (or f-k) and/or High resolution Finite-Wavenumber HR-FK (or HR f-k) analysis. Spatial autocorrelation curves are obtained following the “SPAC” analysis. A description of the SPAC method can be found, for example, in Chavez-Garcia et al. (2005)³, Cornou et al. (2006) or in Gouédard (2008a, 2008b).

These procedures can be done with both Rayleigh and Love waves.

To summarize AVA: 3-component and high sensitivity seismic 2D arrays, recordings of ambient vibrations.

III- Description of the report and first comments

Besides a summary, the deliverable D3-115 (112 pages including bibliography) is organized in 5 chapters:

1. Introduction and objectives (about 2,5 p);

³ *“Cross correlation functions are computed between pairs of stations, and then averaged for different station pairs, at the same interstation distance but with different orientation”.*

2. Acquisition and processing methodology (about 2,5 p);
3. Presentation of surveys, processing and inversion for all investigated stations (**about 93 p**);
4. Discussions (about 7 p);
5. Conclusions and perspectives (1 p).

III. A- Selection of stations, hardware and data processing

The selection of the 9 RAP stations was coordinated with SIGMA WP 2. Selected stations are from the Pyrenean area, an active seismic region that produced the most accelerograms used in seismic studies. The authors decided to first focus on the stations within the accelerometric Pyrenean network, that were considered as “reference stations” within the previous work of Drouet et al. (2010): PYAS, PYLI, PYLL and PYLO. This list has been completed with 4 stations that recorded a large amount of accelerograms: PYOR, PYLU, PYBB and PYAT. Finally, station EPF operated by CEA/DASE/LDG was also retained. The survey took place in September 2012 during 2 weeks.

III. B- Acquisition and processing methodology

Following Hollender et al. (2012) who demonstrated (as others) that better results are obtained from both active and passive methods with a joint inversion of the results, AVA and MASW were applied for this survey.

Data acquisition MASW:

An acquisition seismic line made of 24 vertical and 24 horizontal geophones (all with a 4,5 Hz natural frequency), associated to a Geode acquisition system provided by ISTerre, was used; the active source was provided by a 5 kg hammer, hitting either vertically a metallic plate or horizontally a wooden beam (from D3-115). One or two profiles in both horizontal and vertical polarizations were performed, with an inter-geophone distance of 1 or 2 meters.

Data acquisition AVA:

For passive measurements, the WARAN system developed by Marc Wathelet at the “Institut des Sciences de la Terre” (University Joseph Fourier, OSU Grenoble, UMR 5275) was selected. The WARAN system allows using 10 stations, but only 8 sensors were operated for the last sites characterization due to technical problems. The WARAN acquisition stations were equipped with Lennartz 5s 3-component seismometers, which I personally consider as a very good choice for such studies.

The goal of the processing step is to determine dispersion curves (obtained either from f-k or HR f-k methods) or spatial autocorrelation curves (obtained from AVA following the SPAC analysis). The processing is done on both Rayleigh and Love surface waves.

Processing MASW:

For each site, MASW was processed using the “linear FK” tool of the Geopsy software⁴ in order to retrieve the dispersion curves of Rayleigh and Love waves. MASW processing generally allowed obtaining dispersion curves at high frequencies.

Processing AVA:

Data recorded using passive measurements were analyzed by different ways:

- H/V: Authors started the processing by applying for each “single” point measurement a classical H/V analysis (*D3-115: in order to evaluate the spatial homogeneity of the investigated site, but also to get the fundamental resonance frequency of the site that could be used in joint inversion techniques*).
- FK and HR-FK: FK (f-k) analysis (of multi-station data) is widely recognized as a powerful tool for processing surface waves. The procedure consists of transforming data from the t-x domain into

⁴ <http://www.geopsy.org/> (Wathelet et al. 2008).

the f-k domain and then picking the maxima in the spectrum to retrieve an experimental dispersion curve. The f-k spectrum is strongly influenced by spatial sampling, in other words by a too small number of geophones. Difficulties can be due to an insufficient wavenumber resolution (leading to an inaccurate localization of maxima) which derives from the spatial windowing of acquisition (Foti, 2002). **Questions concern the quality of the phase velocity determination, the discrimination between the different modes and the windowing.**

The authors do not discuss these points neither in their former report, nor in this one.

HR-FK: an improvement of the f-k method, called High-Resolution Frequency-wavenumber, has been introduced by Capon (1969). *“Operating with sliding time windows and narrow frequency bands, this method provides the wave propagation parameters (azimuth and slowness as a function of frequency) of the most coherent plane wave arrivals”* (Gouédard, 2008b)⁵.

The principle of this processing is given in Hollender (D3-115) (rewritten). *“The simultaneous waveform recordings of a group of spatially distributed stations are analyzed in many narrow frequency bands for a number of individual analysis [windows. For each analysis window and frequency band, a grid search is performed in the k domain to retrieve the propagation properties of the most coherent and/or powerful plane wave arrival. The phase velocity of the surface wave at this particular frequency is given by the apparent velocity.”*

The vertical components for each different array were processed using the FK and HR-FK analysis using “Geopsy” software. One should note that the FK and HR-FK lead to obtain Rayleigh waves dispersion curve in a frequency range that depends on the array geometry.

These methods are efficient as the number of noise sources is limited. An increase of this number leads to interferences between the waves generated by each of them, which is not addressed by the method (Gouédard, 2008a).

- Spatial Autocorrelation (SPAC): SPAC allows computing average spatial autocorrelation coefficients for any arbitrary array configurations. It relies on a stochastic ambient noise wave field stationary in both time and space. As the application of the SPAC technique requires perfectly circular arrays, it was difficult to achieve this in Pyrenean sites.

In fact, as we can see from the results presented in this manuscript, SPAC method did not work for several sites of the survey. The SPAC approaches leads to auto-correlation curves that can be converted into dispersion curves. This method is based on two assumptions: 1) the noise sources are randomly distributed; 2) there is one phase velocity per frequency. If the first hypothesis is rarely checked, the method is still acceptable as long as the seismic noise is not very directional; this method is effective in practice as noise sources are numerous and located around the network (Gouédard, 2008).

The geometry of the network is important and must be adapted to the number of sensors and to the site configuration. In this survey, circle geometries are used (1 sensor at the center, 7 or 9 sensors on a circle around the center). Authors measured consecutively 2 or 3 circles with an increasing diameter in order to get the dispersion curves and a wide frequency range.

All the processing was performed with the Geopsy software.

Inversion

The goal of the inversion processing is to convert the dispersion or spatial autocorrelation curves into 1D velocity profiles. It is pointed out that for such non-invasive approaches based on surface wave analysis, non-uniqueness and also misinterpretation in the identification of dispersive curves modes (fundamental or higher modes) can bias the results. However, these “errors” are reduced if we consider the whole available data within the inversion.

⁵ « Une amélioration de cette méthode [f-k], appelée « High-Resolution Frequency-Wavenumber » (HRFK), a été introduite par Capon [1969]. Il proposa de rajouter une pondération pour chaque capteur dans la somme sur les signaux déphasés. Cette pondération est calculée via une optimisation visant à minimiser la réponse du réseau dès qu'on s'éloigne du vecteur d'onde considéré. » (Gouédard, 2008a, PhD thesis).

The inversions were performed using the Geopsy package (<http://www.geopsy.org/>). Authors tried to achieve for each station a joint inversion of the different segments of the Rayleigh wave dispersion curves produced by the AVA array and the MASW survey, the autocorrelation curves when available, the Love dispersion curve at high frequency.

The computations of uncertainties are obtained in the following way (D3-115 deliverable): *“uncertainties linked to the inversion are estimated from the ‘acceptable misfit’ approach that consists to produce not only the ‘best estimate’ velocity profile but also the one that are coherent with the DC curve within a $\pm 1 \sigma$ interval.”* **This needs to be developed.**

The final output is a set of velocity profiles, which are derived in Vs30 values and Soil classes.

III. C- Presentation of surveys, processing and inversion for all investigated stations

For each of the 9 RAP stations, the document is organized in the same manner: station information, measurements, processing and inversion.

Station information

This includes the reasons for the choice, geographic and geologic information (a table - see below an example for station PYAS, figures showing the station location, and pictures realized during the measurement).

Station	City	Department	X Coord (Long)	Y Coord (Lat)	Network	Site	Slope
PYAS	Aspet	Haute-Garonne(31)	0.797255	43.011958	BRGM	Edge of Pyrenean chain	Flat

Measurements

The document presents on a table (see below an example for PYAS) the recording parameters (also for MASW investigation).

Measurments	Numbers of Sensors	Beginning (TU)	End (TU)	Noise/ environnement	Topography	Weather conditions
Array R = 5m	10	10:37:00	11:20:00	Mid-urban	flat	good
Array R = 30m	8	13:58:00	14:58:00	Mid-urban	flat	good
Array R = 50m	8	15:44:00	16:45:00	Mid-urban	flat, with a river at the middle of the array	
MASW N10°E 46m, Dx = 2m	24 vertical geophones V)	11:20:00	11:30:00	Mid-urban	flat	good
MASW N120°E 24m, Dx = 1m	24 vertical geophones(V)	11:30:00	12:30:00	Mid-urban	flat	good

There are however no comments about the selected parameters: for example, which are the (geo)physical reasons to select circles with a diameter equal to 10, 60 and 100 meters for this station with respects to the expected/desirable wavenumber resolution?

Processing

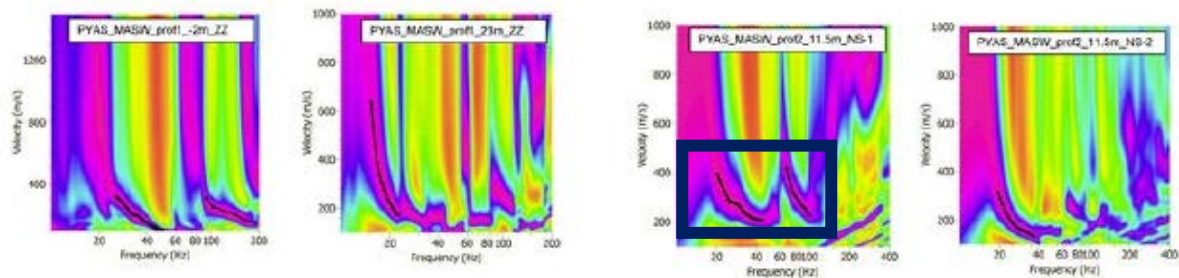
The manuscript presents:

- i) The H/V curves (a figure showing the amplitude of the Fourier spectra computed on 3-C recordings of ambient vibrations at each array receiver);

- ii) a description of the parameters used for FK and HR-FK analysis (a table: see below for station PYAS);

Array	Windows length	Fmin Hz	Fmax Hz	Step	Kmin rad/m	Kmax rad/m	Grid step rad/m	Grid size rad/m	Vmin m/s	Band width
FK										
5 m	70 T	20	40	50	0.4821	3.5203	0.1205	7.041	150	0.1
30 m	150 T	15	25	50	0.1148	0.6070	0.0287	1.214	150	0.1
50 m	200 T	10	20	40	0.0470	0.1145	0.0118	0.2290	150	0.1
HRFK										
5 m	100 T	22	40	30	0.4821	3.5203	0.0241	7.041	50	0.05
30 m	100 T	17	20	50	0.1148	0.6070	0.0057	1.214	150	0.03
50 m	200 T	7	20	40	0.0470	0.1145	0.0024	0.2290	150	0.02

- iii) The results obtained for FK (a set of figures - one for each selected circle - showing the histogram distributions of phase velocities - velocity versus frequency - derived from the ensemble of the wave-propagation estimates obtained for each individual time-frequency cell using the FK method);
- iv) The results obtained for HR-FK (a set of figures as for the FK method);
- v) The results obtained for the SPAC method: a table giving the SPAC analysis parameters (**this is generally not clear in the manuscript to understand how parameters have been selected; for example, the window length - 200 T in this case, where T is the center period of the frequency band -, Fmin and Fmax, ...**), the spatial autocorrelation curves computed for each ring (autocorrelation ratio versus frequency).
- vi) The results obtained for the MASW measurements (again, there are no explanations on the choices made for the configuration of network distance between geophones, location shots ...): a figure (see below part of this figure) showing histogram distributions of phase velocities (velocity versus frequency) derived from the MASW analysis.



The authors say nothing about how - picked manually - the dispersion curves on histograms are pointed (see the black box on the picture number 3).

Inversion

For each station, the manuscript presents:

- A figure showing the dispersion curves derived from AVA and MASW analysis, if both are available;
- A figure showing the Rayleigh and Love dispersion curves (after averaging and resampling the “raw” curves) used for the inversion process at each site;
- A table giving the soil parameterization for the 5-layered model of the parameter space (at each site);

- A figure showing the inverted S-wave velocity profile and the dispersion curves for the “acceptable models” with a misfit equal to one sigma;
- A figure showing the distribution of Vs30 at each site.

Some questions from a reviewer who is not a “daily user” of this kind of studies: a) What is the (geo)physical significance of the phase velocities calculated at very high frequencies (> 40 Hz, for example)? b) How is practically obtained the Vs30 parameter from the inverted S-wave velocity profiles? c) What is the meaning of R0, R1... and L1 (top right of some figures showing the dispersion curves for the “acceptable models”; for example, see figures 71, 85, and 99)? Are they the overtones of the surface waves?

IV- Discussion and other comments

This chapter presents a synthesis of the results obtained and gives some general common features. It is divided into 4 sections: Results synthesis and uncertainty estimation attempt; Methodological learning's; Are there any reference stations? What about on the impact on kappa estimation?

Uncertainties

The authors stress the fact that it is difficult to assess the uncertainties associated to the parameters deduced from the survey at each site: dispersion curves; velocity profiles; Vs30 (one objective of the survey); soil class (as deduced from the Vs30 parameter).

Concerning the velocity profiles, authors used the “acceptable misfit” approach that aims of generating a set of profiles (here, one thousand per site) that produce the same misfit (e.g. one sigma) between the corresponding forward-calculated dispersion curves and the observed dispersion curve. **It would have been interesting to develop on other possible ways, if reasonable, to estimate these uncertainties.**

For Vs30, authors proposed “quite qualitative uncertainty values which take also into account the quality of the acquisition itself and a part of author judgment”.

A table provides a summary of the obtained results for the velocity profiles, Vs30 and soil classes for each site. As already stated, for readers who are not familiar with this kind of studies, this is not easy to properly understand how are obtained the Vs30 estimation from the set of velocity profiles obtained by inversion of the dispersion curves. However, this table is a perfect “*resumé*” of the full work.

On the methodological learning's

Authors point out on the fact that “*surface wave methods can be applied for such application*” (this is understandable in a double sense: a) field conditions were not really the best to apply these array methods; b) these methods yield “valid” results considering the field conditions and the final objectives.)

Anyway, we already know that such surface wave methods should work (the array geometry being adapted to the field conditions). **What is missing, to my opinion, is a general discussion about the limits of each method even if one can find a lot of information in related papers.**

It is also shown that the SPAC method failed in almost cases, but that both FK and HR-FK processing gave positive results in a lot of cases. A table gives a summary of the acquisition geometries (AVA, SPAC) and corresponding processing. On average (everything being considered, acquisition and processing) about 50 % did not lead to usable dispersion curves (very good results for the MASW method, relatively poor results for the AVA methods).

On the reference station

All the Vs30 results obtained in this work for 4 stations being considered by Drouet et al. (2010) as reference stations are much lower (PYAS, PYLI, PYLL and PYLO assumed to have a Vs30 value of 2 000 m/s by Drouet et al.). In this study, these values vary from 540 m/s (PYLO) to 1 150 m/s (PYLI). In addition, even if these Vs30 values for PYLI and PYAS (1 000 m/s) lead to an EC8 soil class A, both stations show a very thin layer of low-velocity material with a thickness of few meters (**however, there is no discussion in the text on the “reliability” - in the sense of what about the vertical resolution - of this thin layer**). It is shown that the 1D transfer functions computed with the “best estimated” Vs30 profiles exhibit a very high frequency site effect (about 20 Hz for PYAS and 30 Hz for PYLI).

The authors conclude that the “A class” information is definitely not sufficient to characterize accelerometric site... and hence propose a new “AA class” that could describe “true” reference site where there are no local high frequency amplification which can bias the records.

The authors write that they don’t find such a “AA” site in their survey.

Concerning Kappa

Kappa, which impact is major on seismic hazard assessment, is a parameter used in the characterization of strong ground motion for high frequencies. It models the linear decay of the acceleration spectrum, in other words the attenuation at high frequencies.

At a scale from few hundred meters to few kilometers (which seems a bit large considering the wavelength of records), a low Kappa is usually interpreted by weakly damped high frequencies and, in contrary, high Kappa values might indicate a high damping for high frequencies (the authors).

In addition, even if the scatter is very large, a global decrease of Kappa with increasing Vs30 is observed (see Van Houtte et al., 2011).

As “rock station” usually shows low Kappa values, hence indicating a weakly damped high frequencies (records have high frequency content), the question arises to know if this is due to a lack of attenuation or to a high frequency site effect. This demonstrates the need of such a survey for the whole RAP network.

The main conclusions of the authors are:

- Reliable results (Vs profile, Vs30, soil class) were obtained in 5 of the 9 RAP stations that were considered in this study;
- The surface-wave methods can be applied for site characterization of accelerometric network stations, even in the case that the field conditions were bad;
- There is no identified reference station (from Vs30) in this study and it is observed a high frequency site effect at 2 stations having a Vs30 close to 1 000 m/s; hence, it is proposed to define a new EC8 AA soil class;
- It is necessary to identify with a flag in the metadata the stations which are “true” reference stations.

Some final comments

The manuscript is a bit long (due to an exhaustive presentation of the measurements and of the results obtained after processing the data), its main part being made of the presentation of the 9 surveys.

It looks like the report was not properly reread before being transmitted. In terms of presentation, figure captions should be completed in order to better clarify their understanding by the reader who is not familiar with such studies. There are still some errors in the text, some of them being due to a “copy & paste” (for my feeling), probably because, for each station, the same reporting structure is logically reproduced (measurements, data processing, inversion, for all the investigated stations).

Even if the document is well presented and easy to read, there is a lack regarding the theoretical description of the methods and their limitations, including the reasons that led to the choice of certain parameter values for the seismic data acquisition in the field (see infra).

Finally, the manuscript looks like an excellent technical report rather than a scientific paper (This is not a criticism!). This is often the case for such field survey. However, it is possible to draw important conclusions from this study:

- It is demonstrated that the use of non-invasive methods is possible for geotechnical site characterization, in hard field conditions; however, it is difficult at this stage to say whether the results obtained are more "reliable" (in the sense of: better than others) than those resulting from other methods (GIM, invasive methods); in addition, positive results are obtained at only 5 of the 9 selected;*
- Regarding Vs30, at some stations, the results are significantly different from those obtained by a method based directly on the use of accelerograms (GIM); this requires further investigation on these non-invasive methods.*

In terms of methodology stricto sensu, as already written, the report should provide a brief theoretical review (not really found in the deliverable D3-37, the reader must look at the literature...) and further explain their implementation, including what are the criteria governing the choice of key parameters (see the main text: it is not explained how these key parameters have been selected; for example, the sliding window length, the Fmin and Fmax frequencies, ...). Other questions are raised directly in the text (for example, the determination of uncertainties, the wavenumber resolution, etc.).

Clearly, this study should be extended to the whole permanent accelerometric network.

Bibliography

- Chavez-Garcia, F.J., Rodriguez, M., and Stephenson, W.R., 2005. An Alternative Approach to the SPAC Analysis of Microtremors: Exploiting Stationarity of Noise. *Bulletin of the Seismological Society of America*, Vol. 95, No. 1, pp. 277–293, February 2005, doi: 10.1785/0120030179
- Capon, J., 1969. High-resolution frequency–wavenumber spectrum analysis, *Proc. IEEE* 57:8, 1408–1418.
- Cornou, C., Ohrnberger, M., Boore, D.-M., Kudo, K., and Bard, P.-Y., 2006. Using ambient noise array techniques for site characterization: results from an international benchmark. In *Proc. 3rd Int. Symp. on the Effects of Surface Geology on Seismic Motion*, Grenoble, 30 August - 01 September, 2006, Bard, P.-Y., Chaljub, E., Cornou, C., Cotton, F. and Guéguen, P. Editors, LCPC Editions, NBT paper.
- Drouet, S., Cotton, F., and Gueguen, Ph., 2010, Vs30, K , regional attenuation and Mw from accelerograms: application to magnitude 3–5 French earthquakes, *Geophysical journal international*, doi: 10.1111/j.1365-246X.2010.04626.x.
- Foti, S., Sambuelli, L., Socco, L., and Strobbia, C., 2002. Spatial Sampling Issues in FK Analysis of Surface Waves. *Symposium on the Application of Geophysics to Engineering and Environmental Problems 2002*: pp. SE18-SE18.
- Geopsy software: <http://www.geopsy.org/index.html>
- Gouédard, P., 2008a. *Techniques de corrélation : aspects méthodologiques et applications à la subsurface*. Thèse de doctorat de l'Université Joseph Fourier, 189p.
- Gouédard, P., Cornou, C., and Roux, P., 2008b. Phase–velocity dispersion curves and small-scale geophysics using noise correlation slantstack technique. *Geophys. J. Int.*, 172 (3): 971-981. doi: 10.1111/j.1365-246X.2007.03654.x.
- Hollender, F., Cornou, C., Bard, P.-Y., and Guyonnet-Benaize, C., 2012. Site characterization (soil classes, Vs30, Vs profile...): review of existing methods and state-of-the-art of non-invasive approaches. SIGMA CS meeting N° 3, Roma, June 2012.
- Van Houtte, C., Drouet, S., and Cotton F., 2011. Analysis of the origins of κ (Kappa) to compute hard rock to rock adjustment factors for GMPEs. *Bull. Seismol. Soc. Am.*, 101, no. 6, 2926–2941.
- Wathelet, M., Jongmans, D., Ohrnberger, M., and Bonnefoy-Claudet, S., 2008. Array performances for ambient vibrations on a shallow structure and consequences over Vs inversion. *Journal of Seismology*, 12, 1-19.